Universitetet
i Stavanger

FACULTY OF SCIENCE AND TECHNOLOGY

MASTER'S THESIS

Study program/specialization: Petroleum Engineering/Drilling	Spring semester, 2009 Open
Author: Chinweike Julius Mba	…… (signature author)

Instructor: Marete Vadla Madland

Supervisor(s): Marete Vadla Madland
Edvard Omdal
Megawati Megawati

Title of Master's Thesis:
The influence of pore pressure on rock-fluid interaction

ECTS: 30

Subject headings: Chalk Strength measurement Creep studies Chemical analyses of fractioned effluents	Pages: 90 Stavanger, 15th June, 2009

ABSTRACT

The experimental work in this thesis was performed at the chalk laboratory in University of Stavanger. The main objective is to determine the overall influence of pore pressure on the mechanical strength of chalk in the presence simple brines, mainly $MgCl_2$ and NaCl with the same ionic strength as in seawater. The tests were carried out at both high and low pore pressures of 40MPa and 0.7MPa respectively. The temperature used during the performance of all the tests was 130^oC.

The chalk samples used in the experiments were from Stevns Klint near Copenhagen in Denmark. Generally the chalk has very high porosity and low content of silica, which confers on it a low mechanical strength.

Each of the samples tested at high pore pressures undergoes four main stages while those carried out at low pressures have three phases. The first phase involves initial building of confining and pore pressures to 1.4MPa and 0.7MPa respectively while cleaning the samples with distilled water. Ramping of confining and pore pressures simultaneously to 41MPa and 40MPa respectively, followed by brine injection is carried out in the second phase. The third phase is hydrostatic loading of the samples to an effective stress of 12MPa, followed by the creep phase and sampling of effluents of the flooded brine. The last stage entails chemical analyses of the fractioned effluents using Ion Chromatography machine. Tests performed at low pressures does not involve the second phase of pressure ramping.

Several problems were encountered during the tests because of the high pressure and high temperature conditions of the tests. Among the tests performed, 6 were accepted as successful, 2 were partially successful while 11 were adjudged as unsuccessful.

Results from the experiments reveal that chalk cores flooded with NaCl are mechanically weaker than those injected with $MgCl_2$ at both high and low pressures. Suggested possible reason for the difference in mechanical strength was that there was dissolution of the chalk and a subsequent precipitation of minerals for cores flooded with $MgCl_2$. The precipitates tend to increase cementation and friction between the chalk grains, making them mechanically stronger. For cores injected with NaCl it was believed that precipitates were not formed which resulted in enhanced compaction taking place. In addition, “accelerating-like” creep was observed on chalk cores exposed to $MgCl_2$ at high pressures but no such creep trend was observed on the rest samples subjected to other test conditions. Accelerating creep has not been reported in previous experiments on chalk.

ACKNOWLEDGEMENT

My profound gratitude goes to my academic supervisor, Marete V. Madland whose guidance and care were enormous throughout the duration of this work.

The Ph.D. students, Edvard Omdal, Megawati Megawati and Bizhan Zangiabadi were of immense assistance in every aspect. I doubt if I could have done this work without their help.

The post-doctoral research staff, Reider Korsnes always came when it matters most, especially at “troubled times”.

I would also like to appreciate the wonderful assistance of all the other laboratory staff not mentioned here. Surely, I could not have had it better.

Stavanger, 15th June, 2009.

Chinweike Julius Mba

TABLE OF CONTENTS

LIST OF FIGURES

LIST OF TABLES

Chapter 1

INTRODUCTION

The experiments performed in this thesis are part of series of studies and research on the compaction/subsidence and borehole stability problems observed in North Sea chalk reservoir oil fields. Seawater is injected with great success into North Sea chalk reservoirs in order to improve oil recovery, but this seawater injection leads also to enhanced reservoir compaction and seabed subsidence. The experiments were therefore designed to understand the chemical interactions taking place between the chalk matrix and seawater, which leads to a mechanical weakening of the chalk. The fundamental objective is to understand the chemical effects from simple brines, mainly $MgCl_2$ and NaCl, which contains the same ions as seawater so that one can fully understand how seawater chemically effect chalk's mechanical strength. In addition, the influence of temperature and pore pressure in the presence of these brines was also considered to play a role in chalk weakening. Hence, the tests were designed to be carried out at initial in-situ reservoir temperature and pore pressure of Ekofisk chalk field. The in-situ conditions are 130^{o}C temperature and about 40MPa (400bar) pore pressure. However, results obtained from the first few tests prompted that similar tests be performed at low pore pressures. This is to enable comparison between results obtained at both pressures in the presence of the two brines.

A lot of time was spent in carrying out the experiments and several problems were encountered because of the high temperature and pressure conditions of the test. A procedure for the different phases of the test was developed. The test material used was chalk from the quarry of Stevns Klint outside Copenhagen in Denmark.

Prior to the tests it was believed that chalk cores exposed to $MgCl_2$ deform more than those flooded with NaCl. Results from the experiments in this thesis show otherwise, where NaCl causes significantly higher deformation of the chalk compared to $MgCl_2$. Also, previous laboratory experiments have not report accelerating creep on chalk. In some of the tests carried out in this thesis, "accelerating-like" creep were observed on chalk cores injected with $MgCl_2$ at 40MPa pore pressures and 12MPa effective stress, but no such creep was seen on cores flooded with NaCl at the same test pressure and temperature.

Chapter 2

THEORY

2.1 Carbonates

Carbonates are sedimentary rocks deposited in marine environments with clear, shallow, warm waters and are mostly of biological origin [Slb, 2007][2]. They make up 20-25% of all sedimentary rocks. About 50% of the world's proven petroleum reserves are preserved in carbonate formations [Roehl et al., 1985][1]. Carbonate rocks are divided into two main groups, limestone and dolomite. Limestone consists of 90% or more of pure calcite (CaCO3) while dolomite consists of about 90% dolomite ($C_aM_g(CO_3)_2$) [Korsnes, 2007][4].

Chalk is a limestone that has maintained its biogenic origin. The particles of chalk originate as skeletons of algae called coccospheres which are approximately 30μm in diameter. The coccospheres constitute of coccoliths which are assemblages of rings made up of calcite plates with a diameter of 0.5 to 2.5μm. In addition to calcite, chalks also contain silica and clay minerals [Fjaer et al.,1992].

Hydrocarbons have been found in chalks in several oil producing regions of the world. Chalks have three main characteristics that interact to differentiate their behaviour from most reservoir rocks. These properties include high porosity, low permeability and soft matrix. The porosity for productive chalk sediments ranges from 30 to 50%. Effects of burial and pore-water chemistry can reduce this porosity to less than 1% [Blanton, 1981][6]. During sediment burying, the low permeability chalk and overlying shale sediments made it difficult for pore fluid to drain the compacting chalk, which resulted in increased pore pressure. Early invasion of hydrocarbons and very low water saturations slowed down the diagenetic process and the high porosity was preserved.

Regardless of porosity, chalks have low permeabilities, usually around 1 to 3 milliDarcy. This is due to smallness of the grains, about 10μm in diameter. Chalk as a reservoir rock is often weak and soft. They are predominantly calcite, which has a hardness of 3 on Mohr's scale [Blanton, 1981][6]. The strength of chalk is determined primarily by the porosity and silica content [Da Silva et al., 1985][17]. But the mechanical properties of high porosity chalks are also strongly dependent on the type of fluid in the pores. Water saturated chalks are relatively weaker than oil saturated or dry chalks [Risnes et al., 2003][3]. This is often referred to as water weakening of chalk.

2.2 Concepts and Definitions

2.2.1 Porosity

The porosity of rock is the ratio of pore volume to the bulk volume of the rock. Mathematically it is defined as:

$$\Phi = V_p/V_b \qquad \text{---------- \{eq. 2.1\}}$$

Where

Φ = Porosity
V_p = Pore volume
V_b = bulk volume

Several factors affect the porosity of rocks. They include size and shape of grains, amount of cementing materials, compaction, uniformity of grain sizes and packing arrangement [Rai, 1998][26]. Porosity can be classified in three different types. The classification is based on the interconnection and communication between the pores.

• Effective porosity: This is the type of porosity where the pores are connected and are able to communicate with other pores. This is the type of porosity that is capable of yielding hydrocarbons.

• Ineffective porosity: The pores are closed and not connected to one another.

• Total porosity: The sum of effective and ineffective porosities.

In this thesis, the porosities used are effective porosities. They are calculated using:

$$\phi = \frac{W_s - W_d}{\rho_s V_p} \qquad \text{---------- \{eq. 2.2\}}$$

where

W_s = saturated weight
W_d = dry weight
ρ_s = density of saturating fluid
V_p = pore volume

2.2.2 Permeability

While porosity determines how much hydrocarbon is stored in the rock, permeability determines if the hydrocarbon can be produced. It is the ability of a rock to transmit fluids. Depending on the number of fluids that saturate a particular rock, permeability can be classified as absolute, effective and relative permeabilities.

Absolute permeability is when the rock is completely saturated with only one fluid while effective permeability is considered when there is more than one fluid

saturating the rock. Relative permeability is the ratio of the effective permeability of a rock to a particular fluid to the absolute permeability of the rock.

Permeability is calculated from Darcy's equation as shown in eq. 2.3:

$$K = \frac{q\mu\Delta L}{A\Delta P} \quad \text{---------- } \{2.3\}$$

where

K = permeability (D)
q = volumetric rate (cm3/s)
μ = fluid viscosity (cP)
ΔL = length of the core (cm)
A = cross sectional area (cm2)
ΔP = pressure drop over the core (atm)

2.2.3 Stress

When studying how materials behave under different loads, it is not only the magnitude of the forces that has to be evaluated. However, the surfaces upon which the forces act on need to be considered. This is because the size of the area upon which the force acts determines the stress. The mathematical definition of stress is as given in equation 2.4.

$$\sigma = F/A \quad \text{---------- } \{2.4\}$$

where

F = total force on one side of a surface area acting to balance all the forces on the opposite side
A = area across which the force acts

In addition to the size of the surface, the orientation of the cross-section relative to the direction of the acting force is also important. If the force acts normal to the surface of the cross-section, the resulting stress is referred to as normal stress. Shear stress results when the force acts along the plane of the cross-section.
In rock mechanics compressive stresses are usually defined as positive entities, while tensile stresses are negative.

2.2.4 Pore pressure

The pore fluid will carry part of the total stresses applied to a rock system, thus relieving the rock matrix from part of the load. Chalk reservoirs are usually under high pore pressures which results from three main causes [Fjaer et al.,1992][5];

• the rate of sedimentation and compaction being higher than the rate of fluid expulsion and migration.
• tectonic loading that leads to undrained shear stress with associated pore pressure development.

• pore fluid generation or expansion by thermal or chemical processes.

Knowledge of the pore pressure in the formation is very important when studying borehole stability during drilling, rock stability during production, and compaction/subsidence [Fjaer et al., 1992][5]. Experiments for this thesis were generally designed for high pore pressures. Results obtained from the first few tests prompted that similar tests be performed at low pore pressures. This is to enable comparison between results obtained at both pressures in the presence of different types of flooding fluids. It is part of series of studies and research on the compaction/subsidence and borehole stability problems observed in North Sea chalk fields.

2.2.5 Effective Stresses

Rocks are porous materials, which consists of a rock matrix and a fluid, which is usually under pressure [Aadnoy, 2003][9]. Assume a porous rock is sealed by a plate as shown in Fig 2.1.

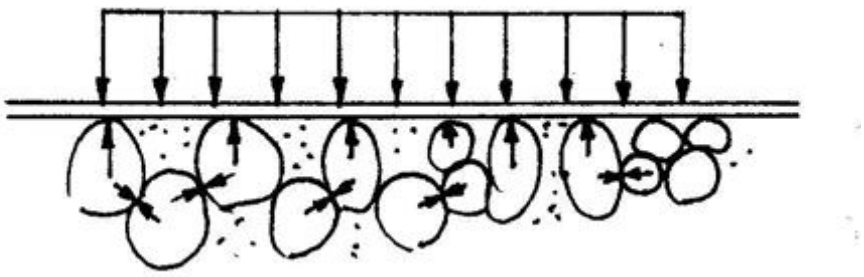

Fig. 2.1 A porous material sealed by a surface [Aadnoy, 2003]

On the outside of the plate is a stress, σ acting. In order for equilibrium to exist, this stress must be balanced by stresses inside the rock on the other side of the plate. Assume that the overburden stress, as an example, represents the total stress as shown in fig 2.1. Inside the rock, this stress is partially taken up by the pore pressure inside the fluid, P_o, and in the rock matrix, σ'. That is, the total stress is equal to the pore pressure plus the effective stress,

$$\sigma = \sigma' + P_o \quad \text{---------- } \{2.5\}.$$

Failure in porous, saturated and permeable rocks is in general governed by the effective stresses [Fjaer et al., 1992][5], which is given by

$$\sigma' = \sigma - P_o \quad \text{---------- } \{2.6\}.$$

2.2.6 Effective Stress Coefficient

The presence of pore fluid in the rock affects both the bulk material and the grains of the solid porous material. [Andersen, 1995][19]. Increasing the pore pressure results in

increase in bulk volume of the rock while the grains tend to be compressed. The bulk compressibility is often very large such that the effect of grain compressibility will be negligible. Introducing a correction factor called effective stress coefficient or Biot's coefficient, α takes care of these effects. This implies that the expression for effective stress changes to

$$\sigma' = \sigma - \alpha P_o \quad \text{---------- } \{2.7\}$$

$$\alpha = 1 - C_m/C_b \quad \text{---------- } \{2.8\}$$

$$= 1 - K_b/K_m \quad \text{---------- } \{2.9\}$$

where

C_m = matrix compressibility
C_b = bulk compressibility
K_b = bulk modulus
K_m = matrix modulus.

Generally, the effective stress coefficient is porosity dependent. It increases with porosity. Common values for chalk range from 0.8 to 1.0. For this thesis, the coefficient is taken to be 1.

2.2.7 Strain

When a body is being loaded the result is displacement or deformation [Aadnoy, 2003][9]. This means that a point on the body is being shifted to another position. Strain is dimensionless parameter; it is defined as deformation divided by a reference length. Mathematically, strain is expressed as

$$E = L_o - L/L_o \quad \text{---------- } \{2.10\}$$

where

L_o = reference length
L = new length after loading

2.2.8 Elastic moduli

The theory of linear elasticity deals with situations where there are linear relationships between applied stresses and the resulting strain [Fjaer et al., 1992][5]. These relationships can be expressed using a group of coefficients called elastic moduli. Some of these coefficients include:

• Young's Modulus, E: this is a measure of the stiffness of the sample under study, that is, the sample's resistance against being compressed by a uniaxial stress.

$$E = \sigma_x/\varepsilon_x \quad \text{---------- } \{2.11\}$$

where σ_x and ε_x are the applied stress and the resulting strain respectively.

• Poisson's ratio, v: is a measure of lateral expansion ε_y relative to axial contraction ε_x.

$$v = -\varepsilon_y/\varepsilon_x \text{ ---------- } \{2.12\}$$

• Shear modulus, G: also known as modulus of rigidity. It is a measure of the sample's resistance against shear deformation.

• Bulk modulus, K: this is a measure of the sample's resistance against hydrostatic compression. It is defined as the ratio of hydrostatic stress σ_p relative to the volumetric strain ε_{vol}.

$$K = \sigma_p/\varepsilon_{vol}. \text{ ---------- } \{2.13\}$$

2.3 Rock Strength and Failure mechanisms

When rock is subjected to sufficiently large stresses, a failure of some kind will occur [Fjaer et al., 1992][5]. Rock strength definition is usually a function of the test carried on the rock. The most important tests used to measure rock strength are the uniaxial and triaxial tests. Uniaxial compressive stress test is when the test is performed with zero confining stress while triaxial test is carried out under non- zero confining stress.

Some basic strength regions in a typical uniaxial stress test are as shown in fig. 2.1.

• Elastic region: the rock deforms elastically and the sample returns to its original state if the stress is released.

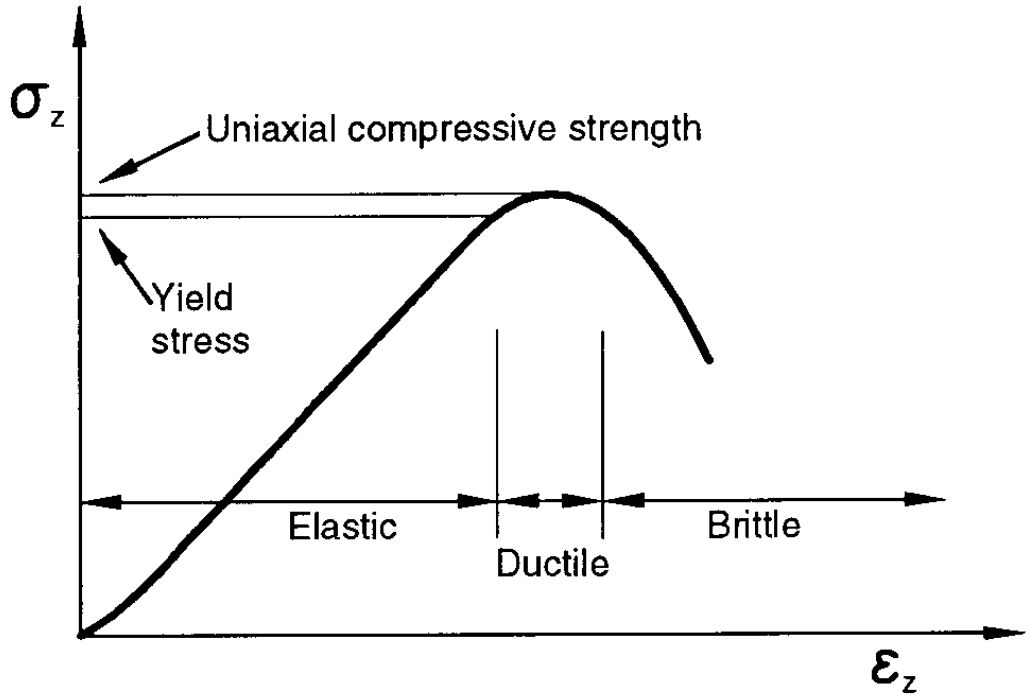

Fig. 2.2 Stress versus deformation in a uniaxial compression test [Fjaer et al., 1992][5]

• Yield point: a point beyond which permanent changes will occur. The sample will no longer return to its original state upon removal of stress.

• Uniaxial compression strength: the peak stress.

• Ductile region: a region in which the sample undergoes permanent deformation without loosing the ability to support load.

• Brittle region: a region in which the sample's ability to withstand stress decreases rapidly as deformation is increased.

A triaxial test is usually performed by increasing the axial and confining loads simultaneously, until a prescribed hydrostatic stress level is reached. Then, the confining pressure is kept constant while the axial load is increased until failure occurs. The most common mode of failure observed in uniaxial and triaxial tests is shear failure. This failure mode is caused by excessive shear stress. Another failure mode is tensile failure, which occurs when the external stresses exceed the tensile strength of the sample. Yield is a type of failure that occurs when there is excess average stress acting on the sample. This failure occurs throughout the material as a breakdown in the structure. This type of failure is also referred to as pore collapse.

Experiments performed in this thesis were hydrostatic tests, such that yield failures are the ones of major interest. A typical volumetric strain versus isotropic stress curve is shown in figure 2.2 [Dahou et al., 1995][11]. Three important phases on the curve are highlighted below:

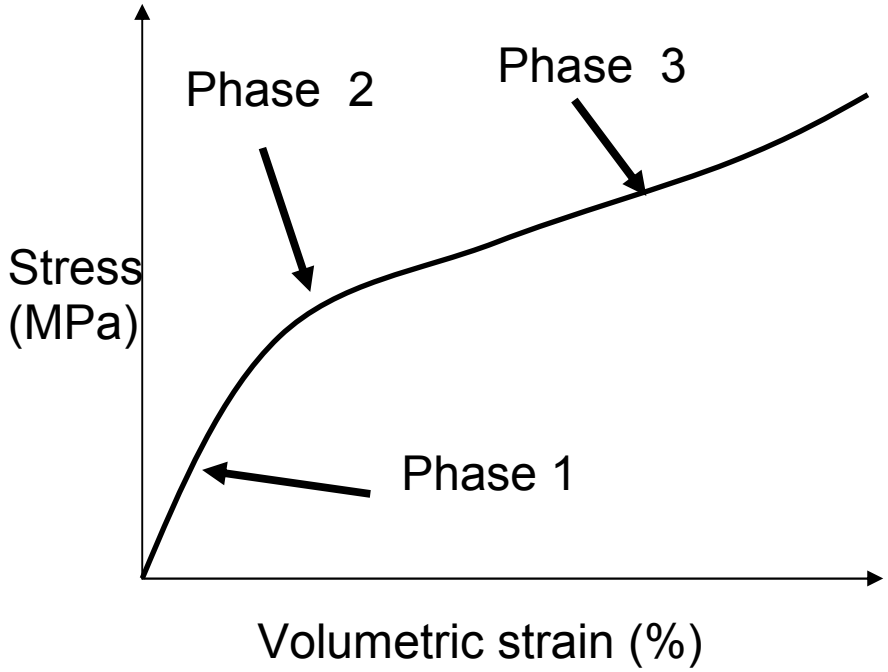

Fig 2.3 Stress-strain curve for chalk in hydrostatic compression

Phase 1: in this region, the chalk response is quite linear and elastic. The volumetric strain is mainly due to the elastic compressibility of the pore system.

Phase 2: the chalk response becomes non – linear with a rapid increase of plastic volumetric strain. This is due to progressive pore collapse by destruction of links between grains.

Phase 3: the plastic strain rate begins to decreases progressively. This is related to decrease of contact surface between grains after a phase of strong pore collapse. This phase is referred to as strain hardening.

2.4 Creep

Creep is a time dependent behaviour. It is deformation that occurs in materials exposed to constant stress and temperature. Creep phenomenon is generally classified into three stages as shown in figure 2.3 [Fjaer et al., 1992][5].

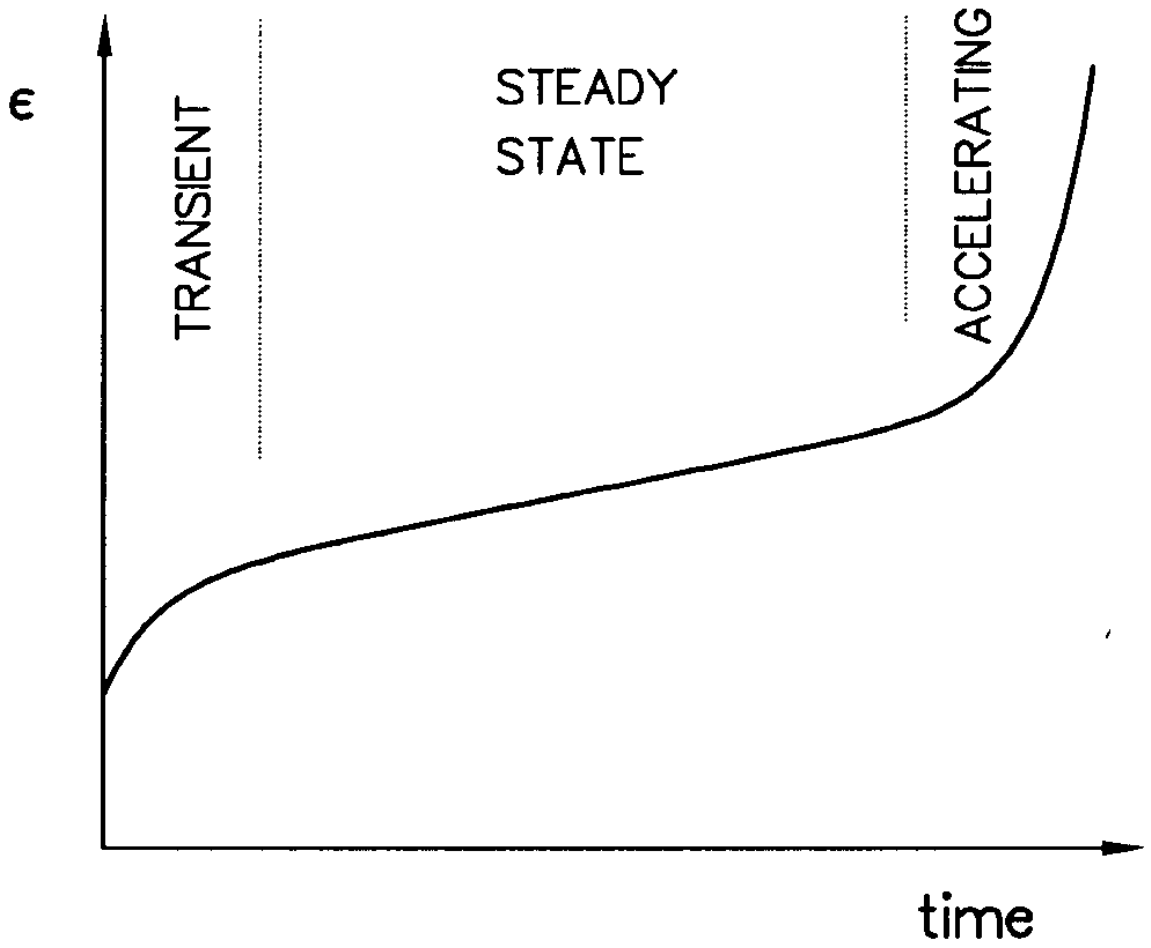

Fig.2.4 Strain versus time for a creeping material

♦ Transient creep (primary creep): this is a region where the rate of time-dependent deformation decreases with time. The deformation during this stage decreases to zero if the applied stress is completely removed.

♦ Steady state creep (secondary creep): The rate of deformation during this stage is constant. If the applied stress is reduced to zero during this stage, the deformation will still exist. This implies that the material is permanently deformed at this stage.

♦ Accelerating creep (tertiary creep): The deformation rate increases with time during this stage, which rapidly leads to failure.

Earlier works on chalk have not reported accelerating creep behaviour, but laboratory experiments carried out in this thesis show significant "accelerating-like" creep on some of the chalk samples tested. This will be presented in chapters 4 and 5.

2.5 Chalk-fluid interactions

Generally, the mechanical strength of chalk depends first on porosity and silica content [Da Silva et al., 1985][17]. The type of fluids present in the pores of high

porosity chalks also determines their mechanical properties. Dry or air saturated chalk is strongest compared to chalk saturated with oil/glycol, while water saturated chalk is the weakest [Risnes et al., 2003][13]. This phenomenon is severally referred to as water weakening of chalk.
Water weakening effect on chalk has caused increased compaction and subsidence in chalk reservoirs flooded with sea water, an example is the Ekofisk field in southern North Sea.

Studies have shown that rock mechanical strength depends on the chemical composition of the saturating and flooding fluids. With regards to hydrostatic yield strength and deformation during creep, chalks exposed to sea water are significantly weaker than those exposed to distilled water [Korsnes, 2007][4]. The overall mechanisms behind the water weakening effect are still not fully understood. Thus far, three different mechanisms have been proposed. They include:

a) physical mechanisms
b) physio-chemical mechanisms
c) chemical mechanisms.

2.5.1 Physical mechanisms

The mechanical strength of chalk has often been related to capillary forces which induce cohesion between chalk grains. Capillary forces occur at the grain surface when contacted by water, which is usually the wetting phase, and between water and non-wetting phase, oil or gas [Korsnes, 2007][4]. These capillary forces tend to pull the grains together, with a consequent increase in cohesive strength. Several researchers have, however, argued that if capillary effects were the main causes of weakening, then dry chalk should therefore be weak. Studies by Risnes [2000][8] shows that dry chalks are actually stronger than water saturated chalks. This led to the belief that capillary forces may be of less significance in causing weakening of chalks, rather other possible mechanisms such as rapid chemical mechanisms could be of more importance [Korsnes, 2007][4].

2.5.2 Physio-chemical mechanisms

Several physio-chemical mechanisms on water weakening of chalk have been proposed. Some of these mechanisms include repulsive forces due to adsorbed dipole layers, van der Waals attractive forces and electrical surface charge [Risnes et al., 2004] [13]. It was concluded that none of these forces were strong enough to cause water weakening of chalk. The new mechanism in terms of physio-chemical effect as proposed by Risnes et al., 2003 is on the activity of fluid on chalk. It was suggested that the added adsorption pressure on chalk grains could contribute to the water weakening effect. The adsorption pressure will act like an increase in the pore pressure, thereby reducing the cohesive strength of chalk.

2.5.3 Chemical mechanisms

The low solubility of chalk ($CaCO_3$) in water has hindered vigorous studies on water weakening of chalk from pure chemical point of view [Madland, 2005][3]. Irrespective of this hindrance, several researchers have suggested different chemical mechanisms that cause weakening of chalk. They include grain to grain dissolution, pressure solution, precipitation, substitution and recrystallization.

Newman in 1983 [18] concluded that compaction is attributed to mechanical failure by dissolution and pressure solution at high stresses. This conclusion was based on experiment carried out on oil saturated cores flooded with equilibrium brine and non equilibrium sea water. The sea water enhanced compaction while the equilibrium brine did not.

Another chemical mechanism as proposed by Hellman et al., 2000, Bjølykke & Høeg, 1997 [16, 20] is pressure solution. An increased stress on chalk grains enhances the solubility of calcite in water. Pressure solution creep in chalk under different stresses as investigated by Hellman et al., 2002 [21] shows that long term creep behaviour seemed to be caused by pressure solution.

The weakening of chalk in terms of chemical dissolution/precipitation was investigated by Heggheim et al., 2005 [22]. The experiment involved aging chalk cores at 130^{o}C in Ekofisk formation brine or modified seawater with four times the concentration of sulphate. The increase in sulphate concentration was to enhance the dissolution by precipitating Ca^{2+} as $CaCO_{3(s)}$. Cores aged in Ekofisk formation brine were relatively stronger than the ones aged in modified sea water.

The impact of certain sea water ions on mechanical strength of high porosity chalks is documented in the studies by Korsnes et al., 2006 [14]. Sea water contain potential determining ions (Ca^{2+}, Mg^{2+}, SO_4^{2-}) which have great impact on the surface chemistry of chalk, especially at high temperatures. The experiment involved hydrostatic and creep tests at different temperatures, using distilled water, synthetic sea water with SO_4^{2-} and synthetic sea water without SO_4^{2-} as flooding fluids. The main conclusions from the experiments were that Ca^{2+} has higher affinity to chalk surface than Mg^{2+} at room temperatures, while at higher temperatures Mg^{2+} will be able to substitute Ca^{2+} from the chalk surface in the presence of SO_4^{2-}. They finally suggested a model to explain the chemical interaction between the intergrain contacts and sea water as enumerated below:

• The presence of strong positive ions (Ca^{2+}, Mg^{2+}) in the aqueous phase will make the chalk surface to be positively charged.
•The positively charged surface will repel the positive ions in the fluid and prevent them to interact with the chalk.
•The presence of SO_4^{2-} which is negatively charged will decrease the surface charge of the chalk, which then allows the positive ions to react with the chalk.
•Mg^{2+} will be able to move into the intergrain contacts and form ion-pair with SO_4^{2-} while substituting Ca^{2+}.
• Thus, SO_4^{2-} acts as a catalyst for the substitution of Ca^{2+} by Mg^{2+} at the grain contacts.

• *The different size of Ca^{2+} and Mg^{2+} cause stress on the chalk surface at the grain contacts, and the mechanical strength of chalk is decreased [Austad et al., 1997]*[15].

Recent studies by Madland et al., 2009 [12] on Kansas chalk showed enhanced weakening when seawater without magnesium was flooded through the cores at 90°C. They therefore suggested that other possible mechanisms such as surface charge and dissolution could be responsible for the weakening. Their argument was based on the fact that since magnesium was not present in the flooded brine there will be no substitution of Ca^{2+} by Mg^{2+} on the chalk. In order to investigate the effect of individual ions in the flooded fluid, they carried out hydrostatic and creep tests, chemical analysis of sampled effluent and mathematical modelling to account for transport and precipitation/dissolution effects. The chalk cores were exposed to different brines such as synthetic seawater (SSW), $MgCl_2$, NaCl and distilled water (DW).

The main conclusion from recent studies by Madland et al., 2009 were that the presence of only magnesium in the injected brine makes the chalk deform similarly as when exposed to seawater. Similar behaviour was also observed on chalk flooded with NaCl and DW within the creep phase. They submitted that substitution may not be the full explanation for chalk deformation. This was based on the fact that analysis of the effluent showed a huge reduction in concentration of Mg^{2+} compared to concentration in the original brine, while the concentration of Ca^{2+} increased tremendously. Hence the amount of magnesium lost inside the core was too much in order to be a consequence of substitution alone. Equilibrium calculation showed that magnesium lost inside the core was precipitated as part of a mineral. Precipitation of this mineral (Huntite, $CaMg_3(CO_3)_4$) lead to a significant dissolution which could explain the enhanced chemical compaction taking place.

Chapter 3

EXPERIMENTAL

The main objective of this work is to study the mechanical strength of chalk in relation to chemical interactions between chalk and some seawater ions at high pore pressures and high temperature. The pressure and temperature values are those of Ekofisk chalk field on the Norwegian sector of the North Sea. They are 40MPa (400bar) initial pore pressure and 130^{o}C. Further tests were also performed at low pore pressures so as to compare with the results obtained at high pressures. The chalk cores were subjected to hydrostatic loading and allowed to creep for days, followed by chemical analysis of effluent samples of the flooded fluid. In order to attain these objectives, each of the tests undergoes four main stages for the high pressure tests and three stages for the low pressure tests. These phases include:

A. High pressure tests

1. Initial pressure build-up phase: this phase involves installing the core sample in a triaxial cell; build initial pressures, 1.4MPa confining pressure and 0.7MPa pore pressure. Clean the core sample by flooding with distilled water, and heat up the cell to 130^{o}C with a heating jacket element. A pressure relief valve was used to remove excess fluid pressure during the heating so that a confining pressure of 1.4MPa is maintained.

2. Pressure ramping phase: This entails ramping confining and pore pressures simultaneously to 41MPa and 40MPa respectively. This was achieved by controlling the flow rates and applying high pressure on the gas side of a Back Pressure Regulator (BPR). The process of ramping was done by keeping a pressure window (effective stress) of 0.7MPa to 0.9Mpa between the confining and pore pressures. Ramping time depends on the pore and confining flow rates used, but care was taken in order to keep within the above pressure window. This is because a higher pressure window will introduce a high and non-uniform effective stress, thereby loading the sample before the required phase. Lower pressure window could, on the other hand cause leakage through the sleeve (if the pore pressure becomes higher than the confining pressure). Ramping at 0.5ml/min on the confining flow rate and 0.025ml/min on the pore flow rate could take as much as 12hours. After attaining these maximum pressures, flooding with the respective brines begins so as to saturate the sample with brine before the loading phase. Brine flooding is followed by effluent sampling of the flooded fluid.

3. Hydrostatic loading phase: The samples were hydrostatically loaded to 12MPa effective stress. This was achieved by keeping the pore pressure constant at 40MPa while increasing the confining pressure to 52MPa by using a constant confining flow rate of 0.05ml/min. A constant pore pressure was maintained by using a back pressure regulator (BPR). After attaining the maximum

confining pressure, the sample was allowed to creep for days. Effluent sampling of the flooded fluid is continued during creep period.

4. Chemical analysis of sampled effluent using Ion Chromatography (IC) machine.

B. **Low pressure tests**.

The procedures for the tests performed at low pressures are basically the same as in high pressure tests, except that in low pressure tests there was no ramping of pressures. Pressure values used were 0.7MPa pore pressure and 1.4MPa confining pressure during the initial pressure build-up, and the samples were hydrostatically loaded to 12MPa effective stress followed by the creep phase.

Flooding brines used in the experiment were 0.219M $MgCl_2$ and 0.657M NaCl, which are of the same ionic strength as in seawater.

3.1 Sample material

Core materials from chalk reservoirs are usually in limited supply. The presence of chalk formations in several places in Europe makes it possible to find outcrop chalks with properties similar to that of reservoir chalks [Madland, 2005]. High porosity outcrop chalk was used in the experimental work, and it came from the quarry of Stevns Klint near Copenhagen in Denmark. It is of Maastrichtian age and has low silica content. The general properties of the chalk used are shown below:

Age	Maastrichtian
Porosity	39 – 43 % (typical values are 48%)
Silica content	< 2WT%
Permeability	3 – 5mD

3.2 Sample preparation

3.2.1 Drilling

Chalk block as obtained from the quarry is drilled with a laboratory coring machine. The machine uses an oversize coring bit of about 42mm diameter with circulating water as the cooling fluid.

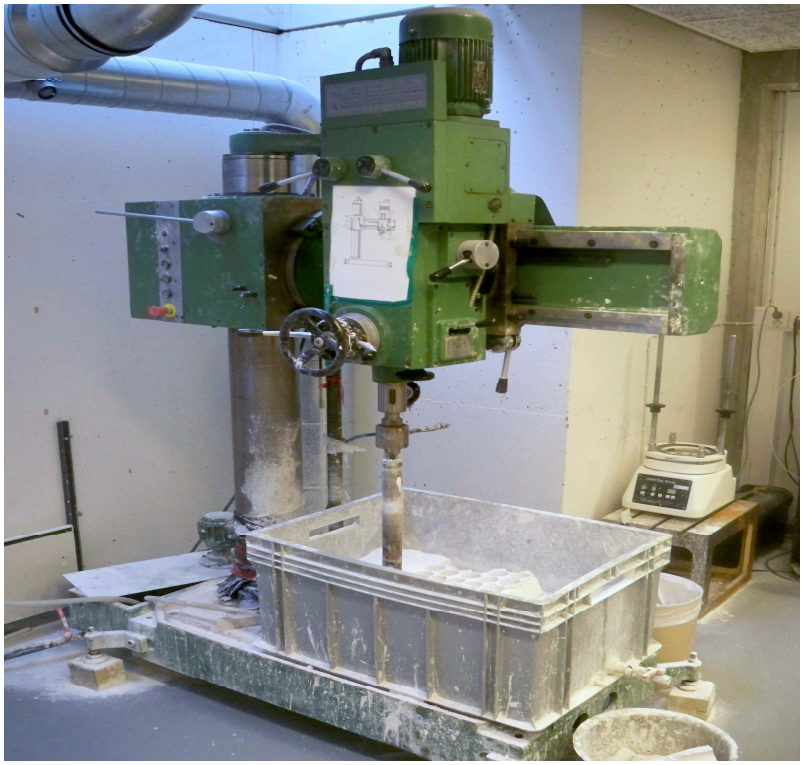

Fig.3.1.The coring machine

3.2.2 Drying

The drilled cores were dried for about 24hours in a heating oven at a temperature of 110^{o}C – 120^{o}C.

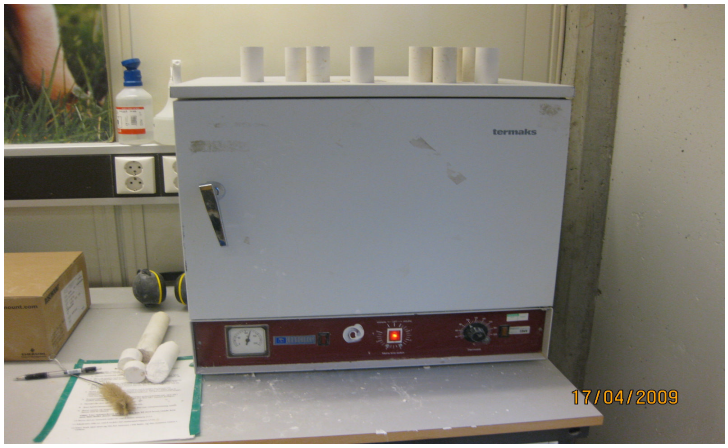

Fig.3.2 The heating cabinet

3.2.3 Shaping

The samples were shaped in a lathe machine (fig. 3.3) to the appropriate diameter. For the purpose of this work, the cores were shaped to a diameter of 38.1mm.

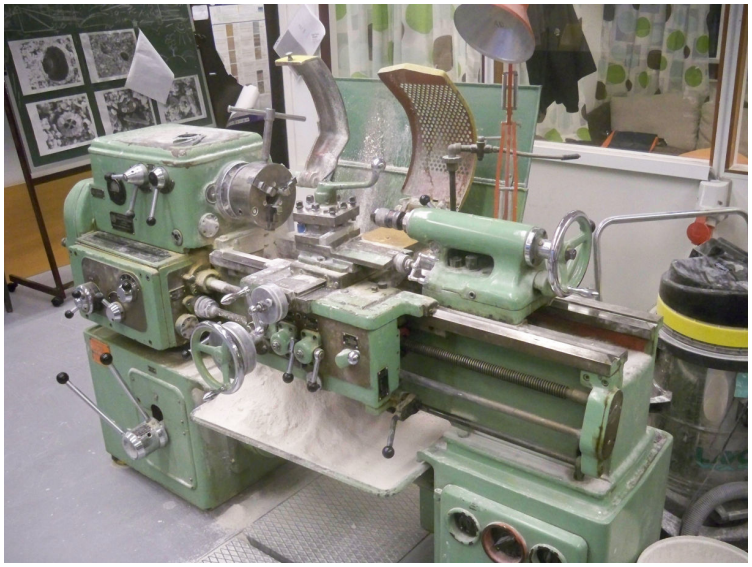

Fig.3.3 The lathe

3.2.4 Cutting

A diamond saw cutting machine was used to cut the chalk samples to the desired length of approximately 80mm, which is the required length for the test cell used. The samples were further dried in the heating cabinet for at least 24 hours.

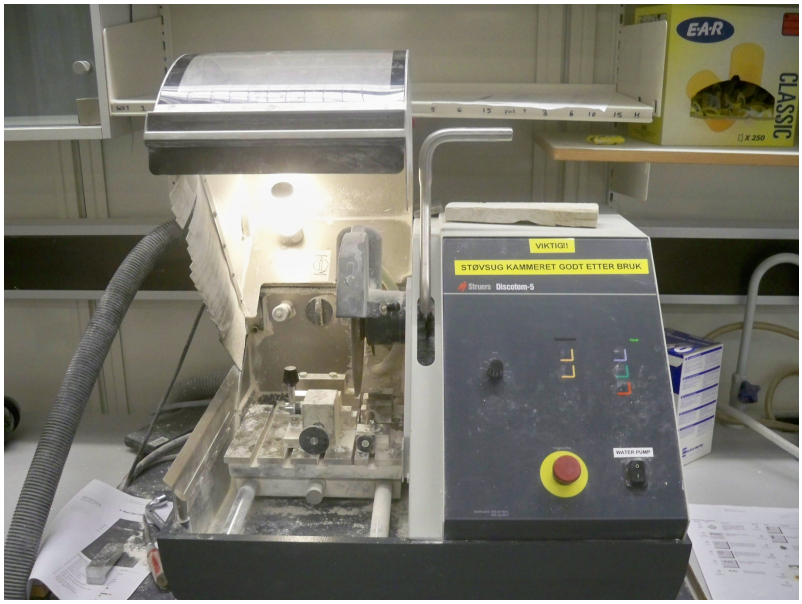

Fig. 3.4 Diamond saw

3.2.5 Saturation and porosity determination

The dry weights of the samples were measured and the dried samples placed in glass container connected to a vacuum pump (fig. 3.5). The vacuum pump is also connected to a distilled water storage unit through the glass container. On attaining the required vacuum (when all the air inside the samples must have been evacuated), the samples were saturated with distilled water. Finally the saturated weights were measured and these values were used to determine the porosity.

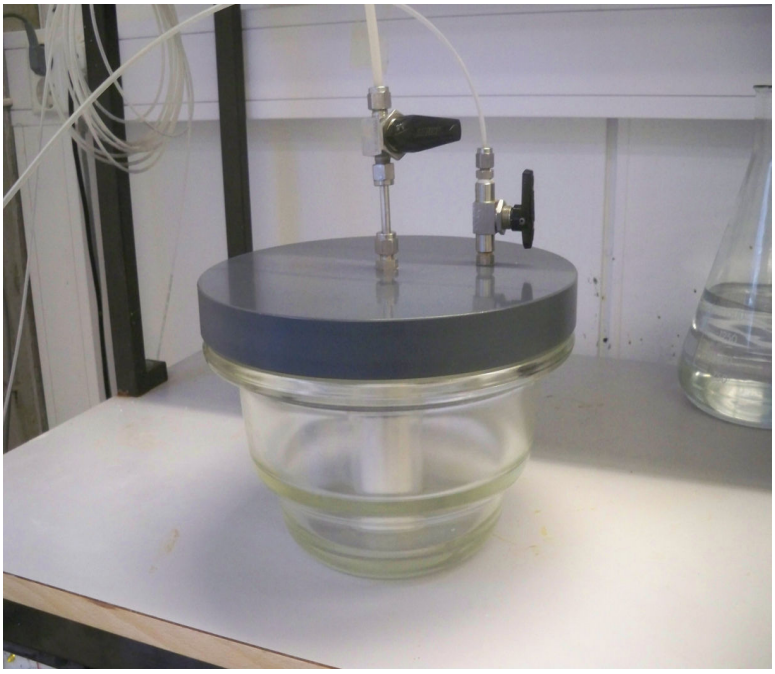

Fig. 3.5 vacuum container

3.3 Test Equipment

3.3.1 The triaxial cell

The test cell used for the experiments is designed for cylindrical samples with diameter of about 38mm and length close to 80mm. The sample is placed inside a transparent shrinking sleeve and mounted in the lower part of the cell. External stresses on the sample are provided by two high pressure piston pumps, one for the confining pressure and the other for axial pressure. The pumps are of Gilson types. For the purpose of this work, the pumps are defined as pump 1 for the axial and pump 2 for the confining. The pumps are controlled by adjusting the flow rates of fluid either directly from the pump system or from the computer software. The computer software used for the experiment is called Lab View. It was used to control the test set up and for real-time data logging.

A steel cylinder within the middle chamber houses the hydraulic oil which applies the confining pressure. An external Linear Voltage Displacement Transducer (LVDT)

connected to the piston on the upper chamber measures the axial deformation. The cell has no facility to measure lateral displacement of the sample.

There are also two high pressure pumps connected to the pore pressure line, one upstream and the other downstream. The pump connected upstream to the pore pressure line is defined as pump 3. A hole in the upper part in the bottom chamber allows the sample to be flooded with the desired fluid. The down stream pump serves as a back pressure regulator, which allows the system to carry out tests at high pore pressures. A special heating system connected to the steel confining chamber allows the cell to be heated to the desired temperature of 130^{o}C.

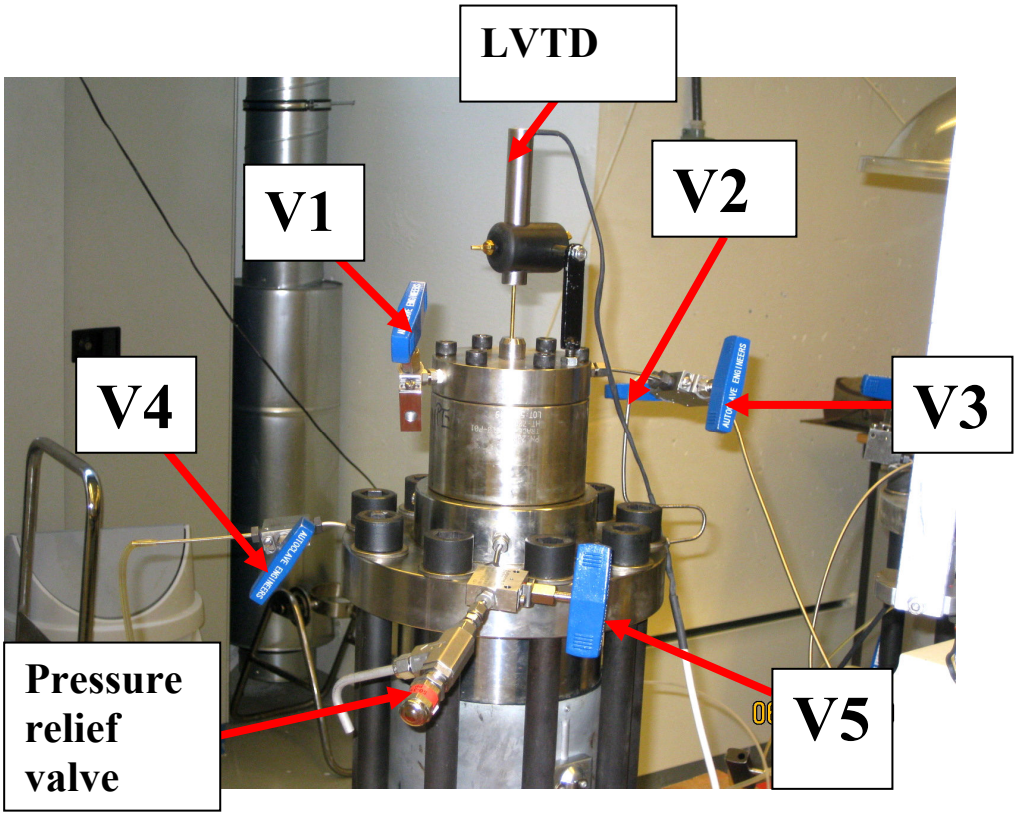

Fig. 3.6 The triaxial cell showing the main valves

3.3.2 The Back Pressure Regulator (BPR)

The BPR is connected to the downstream pump of the pore pressure line in order to support and control pore pressure from the back side. It consists of a two-steel cylinder (fig. 3.7), with one end connected to the pore pressure line and the other end to a pump. Inside the BPR is a steel plate (fig. 3.8) of about 39mm which balances the fluid pressure from both sides of the pump and the pore pressure line.

Usually, the BPR is set to a certain pressure limit which corresponds to the required pore fluid pressure. Whenever the pore pressure exceeds the set pressure on the BPR, the excess fluid will be expelled through a hole inside the pore pressure side of the

BPR. This is made possible by the steel plate inside the BPR. The steel plate tends to push back any excess fluid pressure from the pore pressure line. The excess fluid is thus expelled and the pore pressure is maintained at the set limit. In the first few experiments performed, a Gilson pump was used for the BPR. The Gilson pump can only receive fluid from the reservoir and deliver to the system, but it cannot receive fluid from the system. This and other limitations of the Gilson pump gave some problems, such as fluctuating pore pressure (as explained in section 3.6.2) during the experiments. As a result of potential problems posed by the Gilson pump, an ISCO pump was later used. The ISCO pump was able to maintain a constant pressure because of its ability to deliver to and receive fluid from the system.

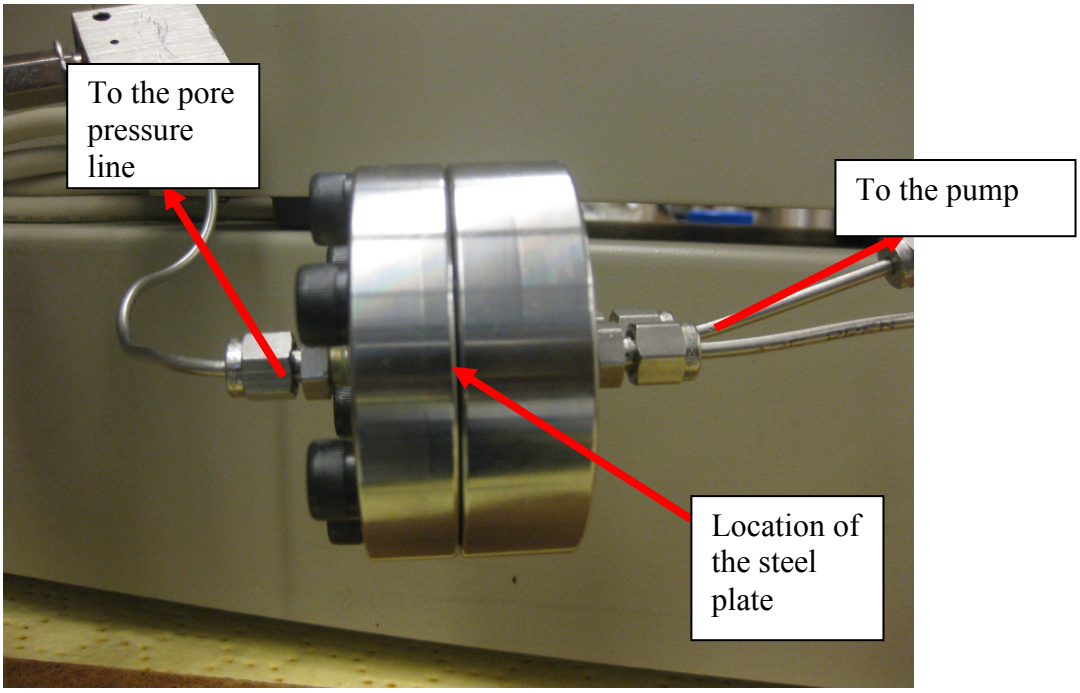

Fig. 3.7 The BPR

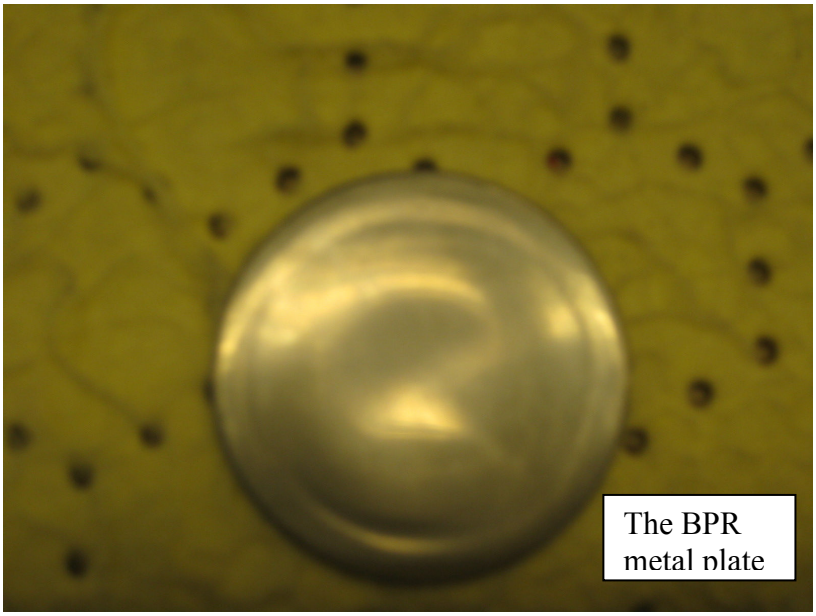

Fig. 3.8 The metal plate used inside the BPR

3.3.3 The flooding cell

A flooding cell was used to flood the respective brines during the experiment (fig. 3.9). The cell has two chambers separated by a piston. The lower chamber is filled with brine while distilled water is pumped into the upper chamber from pump 3. This is to ensure that brine continuously flow out of the lower chamber when needed, into the flooding circuit.

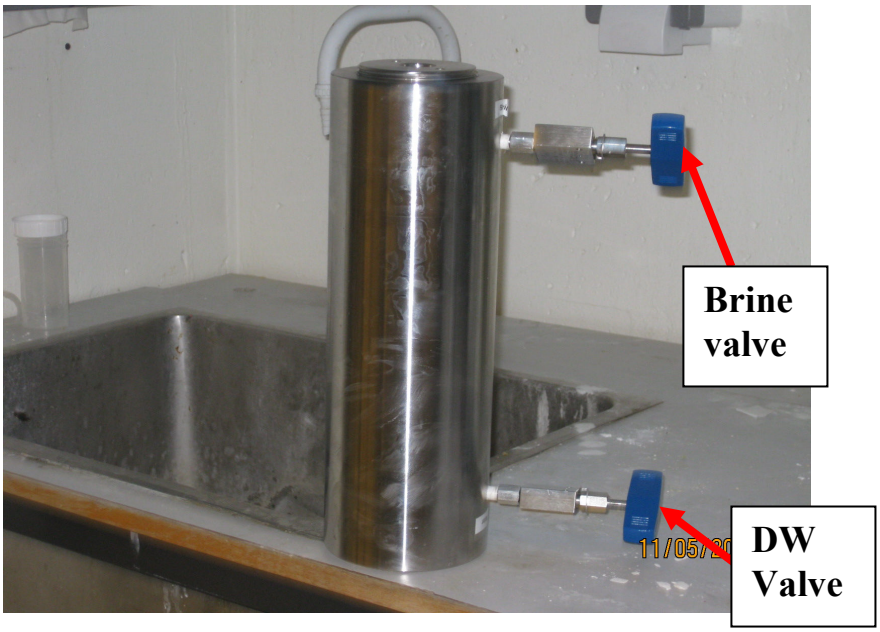

Fig. 3.9 The flooding cell

3.3.4 Gauges

There were four external pressure gauges and one temperature gauge used in the experiment. The gauges read real time pressures and temperature during the experiments. The pressure gauges include:

- the pore pressure gauge
- the differential pressure gauge, which measures the pressure difference between the top and bottom of the sample
- the axial pressure gauge which measures the pressure of the axial piston
- the confining pressure gauge.

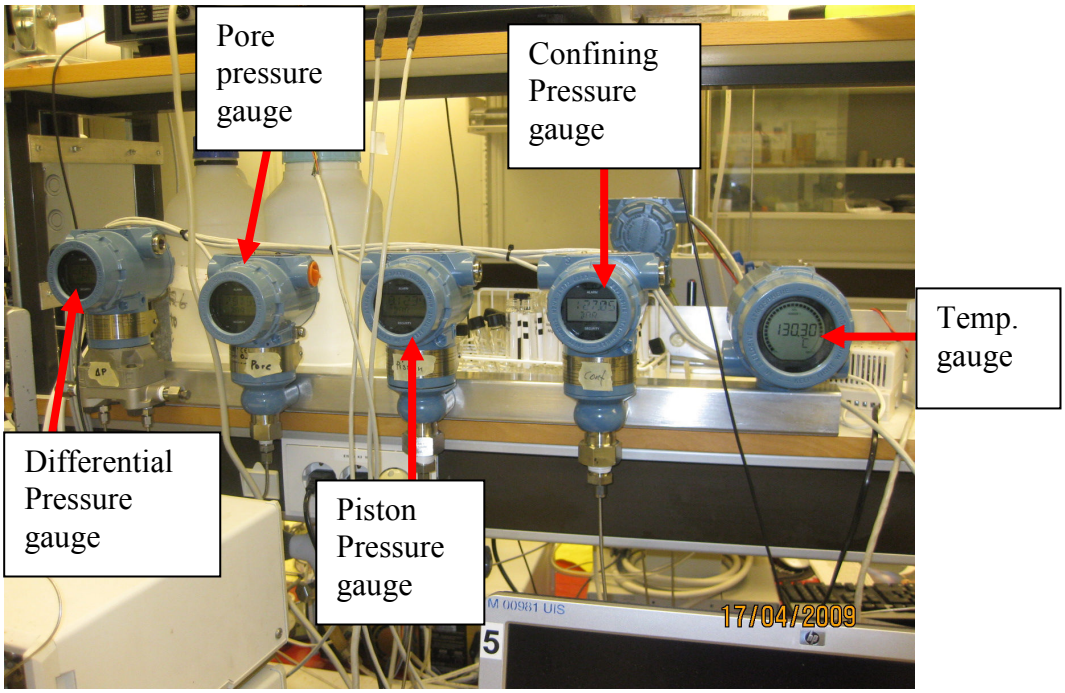

Fig. 3.10 Pressure & temperature gauges

3.4 Experimental setup: mounting procedure

3.4.1 Triaxial cell

1. Place two rubber-rings at the top and bottom parts of the core plug.
2. In order to prevent chalk particles into the flow line, place two filters at both ends of the plug.
3. Place the sample inside a transparent shrinking sleeve.
4. Install the sample and sleeve on the lower part of the cell.
5. Heat the sample using a heating gun. This is to ensure the sample is tightly fitted into the sleeve to prevent communication between confining and pore fluid.

6. Install the steel cylinder of the middle chamber and fill-up with confining oil. The steel cylinder has the heating element attached to it. The heating element heats up the cell to the required temperature of 130^{o}C. Before pouring the hydraulic oil, ensure the outlet valve for the confining oil is closed.
7. Install the upper part of the cell. Before doing this, ensure the axial piston is fully raised and the confining valve opened in order to expel any air inside the confining chamber.
8. Fasten the different parts of the cell with bolts.
9. Install the external axial LVDT on top of the upper part of the cell. The axial displacement rod should be free to move so that it can follow the displacement of the piston.

3.4.2 Refilling the flooding cell

1. Close the valves connecting the brine and DW chambers to the circuit.
2. Disconnect the cell from the main system.
3. Place the cell in reverse position, that is, the DW chamber should be down and the brine chamber up.
4. Connect compressed air pipe to the brine side if the valves. The essence of this is to flush out the DW and to push the piston down to the DW side of the cell.
5. Remove the end seal and threaded cap from the top of the cell, using the special tools meant for this purpose. See fig. 3.11.
6. Clean the cell and rinse with the brine to be used.
7. Fill cell with brine and replace end seal and threaded end-cap. Ensure that no air was locked by tilting the cell when replacing the seal and end-cap.
8. Replace the cell to the system, with the DW end on top and the brine chamber down.

Fig. 3.11 Tools for removing end seal and end cap

3.5 Test procedure

As mentioned earlier, there were four main phases in each of the samples tested. The test procedure for each of the samples will be discussed under the following:

- Initial pressure build-up, 1.4MPa on confining and 0.7MPa pore pressures, followed by cleaning with distilled water (DW)
- Ramping confining and pore pressures by rate control to 41MPa confining and 40MPa pore pressures.
- Hydrostatic loading to 12MPa effective stress, followed by creep.
- Chemical analysis of fractioned effluent.

As explained in section 3.0, there was no ramping of pressures for the low pressure tests. For the purpose of this thesis, the pressures and flow rates on the different pumps will be defined as follows:

- Axial pressure in pump 1 = P1
- Confining pressure in pump 2 = P2
- Pore pressure in pump 3 = P3
- BPR pump = P4
- Flow rate in pump 1 = Q1
- Flow rate in pump 2 = Q2
- Flow rate in pump 3 = Q3

3.5.1 Initial pressure build-up and cleaning with distilled water (DW)

1. Install sample in triaxial cell
2. Start the computer programme and identify the sample with a name
3. Set Q2 to 2ml/min
4. Set maximum P2 to 0.7MPa.

In order to ensure that no air is trapped inside the confining chamber, open the confining valve (V5). Dripping of oil through the valve signifies air removal.

5. Close the confining valve (V5) when all air must have been evacuated.
6. Observe the plot of confining pressure (y – axis) versus time (x – axis)
7. Set x and y – axis on auto scale
8. When the confining pressure gets to 0.7MPa, begin to build pore pressure
9. Set Q3 to 0.25ml/min
10. Set maximum P3 to 0.7MPa
11. Set P4 (BPR) to 0.7Mpa
12. Increase maximum P2 to 1.4MPa.
13. Observe plot of confining pressure (y – axis) versus pore pressure (x – axis)
14. Build P2 and P3 simultaneously to 1.4MPa and 0.7MPa respectively, keeping effective stress of about 0.7MPa. This is achieved by adjusting Q2 and Q3. If P3 exceeds 0.7MPa, there should be dripping of water from the rubber hose connected to the BPR. In this way, the excess pressure is bled-off and P3 is restored to 0.7MPa.
15. Switch on the heating device so as to increase the cell temperature.

16. Connect a Pressure Relief Valve on the confining valve (V5). The need for this valve is to expel any excess confining oil that may increase P2 when the oil expands with increasing temperature.
17. When the temperature gets to 130^{o}C, adjust the Pressure Relief Valve until P2 stabilizes at 1.4MPa.
18. Leave the whole set up for about 24hours. In this way, the sample is cleaned with DW within this period.

3.5.2 Ramping confining and pore pressures, followed by brine flooding

1. Set maximum P3 to 40MPa
2. Set maximum P2 to 41MPa
3. Set P4 (BPR) to 40MPa
4. Set Q3 to 0.05ml/min
5. Set Q2 to 0.5ml/min
6. Build P2 and P3 simultaneously to 41MPa and 40MPa respectively, keeping effective stress of about 0.7MPa. This is achieved by adjusting the Q2 and Q3.
7. When maximum P2 and P3 are attained, begin to flood with brine by opening the brine valve and closing the DW valve.
8. Begin to take effluent samples using the sampling bottle.
9. Begin to lower the piston by:

- close valves V1 and V2
- open valves V3 and V4.
- Set maximum P1 to 0.85MPa
- Set Q1 to 0.05ml/min.

10. Leave the whole set up for about 24hours.

For low pressure tests, maximum P1 should be set to about 0.3MPa when lowering the piston. This is because the friction encountered during low pressure tests is small compared to high pressure tests. Also the reason for lowering the piston after pressure ramping is to ensure the piston has landed on the core before hydrostatic loading.

3.5.3 Hydrostatic loading and creep phase

1. Set Q2 to 0.05ml/min
2. Set maximum P2 to 52MPa (i.e. 12MPa effective stress)
3. Observe plot of confining pressure (y – axis) versus axial movement (x – axis).A linear increase in confining pressure with axial movement signifies the piston is moving down as required.
4. In order to overcome friction against the piston, increase maximum P1 to between 1.1 to 1.5MPa in steps of 0.5MPa.
5. When maximum P2 of 52MPa is attained, set Q2 to 0.5ml/min
6. Observe plot of axial movement (y – axis) versus time (x – axis)

7. Allow the sample to creep for days, while taking effluent samples at least ones everyday.

3.5.4 Stop test and dismantle

1. At the end of creep period, close the brine valve and open the DW valve
   Set Q3 to 0.1ml/min for about 160minutes
2. Switch off the temperature
3. Raise the piston by:
- open valves V1 and V2
- close valves V3 and V4
4. Gradually reduce P2 and P3 to zero and P4 to about 0.7MPa
5. Dismantle cell

3.5.5 Chemical analysis of effluent samples

Analysis of the effluents sampled during brine flooding is done using Ion Chromatography (IC) machine.

1. Dilute samples to 50 times lower than the original concentration using a dilution machine.
2. 2ml of samples are put inside the tray and analysed by IC. This is done by:
- Prime both pumps (at cation and anion sides)
- Increase the pump pressure stepwise by changing the flow rates from 0.2 – 1ml/min.
- Then IC is ready
3. Run the measurement

Processing time for cation is about 30min and anion is 20min.

3.6 Problems encountered

Several problems were encountered in the course of performing the experiments. These problems resulted in delays and failures of several tests after few days. Some of these problems are highlighted below.

3.6.1 Leakages

This was one of the greatest challenges during the tests. Leakages occurred through the sleeve inside the triaxial cell, resulting in invading of confining oil to the sample. There was also, occasional leakage of the flooding cell and leakage through the couplings connecting the numerous flow lines. These leakage problems were mainly attributed to the high temperature and pressure conditions the tests were subjected to.

3.6.2 BPR problems

The BPR normally uses a plastic or aluminium plate which helps to regulate the pore pressure. It was earlier anticipated that this plate could not withstand the test pressure, hence a steel plate was used and it functioned quite well. The steel plate was machined from the mechanical workshop in University of Stavanger.

During the first few tests, a Gilson pump was used for the BPR. The Gilson pump uses hydraulic oil supplied from an external reservoir. It was observed that pore pressures were higher and steady at night, but reduces below set limits during the day. It happened that at night, the room temperature was high and steady. Therefore the reservoir oil expands and more oil was pumped into the Gilson pump, thereby keeping the BPR pressure high enough to equalize the pore pressure. As a result of lower and fluctuating temperature during the day, the pump receives lesser oil such that BPR and pore pressures were lower and unsteady. This causes fluctuation of the pore pressure which then resulted in non-uniform effective stress on the sample.

Fig. 3.12 Hydraulic oil used by the Gilson pump.

Initial attempt to resolve this problem was to replace the hydraulic oil with water, but this does not provide effective solution. This is because the Gilson pump only has the capability of receiving fluid from the reservoir and delivers to the system, but not able to receive fluid from the system. An ISCO pump was later used in place of the Gilson pump. ISCO pump was chosen because it can deliver to and receive fluid from the system. In addition, it does not use external reservoir fluid, rather it has internal cylinder of about 266ml which is manually filled with water. This pump proved a better alternative for the BPR.

Another problem encountered was failure of the O-ring inside the BPR, especially in high pressure tests. This results in series of unexpected leakages through the BPR and

a subsequent loss of pore pressure. In order to reduce or possibly avoid this problem, the BPR has to be disconnected and the O-ring inspected before every test.

3.6.3 Pump problems

On many occasions, there was failure in communication between the Gilson pumps (pumps 1, 2 & 3) and Lab View. Usually, this caused the pumps to stop working. The problem was solved by turning off and on the pumps and re-starting the Lab View. This implies having the data log for the test on different files.

3.6.4 Non-uniform pressure readings

The pressure readings on the Gilson pumps, Lab View and pressure gauges were usually not the same. The pressure readings may sometimes differ by as much as 0.2MPa between the Gilson pump and Lab View. Consistent results were obtained by sticking to only one pressure reading – the one on Lab View, while the others were used more as references.

3.6.5 Temperature Fluctuations

There was temperature fluctuation from the cell's heating element, especially in the last batch of tests carried out. The cyclic fluctuation in temperature varied between less than 129^{o}C to more than 130^{o}C. This causes a cyclic response in confining pressure, and a subsequent non-uniform and fluctuating effective stresses on the sample. Attempt to remedy the situation was not successful as it was discovered the problem is related to calibration of the heating element.

Chapter 4

RESULTS

In this chapter, the results for the different phases of the experiment will be briefly presented. Detailed results and comparisons between different test scenarios will be presented in chapter five. For all the tests carried out, the focus areas are during the hydrostatic loading phase and the subsequent creep phase. The general test procedure was developed (as explained in section 3.5) such that the results presented in this chapter are representative results for the different test samples.

The test results will be presented in six different sections, which will reflect the various phases of the experiments.

In section one, porosity calculation for the samples used in the test will be presented.

Section two presents the typical pressure history encountered during the experiments. Pressure histories covered are both for tests carried out at high confining and pore pressures and the ones at low pressures.

The results obtained during the hydrostatic loading phases are presented in section three. These include the yield curves and methods of determining the yield strength for each sample.

Different creep curves were obtained during the phases. The creep curves and creep strains obtained depends on the flooding fluid and the test pressure. These results are presented in section four.

There was continuous sampling of effluent during brine flooding. Results of the analyses of fractioned effluent are presented in section five.

As explained in section 3.6, some tests were not successful. The failed tests and possible reasons for their failures are presented in section six.

4.1 Porosity calculation

Generally, Stevns Klint chalk is known to be of high porosity. Several researchers have calculated porosity of 40% and above. However, the porosity values obtained in some of the test samples were somewhere below 40%, while the majority were within the anticipated range.

Table 4.1 Porosity calculation

Sample name	Volumetric variables			Sample Weight		Pore volume relatives		
	L (mm)	D (mm)	Matrix Vol. (mm3)	Dry (g)	Sat. (g)	∆ Wt. (g)	Pore Vol. (mm3)	Porosity (%)
Core A	79.50	38.20	91113.92	140.77	176.14	35.37	35370	**38.82**
Core B	78.24	38.20	89435.27	137.43	175.32	37.89	37890	**42.37**
Core C	80.00	38.10	91207.56	139.11	177.97	38.86	38860	**42.61**
Core D	76.14	38.10	86806.80	131.62	169.63	38.01	38010	**43.79**
Core E	79.10	38.10	90181.47	139.46	177.59	38.13	38130	**42.28**
Core F	80.64	38.20	92178.68	146.32	183.50	37.18	37180	**40.33**
Core G	80.20	38.20	91675.72	138.38	178.13	39.75	39750	**43.36**
Core H	80.00	38.20	91447.11	142.03	176.98	34.95	34950	**38.22**
Core I	79.00	38.20	90540.88	137.54	173.08	35.54	35540	**39.25**
Core J	79.00	38.10	90067.47	135.33	174.31	38.98	38980	**43.28**
Core K	80.00	38.10	91207.56	140.28	175.83	35.55	35550	**38.98**
Core L	80.00	38.20	91447.11	140.75	181.11	40.36	40360	**44.13**
Core M	79.50	38.10	90637.51	138.78	178.11	39.33	39330	**43.39**
Core N	80.00	38.20	91447.11	141.99	181.79	39.80	39800	**43.52**
Core O	79.50	38.10	90637.51	138.62	177.88	39.26	39260	**43.31**
Core P	81.40	38.00	92317.17	139.28	178.84	39.56	39560	**42.85**
Core Q	80.80	38.10	92119.64	139.40	179.37	39.97	39970	**43.39**
Core R	79.00	38.10	90067.47	138.33	177.69	39.36	39360	**43.70**
Core S	80.30	38.10	91549.59	138.89	177.36	38.47	38470	**42.02**
Core T	80.90	38.20	92475.89	140.58	180.07	39.49	39490	**42.70**

As can be seen on table 4.1, samples A, H, I and K have porosity values less than 40%, while the rest of the samples have little variations in their porosities. Since the samples were drilled from the same chalk block, it was expected that their porosities should be relatively similar. As a result of these variations, the samples (except for Core A) were measured again and the porosities re-calculated. The new results obtained were quite similar to the previous porosity values. The variations in porosity may be attributed to differences in depositional texture of the chalk. In order to have comparable results, samples with similar porosities were used for the tests except for core A, which was already being tested before the porosities were re-calculated. Cores H, I and K were actually tested but they were among the tests that failed after few days.

4.2 Pressure History

As mentioned earlier, the tests were originally designed for high pressures (40MPa pore pressures and 52MPa confining pressures). But some of the tests were performed at low pressures (0.7MPa pore pressures and 12.7MPa) confining pressures) in order to compare with the results obtained at high pressures. The test procedure is the same

in both cases, except that ramping of pressures was not applicable for low pressure tests. High pressure tests were carried out using the two brines, $MgCl_2$ and NaCl as the flooding fluids. The pressure history when using both brines is basically the same.

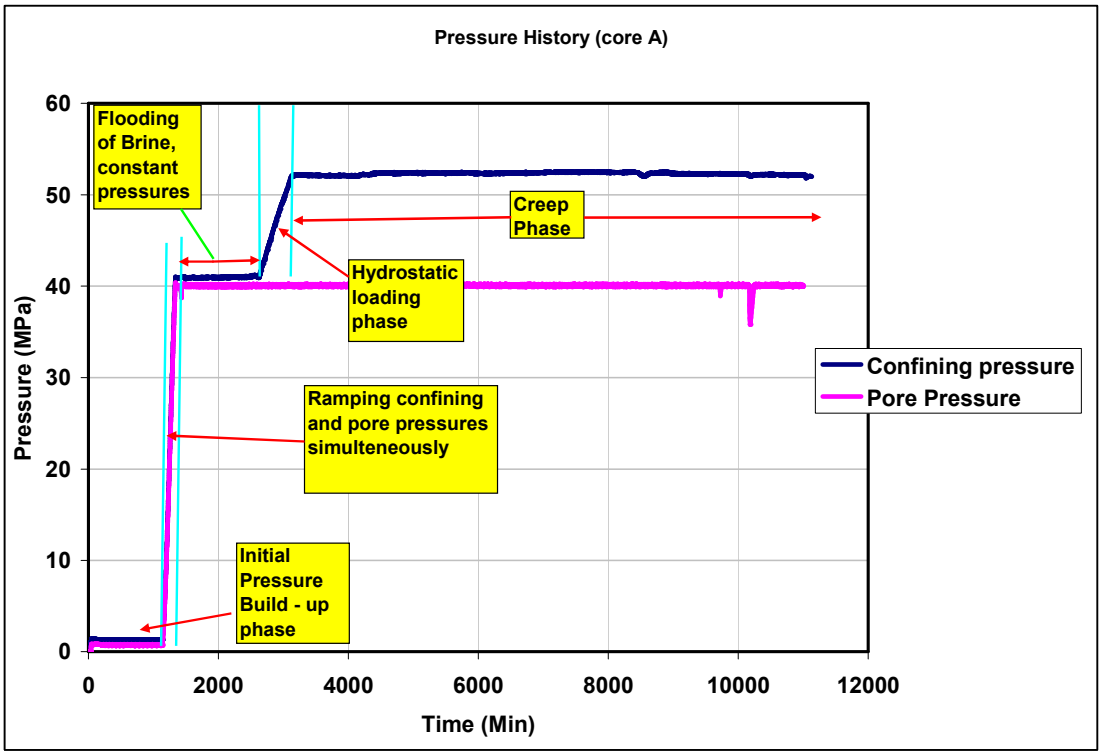

Fig. 4.1 Pressure History for Core A

Fig. 4.1 shows the pressure history for core A. The four main phases of the test are as indicated on the figure.

During the initial pressure build-up phase, the test samples were flooded with at least 4PV of distilled water. This was done in accordance with the procedure for preparing outcrop chalk, developed by Puntervold et al., 2007 [27]. The essence of this was to remove SO_4^{2-} ions which might be present in the sample due to possible seawater contamination, as Stevns Klint is located close to the sea.
The second phase which involved simultaneous ramping of confining and pore pressures was also carried out while still cleaning with distilled water. The samples were later exposed to the respective brines after the ramping operation. Hydrostatic loading was achieved by flooding about 2PV per day of brine, followed by the creep phase. The strain developed during hydrostatic loading and creep for core A is shown in fig. 4.2. As expected, there is no axial strain developed during initial pressure build-up and pressure ramping because the piston has not landed on the sample. However, it is documented in the studies by Omdal et al., that there is usually minor deformation in the radial direction during these phases. As already mentioned in section 3.3.5, the cell used for these experiments has no facility to measure radial deformation.

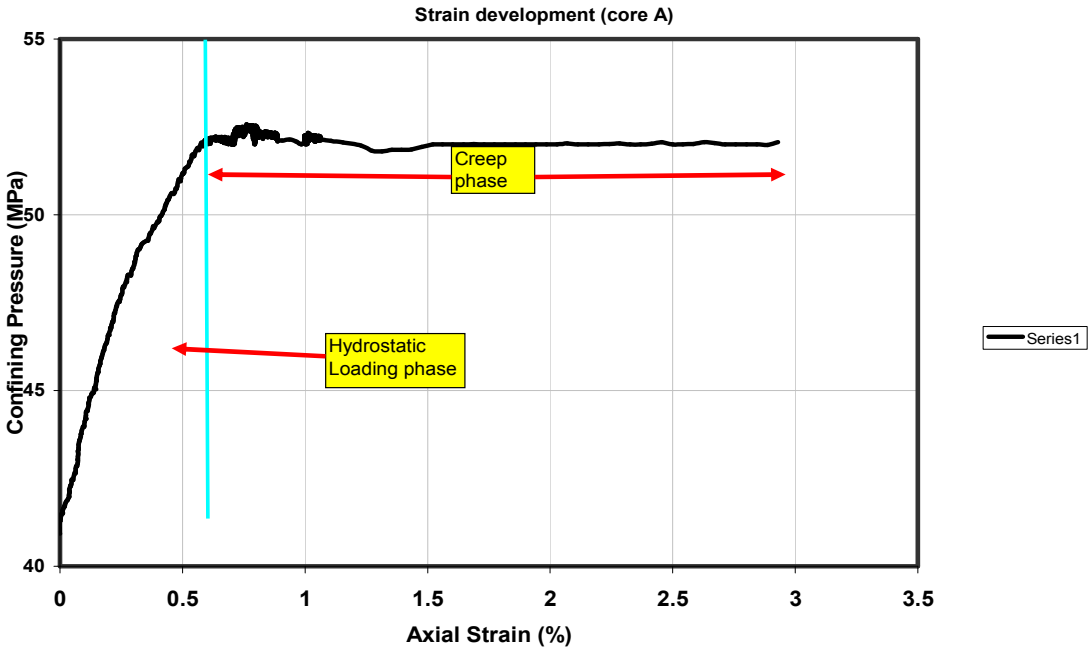

Fig. 4.2 Strain development during hydrostatic loading and creep for Core A

Fig. 4.3 is the pressure history for core G performed at low pressures. Just as in tests at high pressures, the initial pressure build-up phase is to build pore and confining pressures of 0.7MPa and 1.4MPa respectively, followed by brine flooding in order to fully saturate the sample with brine. The hydrostatic loading phase involves exposing the sample to effective stress of 12MPa, and then allowed to creep for at least five days. The pressure histories for other samples tested are shown in Appendix A.

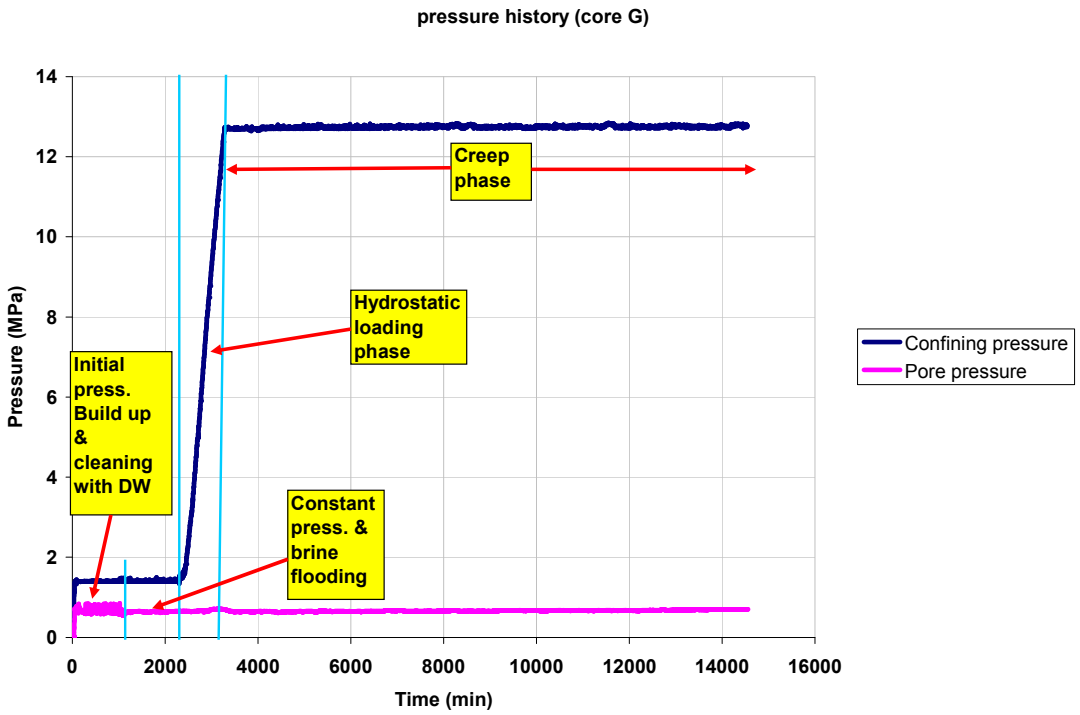

Fig. 4.3 Pressure history for Core G

4.3 Hydrostatic Loading phase

The high porosity of the test samples makes them vulnerable to fail by pore collapse under hydrostatic loading. As explained in section 2.3, the samples' response is linear in the elastic region because the deformation is mainly due to elastic compressibility of the pore system. At the onset of hydrostatic yielding/pore collapse, the samples' response becomes non-linear with rapid increase in volumetric strain. This results in decline in porosity and high compressibility of the samples. After the phase of strong pore collapse, the plastic strain begins to decrease progressively. This is the plastic region. The yield stress or pore collapse stress is therefore the region between the elastic and plastic region on stress-strain curve.

Based on the above information, yield stress of the samples used in this thesis is determined at the point where the stress-strain plot becomes non-linear. This is obtained by drawing a straight line into the stress-strain plot from the elastic region, and a corresponding straight line from the plastic region. The point of intersection between these lines is taken to be the yield stress. Fig. 4.4 illustrates this method for core C.

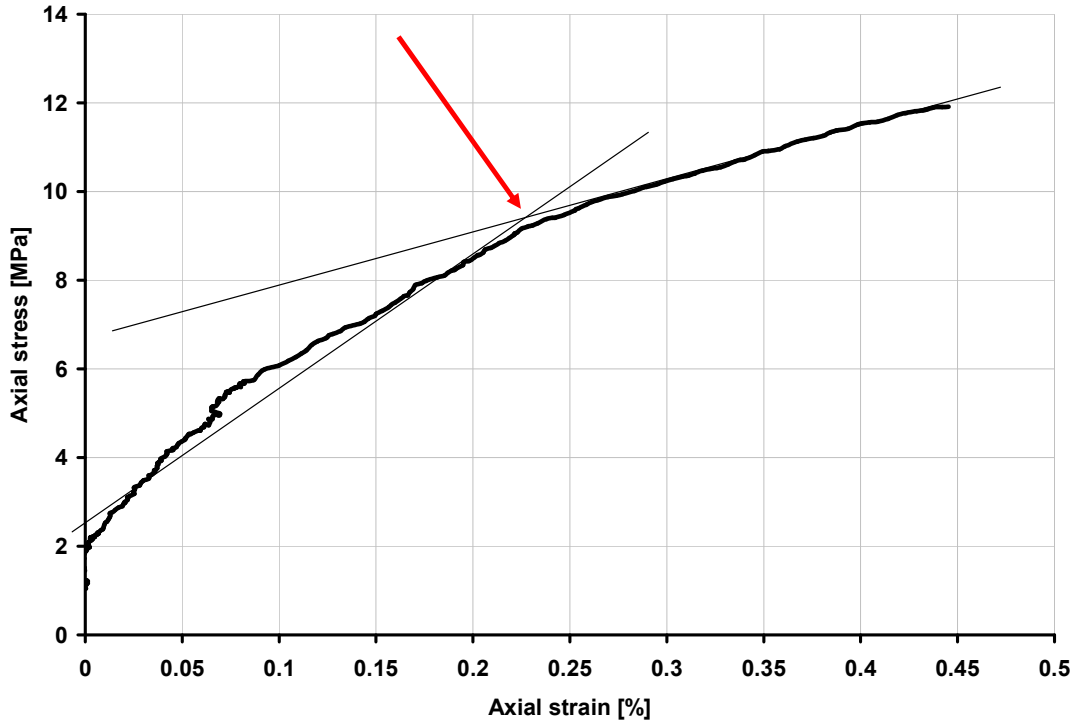

Fig. 4.4 Yield point for core C determined by method 1

Looking at the stress-strain plot of fig.4.4, the region within the elastic phase seems to have more than one slope such that one may be tempted to suggest that the yield point is around 6MPa. Closer examination will show that this is not actually the case because there could be some distortion within this phase. The distortion might be in the form of "hanging of the piston". The plastic phase is normally characterised by a smooth and linear trend with one slope on the stress-strain curve as seen in fig. 4.4. Therefore the yield point was chosen as the transition to the plastic phase, which in

this case is 9.23MPa. This yield value agrees relatively well with the yield values obtained for the rest test samples.

In order to cross-check the yield values obtained using the above method; an alternative method was also used. This method involves plotting the axial stress developed during hydrostatic loading against the differential pressure over the sample. Generally, there will be decrease in permeability during yielding, as documented in studies by Korsnes et al., 2006[24]. With reference to Darcy's law (equ. 2.3), a decrease in permeability will result in a proportionate increases in pressure drop over the sample. Hence, yield is determined where there is rapid increase in differential pressure over the sample. Fig 4.5 illustrates this method as used on core C also.

The determination of yield values from the plot of axial stress versus the axial strain is in this thesis, referred to as METHOD 1 while the yield values determined from a plot of axial stress versus differential pressure is METHOD 2.

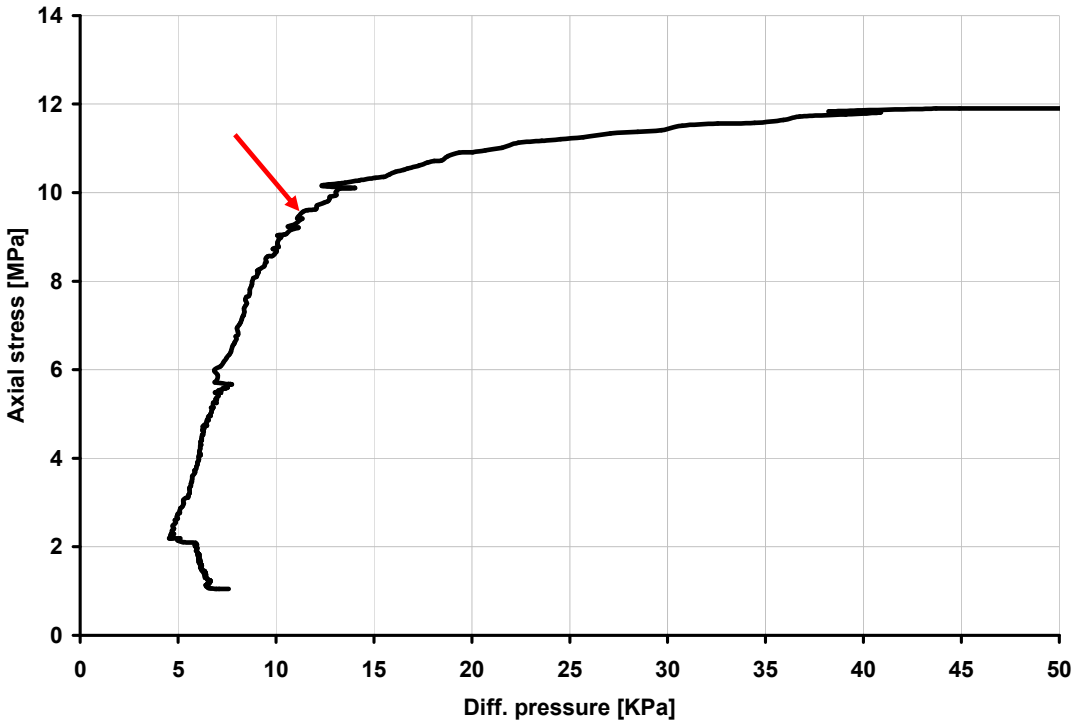

Fig. 4.5 Yield point for core C determined by method 2

From fig. 4.5, there seems to be a change in slope between 6MPa and 9MPa axial stress which is close to what obtains in fig. 4.4. This region is followed by a region of possible initiation of pore collapse where it could be argued that the weaker grains collapsed first, followed by the general collapse of the stronger grains. At this phase of pore collapse, the differential pressure began to increase rapidly and the yield point was taken to be 9.4MPa.

Method 2 was not easily used to determine the yield stress for all the samples because of fluctuation in differential pressure. The differential pressure may not increase linearly with axial stress as seen on core C because of effect from the BPR. As

explained in section 3.3.6, the BPR is set to a certain pressure limit such that any excess fluid pressure through the sample is expelled. It then implies that when the fluid pressure through the sample becomes high, the differential pressure increases, while the reverse is the case when the excess fluid pressure is expelled and then becomes low.

Table 4.2 shows the yield values and bulk modulus for the samples. The bulk moduli were found from slope of the straight line in the elastic region of fig.4.4 and dividing by a factor of 3. From fig. 4.4, x – axis of the plot shows the axial strain, but bulk modulus is based on volumetric strain. In a hydrostatic test, the volumetric strain is assumed to be three times the axial strain, and that explains the reason for dividing the obtained slope by a factor of 3.

Table 4.2 Yield values and bulk modulus of the samples

Sample name	Flooding fluid	Pore press (MPa)	Yield values (MPa)		Kb GPa
			method 1	method 2	
A	$MgCl_2$	40.00	8.39	–	0.86
B	$MgCl_2$	40.00	9.20	9.39	0.92
C	$MgCl_2$	0.70	9.23	9.40	1.39
D	$MgCl_2$	0.70	7.32	–	0.64
G	NaCl	0.70	7.52	7.35	0.63
M	NaCl	40.00	8.22	–	0.57
N	$MgCl_2$	40.00	7.66	8.32	0.72
O	$MgCl_2$	40.00	8.13	–	0.61

4.4 Creep Phase

Different types of creep curves and creep strains were observed from the tests. The differences depend on test pressure and flooding fluid a particular sample was exposed to. As already mentioned, the experiments were originally designed to be carried out at high pressures with different brines. Results obtained from the first few tests necessitated that similar tests should be performed at low pressures in order to have a reasonable comparison. Previous laboratory experiments have not reported accelerating creep on chalk. Tests performed in this thesis at high pore and confining pressures shows significant “accelerating-like” creeps. These observations prompted that similar tests should be performed at lower pressures and possibly with different types of brines. Fig. 4.6 is the creep curve for core A. As can be seen from the figure, “accelerating-like” creep began to develop after about 5000minutes of creep (after flooding about 9.3PV of 0.219M $MgCl_2$).

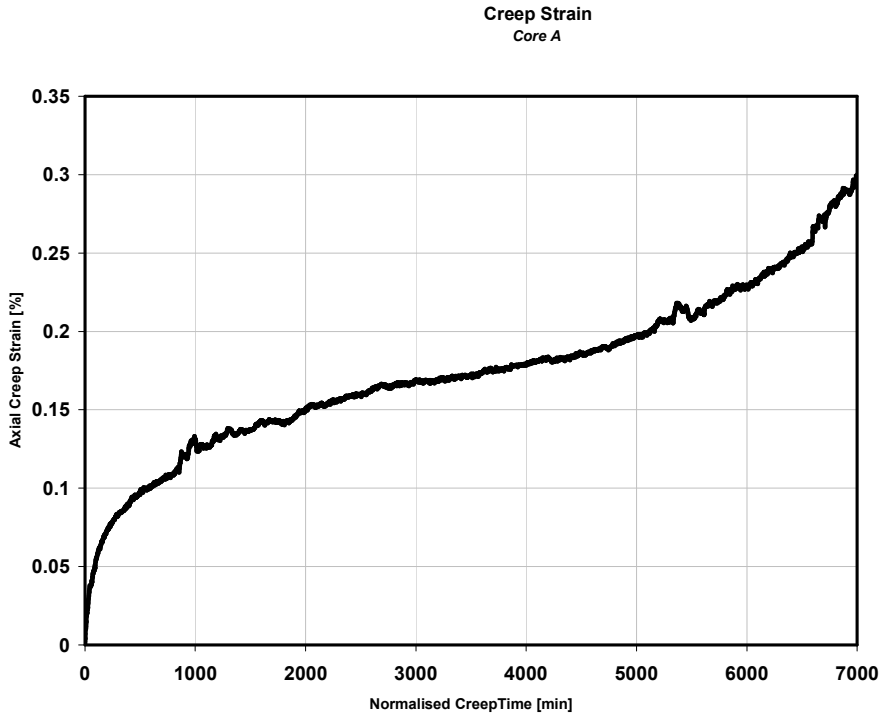

Fig. 4.6 Creep curve for core A

Core M was subjected to the same experimental condition but with 0.657M NaCl as the flooding fluid. In this case, "accelerating-like" creep was not observed as can be seen in fig. 4.7. Other tests performed under similar conditions show "accelerating-like" creep when the samples were exposed to $MgCl_2$, but no such creep was observed when NaCl was used.

Tests on Core C and Core G were carried out at low pore pressures of 0.7MPa and hydrostatically loaded to effective stress of 12MPa. Core C was exposed to 0.219M $MgCl_2$ while Core G was flooded with 0.657M NaCl. For these tests, steady state creeps were rather observed as seen in fig.4.8 and fig. 4.9. Other creep curves for all the samples are presented in Appendix C.

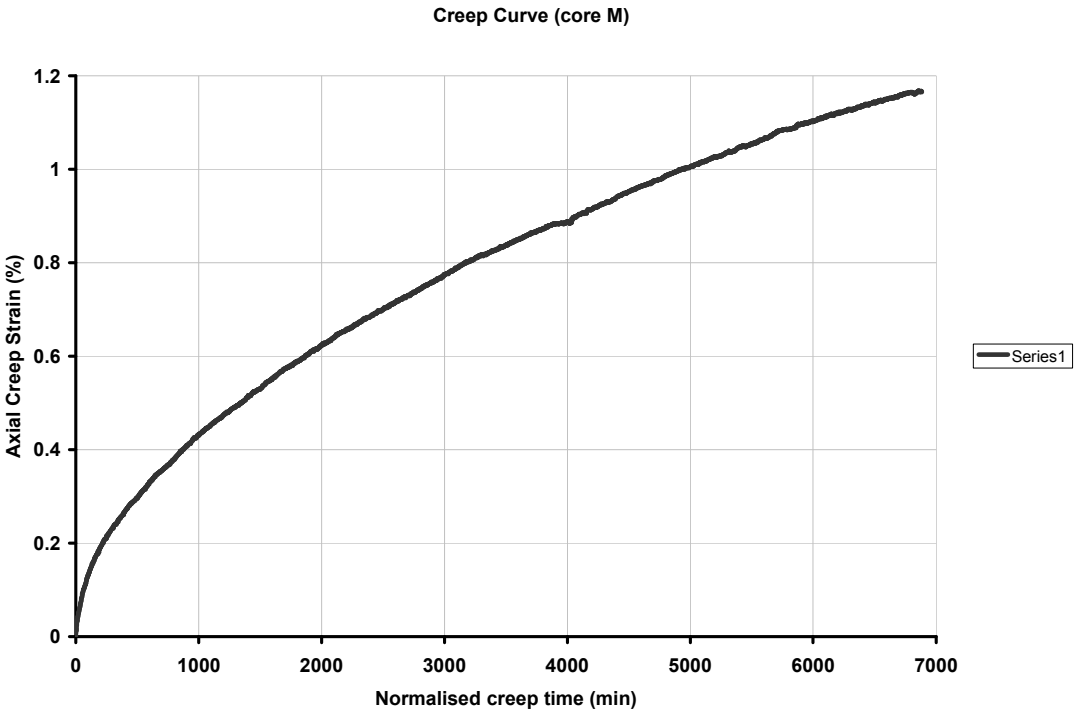

Fig.4.7 Creep curve for core M

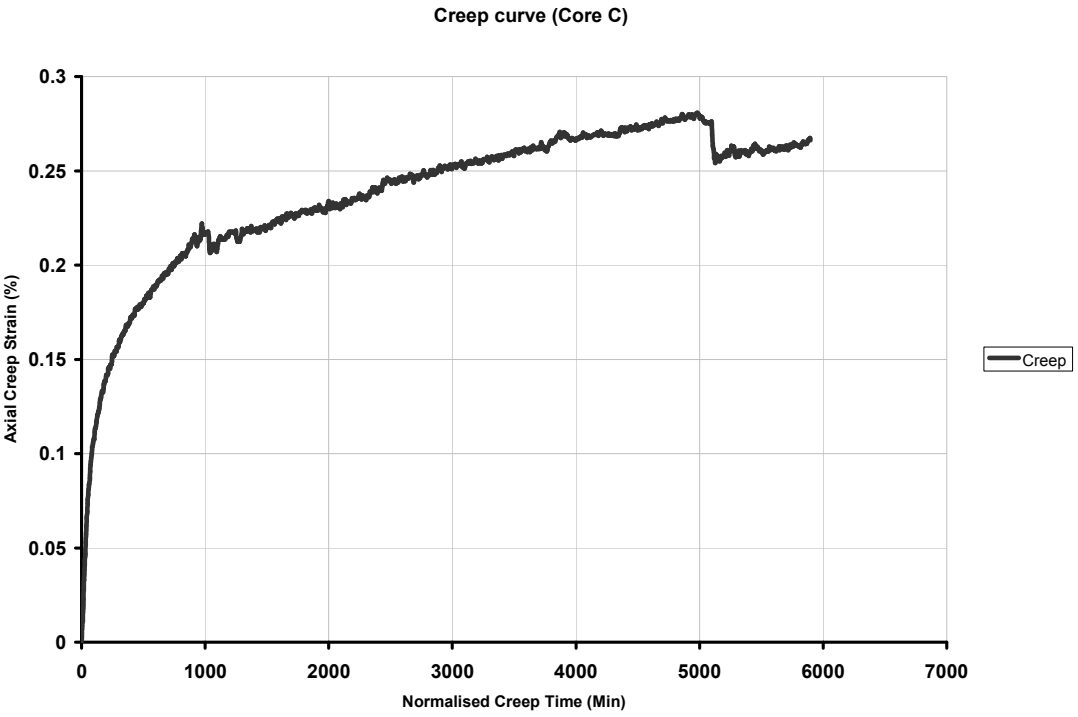

Fig. 4.8 Creep curve for core C

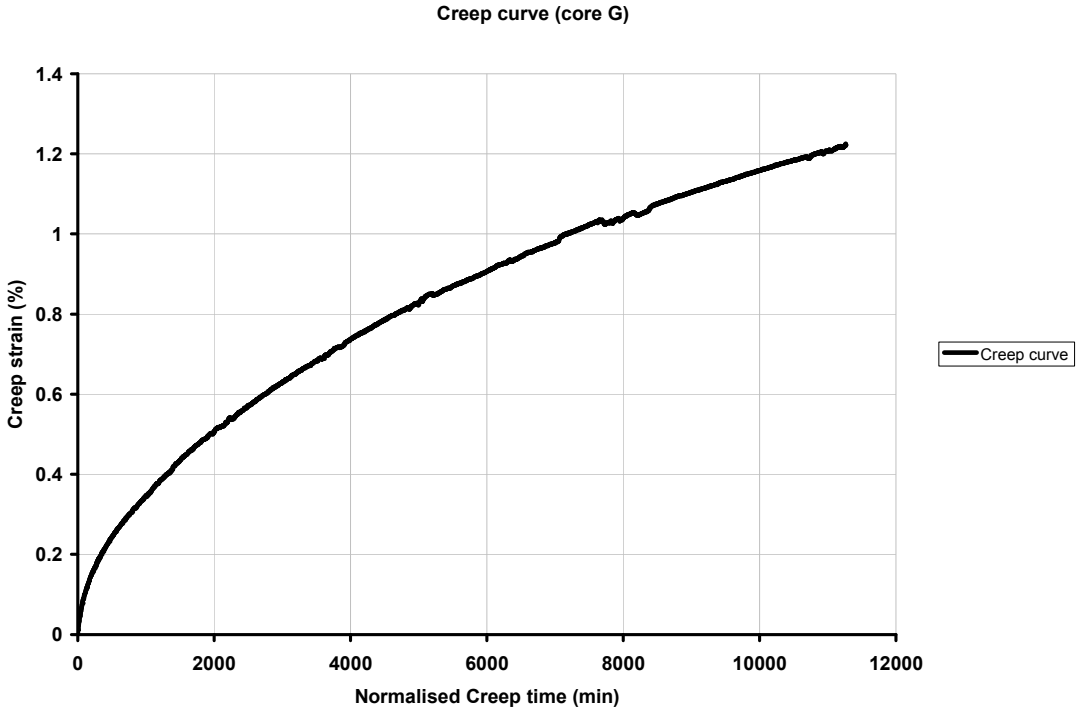

Fig.4.9 Creep curve for core G

Table 4.3 summarizes the creep type, test pressure, flooding fluid and creep strain obtained after 6000minutes of creep for all samples tested. From the table, it can be seen that samples subjected to same test conditions have similar strain values within the same time period. The deformation during creep at different test conditions varies significantly between the different samples. For example, cores A, B and C flooded with $MgCl_2$ deformed by 0.228%, 0.220% and 0.280% respectively after 6000minutes of creep. The variation in creep strain for these samples is relatively small, compare to cores G and M flooded with NaCl which deformed by as much as 0.913% and 1.166% respectively during the same time period.

Further discussion on possible reasons for these variations will be presented in chapter 5.

Table 4.3 Creep summary

Sample name	Flooding fluid	Pore press (MPa)	PV	Strain (creep after 6000mins) %	Total creep (%)	Creep type
A	$MgCl_2$	40.00	13.32	0.23	0.30	Accelerating
B	$MgCl_2$	40.00	24.58	0.22	0.42	Accelerating
C	$MgCl_2$	0.70	10.93	0.28	0.28	Steady state
D	$MgCl_2$	0.70	27.11	0.48	0.60	Steady state
G	NaCl	0.70	19.48	0.91	1.22	-
M	NaCl	40.00	11.73	1.10	1.16	-
N	$MgCl_2$	40.00	18.28	1.29	1.31	-
O	$MgCl_2$	40.00	14.26	-	-	-

4.5 IC Results

Chemical analyses of the fractioned effluent are easily comparable. Fig. 4.10 and 4.11 are the IC results of effluents from cores B and G, which are representative results for all the samples flooded with $MgCl_2$ and NaCl respectively. The IC result can either be plotted as ion concentration (y-axis) versus flooded pore volume (x-axis), or as ion concentration versus sampled time of the effluents. Both plot types are shown in fig.4.10 and 4.11. The chemical analyses performed show that when $MgCl_2$ is flooded through the sample, a significant amount of magnesium is lost inside the core while a considerable amount of calcium is detected in the effluent. Cores flooded with NaCl did not show any significant reaction as NaCl is inert with chalk ($CaCO_3$). This result is shown in figure 4.11.

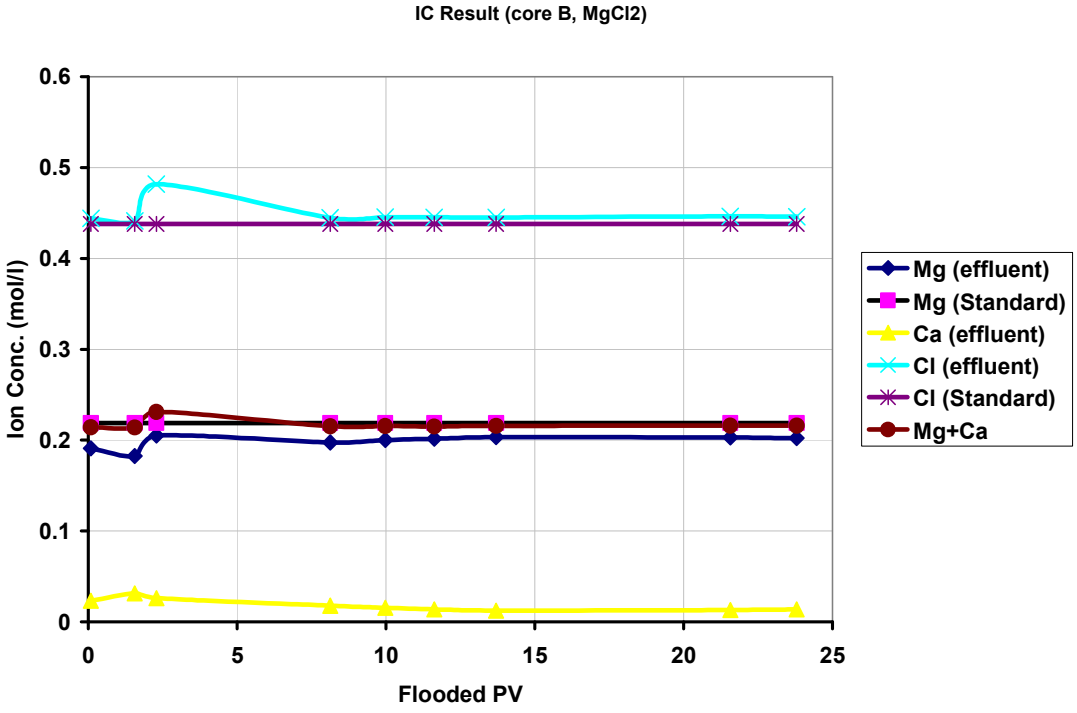

Fig. 4.10 IC result for Mg^{2+}, Ca^{2+} and Cl^- ions in sampled effluent for core B flooded with $MgCl_2$

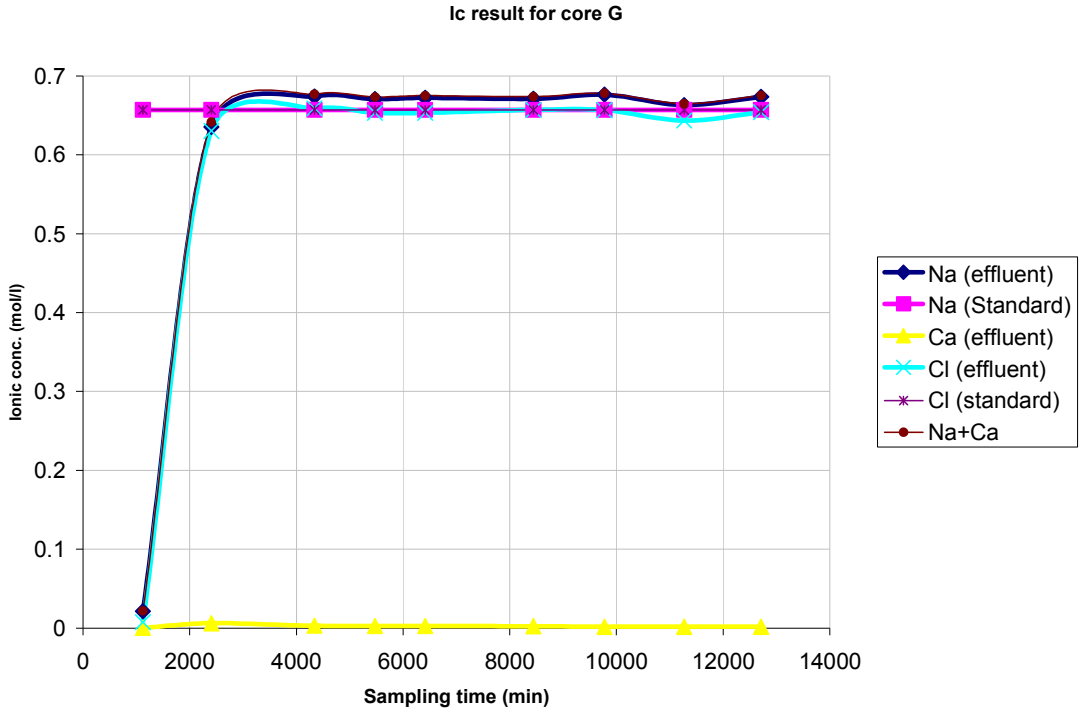

Fig. 4.11 IC result for Na^{+}, Ca^{2+} and Cl^{-} ions in sampled effluent for core G flooded with NaCl

The drastic increase in concentration was because within the start-up of any flooding the effluent will be a mixture of distilled water and actual brine since all the cores were saturated with distilled water from the very beginning.
Also, the flooded fluids tend to be more alkaline after passing through the samples compared to the original brines. For example, the average PH of effluents fractioned from core B is 7.59 while the PH of original $MgCl_2$ is 5.59. This can be seen in table 4.4. This is because when carbonates dissolve ($CaCO_3$) they release HCO_3^{-} and CO_3^{2-} ions into solution, providing alkalinity (Jury, 2009)[25].

Table 4.4 pH of fractioned effluent for core B

Sample number	sampled time (min.)	PV	pH
1	1431	0.09	7.63
2	2462	1.56	7.68
3	2981	2.28	7.69
4	7188	8.12	7.27
5	8519	9.97	7.28
6	9704	11.62	7.75
7	11204	13.70	7.63
8	16869	21.57	7.65
9	18474	23.80	7.77
$MgCl_2$ (standard)		–	5.59
$MgCl_2$ (undiluted)		–	5.71

The pH values for core B is a representative of the pH for all the other samples. The pH values for the other test samples are shown in Appendix D.

4.6 Failed tests

Some of the experiments were not successful because of the reasons explained in section 3.6. The possible causes for each of the failed tests are given in table 4. 5.

Table 4.5 Failed tests and causes of the failures

	Causes of failure					
Sample name	Leakages through the;			BPR problem		Temp. fluctuation
	core sleeves	flooding cell	couplings	loss of pore pressure	failure of O - ring	
core E	√				√	
core F	√					
core H		√		√		
core I				√		
core J			√	√		
core K	√					
core L		√				
core P				√	√	
core Q			√		√	
core R						√
core T						√

Chapter 5

DISCUSSION OF RESULTS

This chapter contains the detailed results from each of the main phases of the experimental work. It is divided into three main sections;

♦ hydrostatic/isotropic loading phase

♦ creep phase

♦ chemical analysis of the fractioned effluents

Each of the phases presents the influence of pore pressure and brine composition on the sample, that is, the sample's mechanical and chemical behaviour at high and low pore pressures when exposed to $MgCl_2$ and NaCl. Therefore in each phase, a comparison will be made based on the effects of pore pressure (high and low pressures) while flooding with the same and/or different brines and the effects of brine ($MgCl_2$ and NaCl) while testing at high and/or low pore pressures.

5.1 Hydrostatic loading phase

5.1.1 Brine effects at high pressures

Fig. 5.1 presents the yield curves for cores A, B, M, N and O. Tests on these samples were carried out at 40MPa pore pressures and hydrostatically loaded to 12MPa effective stress according to the procedures described in section 3.5. While cores A, B and N were exposed to 0.219M $MgCl_2$, core M was flooded with 0.657M NaCl. As already mentioned in section 3.0, these brine concentrations are of the same ionic strength as in seawater.

The yield curve for core N may not be a good comparison to the rest samples because of inconsistent pore pressure during the loading. This is because there was drop in pore pressure to 39MPa for about 15minutes on two occasions as reflected by the two loops on the curve. That is, on these two occasions the effective stresses increased rapidly and after the pore pressure was restored the core have compacted such that the original curve trend was no longer maintained. Therefore a good comparison will be for the samples that were subjected to the same test conditions.

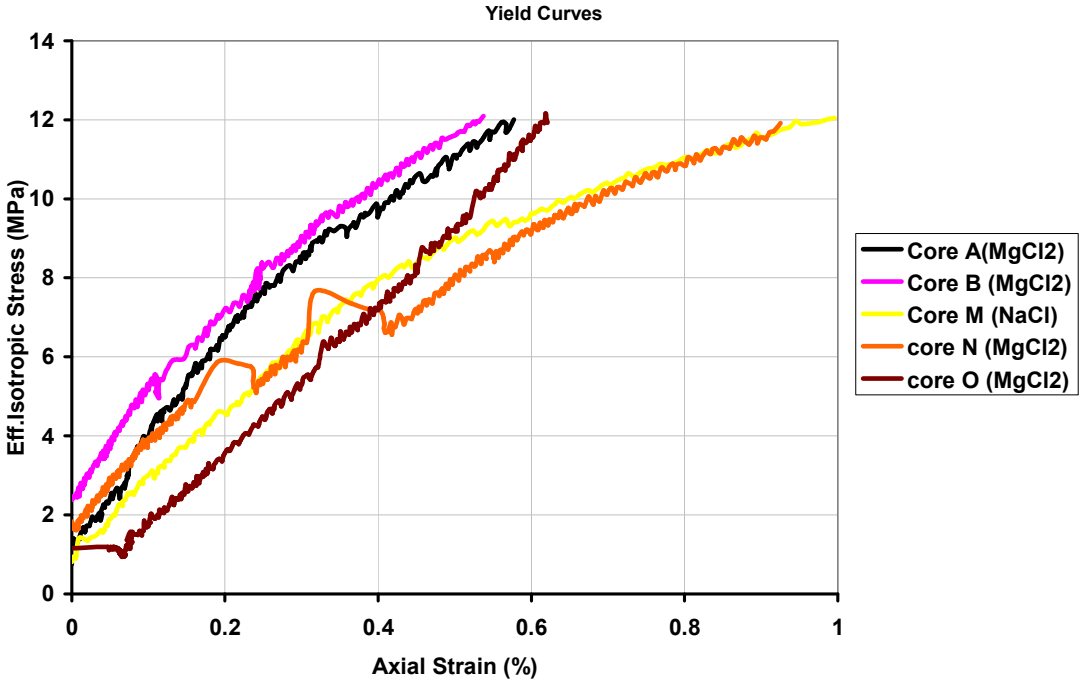

Fig. 5.1 Stress-strain curves for cores A, B, M, N and O

From fig. 5.1, it can be seen that core M deformed by more than 40% at maximum hydrostatic load than cores A and B. While cores A, M and O have similar yield stress of 8.39MPa, 8.22MPa and 8.13MPa (table 5.1) respectively, core B has a higher yield strength value of 9.2MPa. Core N was recorded to have a yield value of 7.66MPa and a strain of 0.925% at maximum load but it may be difficult to conclude that these are the exact values because of the problem explained above. Though, it may be argued that the high strain on core N is relatively large to be as a result of "just" additional 1MPa effective stress. Hence other factors may equally contribute as well.

Theory states that mechanical strength of chalk depends on, among other factors, porosity and silica content [Da Silva et al., 1985][17], type of fluid in the pores [Risnes, 2000][8], and effective stress imposed on the chalk [Blanton, 1981][6]. Cores M, N and O have similar porosities of about 43% while core B has about 42% and core A's porosity is a little below 39% (not re-calculated like in other samples as explained in section 4.1). High porosity chalk is generally weaker than chalk with lower porosity. It could therefore be that the higher strain obtained in core M (and possibly core N) may be as a result of the higher porosity. The flooding fluid used on core M (NaCl) may also have an effect on the deformation at maximum hydrostatic load, but this may be difficult to conclude at this stage since only one test was successfully carried out at high pressure while injecting NaCl brine.

5.1.2 Brine effects at low pressures

Fig. 5.2 shows the yield curves for cores C, D and G. Cores C and D were flooded with $MgCl_2$ while core G was exposed to NaCl. All the tests were performed at 0.7MPa pore pressure and loaded isotropically to effective stress of 12MPa.

It can be observed from the figure that the results on these samples are not relatively comparable especially in terms of the brine used. While cores D and G have similar yield strengths of 7.32MPa and 7.52MPa respectively, core C has a higher yield value of 9.23MPa. Core G developed a strain of 0.72% and core C 0.445%. Core D on the other hand deformed by 0.81%, about 45% more than core C which was exposed to the same brine. The major factor that could cause these variations in mechanical strength may be the samples' porosities. Core D has a porosity of 43.78%, core G has 43.35% while core C has a lower porosity of 42.60% and hence the strongest of the three.

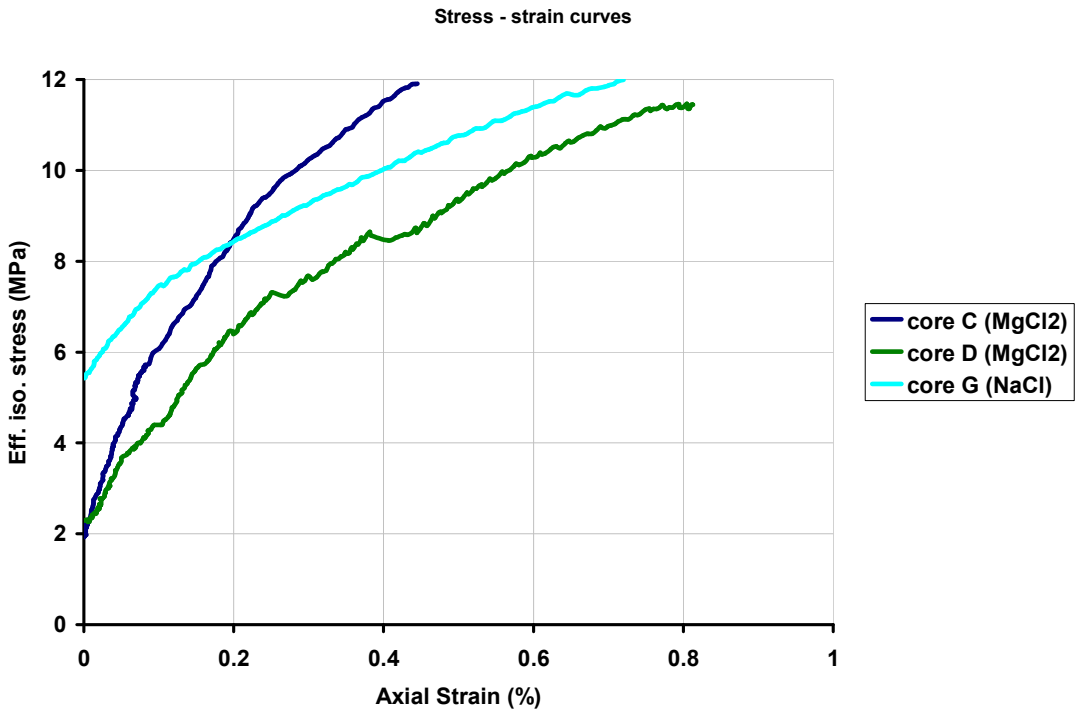

Fig. 5.2 Stress-strain curves for cores C, D and G

5.1.3 Pressure effects, $MgCl_2$ brine

Fig. 5.3 presents the stress-strain curves for cores A, B, C ,D and O. Tests on cores A ,B and O were performed at 40MPa pore pressures and 0.7MPa pore pressures on cores C and D. All the samples were flooded with 0.219M $MgCl_2$ and isotropically loaded to effective stress of 12MPa.

As can be observed from the figure, there is no strict trend on the sample's deformation at maximum hydrostatic load with respect to pore pressure. Cores A, B

and O have deformations of 0.577%, 0.537% and 0.62% respectively at maximum load, while core C deformed by 0.445% at the same effective stress. However, core D which was subjected to the same pressure as core C deformed by as much as 0.855% at maximum load. In addition, the yield strength of core D is small compare to the rest four (table 5.1). Core D has yield strength of 7.32MPa while the yield strengths of cores B and C is about 9.2MPa and cores A and O are 8.39MPa and 8.13MPa respectively.

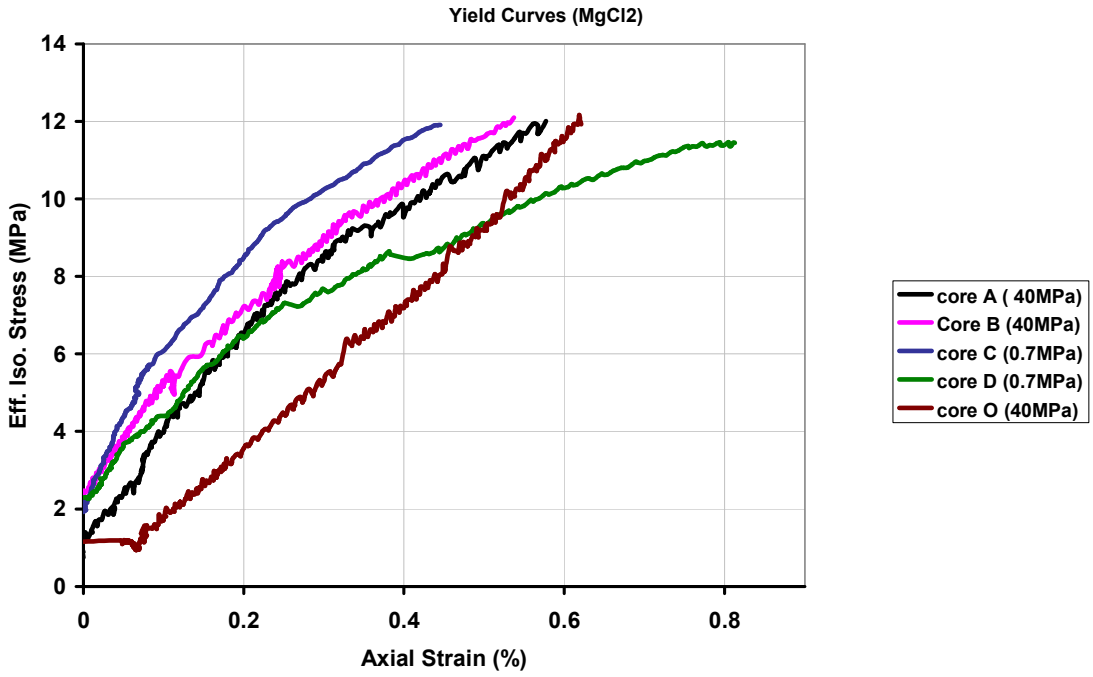

Fig.5.3 Stress-strain curve for cores A, B, C, D and O

Since these samples were exposed to nearly the same effective stress and flooded with the same brine, their differences in porosity may be the possible reason for variation in their mechanical strength. As already mentioned, high porosity chalk generally deforms more than chalk with lower porosity. While cores B and C have similar porosities of about 42% and core A has 38.82% (not re –calculated as explained in section 4.1), core D has higher porosity of 43.78%. This may explain the lower yield stress and higher deformation observed on core D.

5.1.4 Pressure effects, NaCl brine

Tests on core G was at 0.7MPa pore pressure and 40MPa on core M. Both samples were flooded with 0.657M NaCl and loaded hydrostatically to effective stress of 12MPa. From fig. 5.4 core M has yield strength of 8.22MPa while core G yielded at 7.52MPa. In addition, core M developed a strain of 0.988% at maximum load while core G deformed by 0.72% at the same effective stress. In this case, it might be difficult to attribute these variations to difference in porosity because the two samples have similar porosities of about 43%. Also from the explanation in section 5.1.2, the

influence of pore pressure does not seem to affect the mechanical strength of chalk. This is also in line with studies by Breivik, 2007 [7].

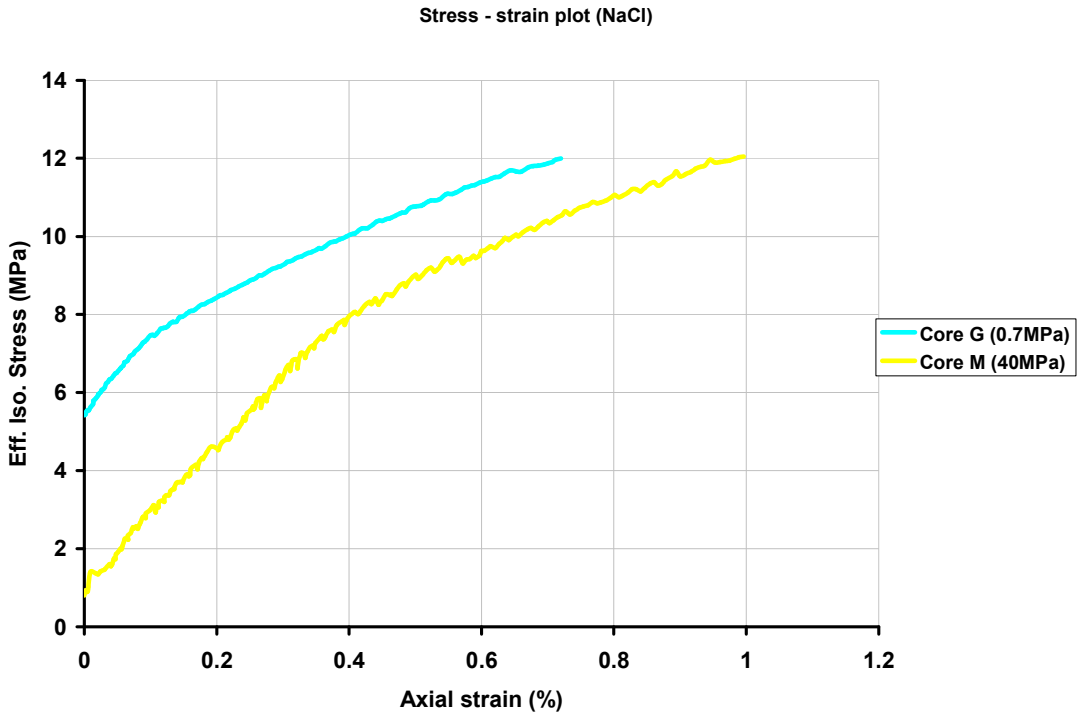

Fig. 5.4 Stress-strain curves for cores G and M

5.1.5 Combined yield curves

Fig. 5.5 shows a plot of the yield curves for all the samples tested. From the figure, it can be observed that yield values do not tend to be affected by pore pressure differences. The yield values vary between 7.5MPa to 9.30MPa within normal scatter, with the average yield value being 8.22MPa.

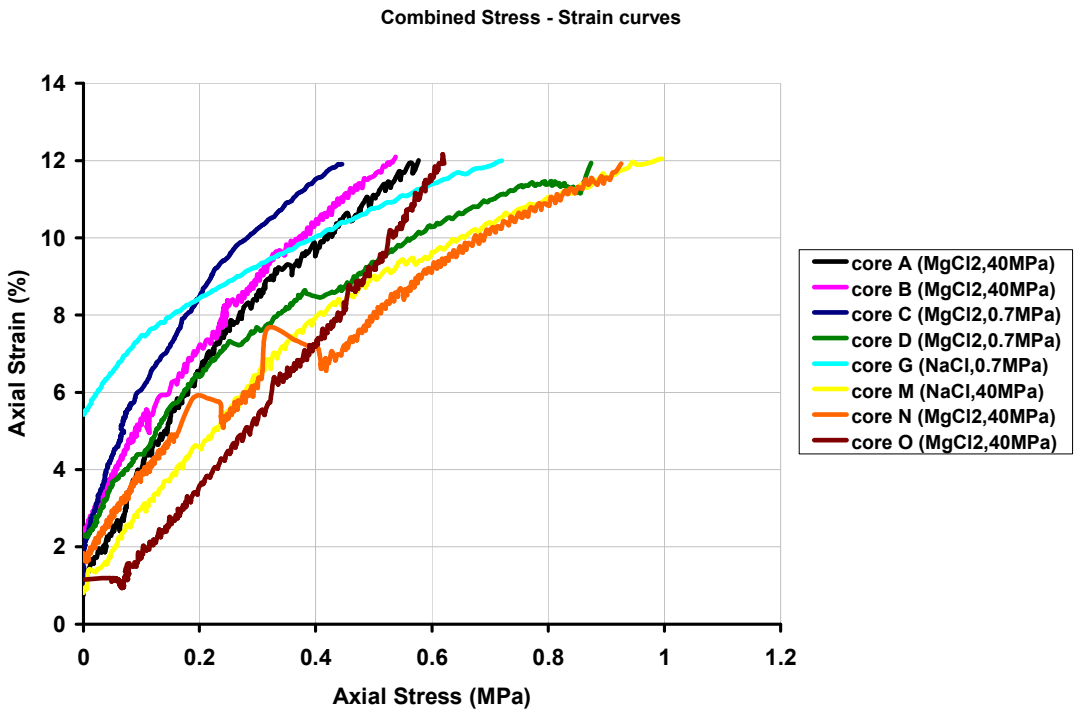

Fig. 5.5 combined stress-strain curves

Table 5.1 shows a summary of the yield stress and strain developed at maximum hydrostatic load for each sample. As explained in section 2.2.5 failures in porous and saturated rocks are governed by the effective stress, such that the absolute pressure values do not affect the test samples. Tests performed by Breivik (2007) on Stevns Klint chalk at different pore pressures while flooding with synthetic sea water also reveals that pore pressure does not affect the yield strength of chalk. The test samples had average porosity of 48% and average yield strength of 6.6MPa. As mentioned earlier, rocks with high porosities are mechanically weaker than those with lower porosities [Da silva et al., 1985][17]. Since the samples used for this thesis work have average porosity of 42%, the higher yield strength of 8.22MPa should therefore be expected.

Table 5.1 Yield strength and strain at maximum load for the samples

Sample name	Porosity (%)	Flooding fluid	Pore press (MPa)	Yield Str. (MPa)	Strain at max load (%)	Kb GPa
A	38.82	$MgCl_2$	40.00	8.39	0.58	0.86
B	42.36	$MgCl_2$	40.00	9.20	0.54	0.92
C	42.60	$MgCl_2$	0.70	9.23	0.45	1.39
D	43.79	$MgCl_2$	0.70	7.32	0.81	0.64
G	43.36	NaCl	0.70	7.52	0.72	0.63
M	43.39	NaCl	40.00	8.22	0.99	0.57
N	43.52	$MgCl_2$	40.00	7.66	0.93	0.72
O	43.32	$MgCl_2$	40.00	8.13	0.62	0.61

The samples' deformation at maximum hydrostatic load of 12MPa is not easily comparable. While core M which was exposed to 40MPa pore pressure and flooded with NaCl developed a strain of 0.988% at maximum load, core D deformed by as much as 0.81% at a lower pressure of 0.7MPa on being flooded with $MgCl_2$. On comparing deformations on cores A, B, C and O with cores M and G, it will appear that samples flooded with NaCl tend to be weaker than those flooded with $MgCl_2$. The strain developed for core N was recorded to be 0.925%, but the loss of pore pressure as explained in section 5.1.1 should be taken into consideration.

The mechanical strength of the samples seems to be consistent with their bulk modulus. As defined in section 2.2, the bulk modulus is a measure of the sample's resistance against hydrostatic compression. With the exception of core C, the samples' bulk moduli vary between 0.567GPa to 0.924GPa, with the average being 0.705GPa. Core C seems to be exceptionally stronger than the rest samples. This is reflected in the high bulk modulus of 1.39GPa and lower deformation of 0.445% at maximum hydrostatic load. Though core M has the lowest bulk modulus of 0.567GPa, its high yield value of 8.22MPa signifies that it is naturally not the weakest of the samples. Rather it may be argued that the high strain developed by core M is as a result of the flooding fluid used on the core. It is also worth noting that the bulk modulus for core N is not consistent with the recorded deformation. This also has to do with fluctuation in pore pressure as explained in section 5.1.1.

5.2 Creep phase

One of the main focus areas of this thesis is to investigate the influence of pore pressure on chalk deformation during the creep phase, when the chalk is exposed to different brines. Previous work by Breivik (2007) did not show tangible correlation between pore pressure and creep deformation. In those tests, pore pressure was varied between 0.7MPa to 35MPa and only one type of brine, synthetic sea water was used. The few results that could be correlated in the studies of Breivik shows a decreasing trend in creep deformation with increasing pore pressure. In this thesis work, $MgCl_2$ and NaCl with ionic strength as in sea water were used at both high and low pore pressures. The results obtained during the creep phase for the different test scenarios are presented in this section. The creep curves for cores N and O are excluded in the comparisons within this section. This is because of high fluctuation in pore pressure during the creep phase of the tests for these samples. It was therefore believed that values and creep trends obtained from these two samples may not be easily compared to the rest samples. However, the creep curves for these samples will be presented in Appendix C.

5.2.1 Brine effects at high pressures

Fig. 5.6 presents the creep curves for cores A, B and M. Cores A and B were flooded with $MgCl_2$ while NaCl was flooded through core M. All the samples were subjected to the same pore pressure of 40MPa and effective stress of 12MPa during their creep periods.

It can be observed from the figure that core M deformed by more than a factor of 3 compared to cores A and B. It may be quite difficult to attribute the huge difference in deformation to the higher porosity of core M because it has just 1% porosity more than core B. In addition, "accelerating-like" creep began to develop on core A after about 5000minutes and after about 10000minutes of creep on core B, but no such trend was observed on core M. Since the test conditions for the three samples were similar, save for the brine, it may not be completely out of place to believe the higher deformation of core M to be as a result of the injected brine. However, it may not be quite easy to make a definite conclusion on this since only one test was successfully carried out at high pressures with NaCl brine.

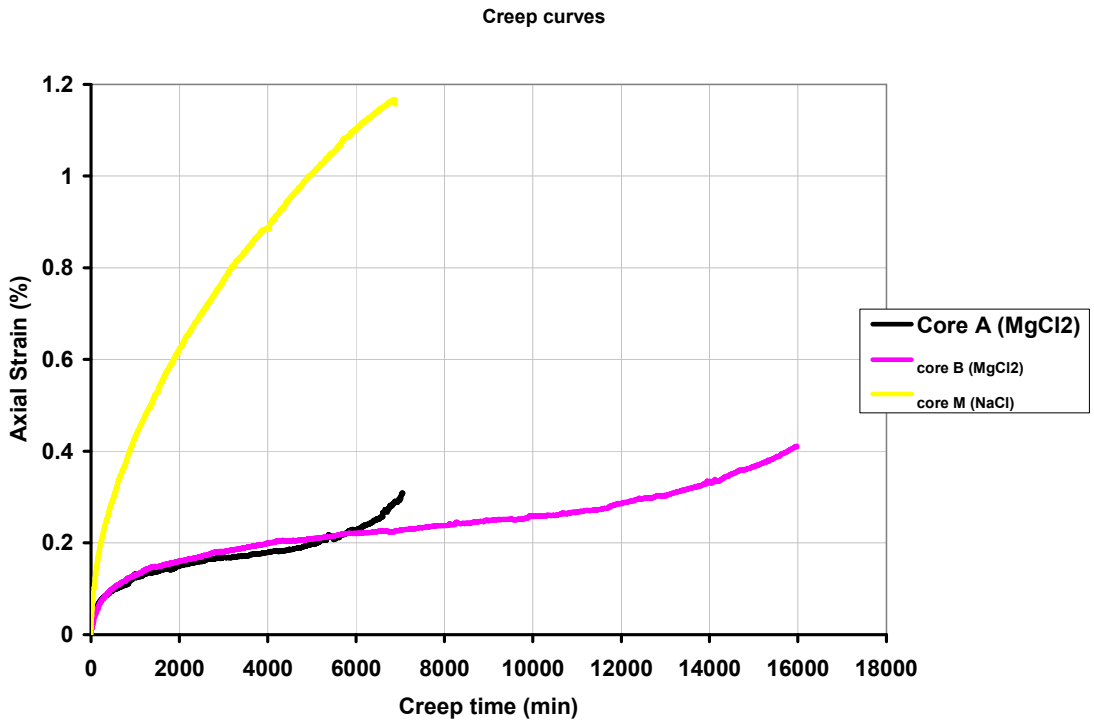

Fig. 5.6 Creep curve for cores A, B and M

Recent studies by Madland et al., (2009)[12] points to dissolution and precipitation as possible chemical mechanisms that cause weakening of chalk. In the light of this, it becomes imperative to understand the differences in chemical effects of $MgCl_2$ and NaCl on chalk, as it relates to dissolution and precipitation. This will be pursued a little further as presented in section 5.2.6.

5.2.2 Brine effects at low pressures

The creep curves for cores C, D and G is shown in fig. 5.8. Cores C and D were flooded with $MgCl_2$ while core G with NaCl. All the tests were performed at 0.7MPa pore pressure and subjected to effective stress of 12MPa during the creep period.

Considering the creep strain developed by the samples, it can be seen from fig. 5.7 that core G deformed by more than factors of 4 and 2 compared to cores C and D respectively, within the same creep period of about 6000minutes. The higher creep

strain on core G may not be attributed to the porosity because core D even has a little higher porosity than core G (table 4.1). The high deformation obtained on core G is in line with the result obtained by Kulathilagan, (2009)[40]. The test involves injecting distilled water, followed by NaCl at low pressures through the chalk core, fig. 5.8. It was observed that the creep strain increased from about 0.8% to more than 1.4% when flooding was changed from DW to NaCl. Knowing that tests on cores C, D and G were subjected to the same pore pressure and exposed to similar effective stress, it becomes reasonable therefore to argue that the presence of NaCl in core G accounts for the high creep strain.

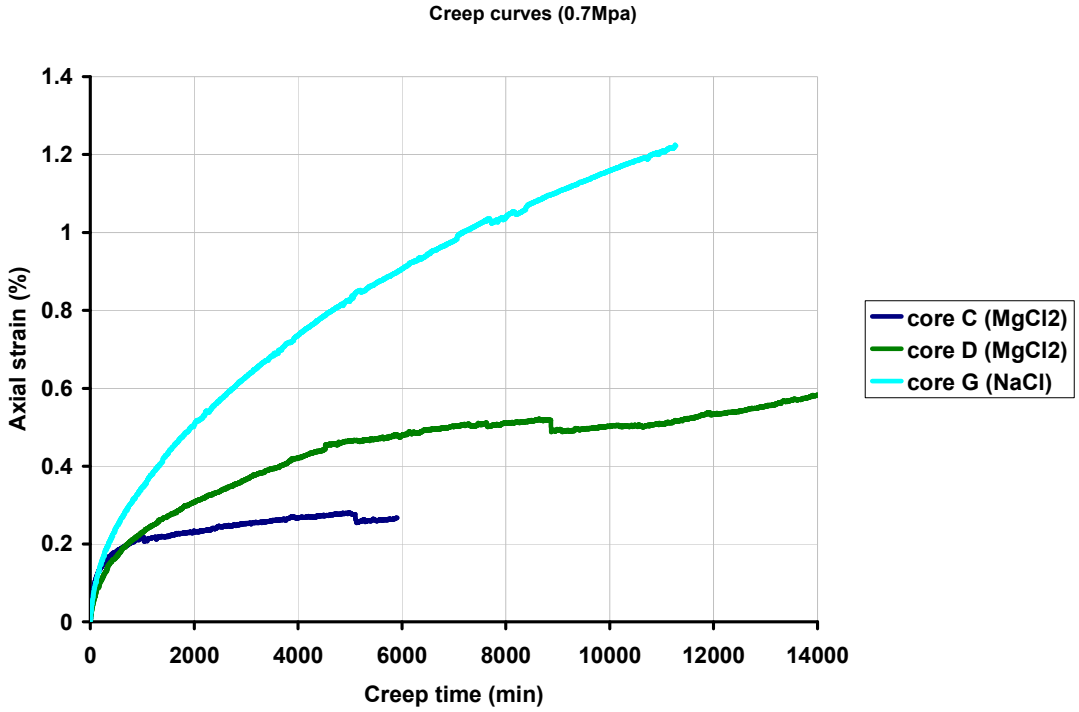

Fig. 5.7 Creep curves for cores C, D and G

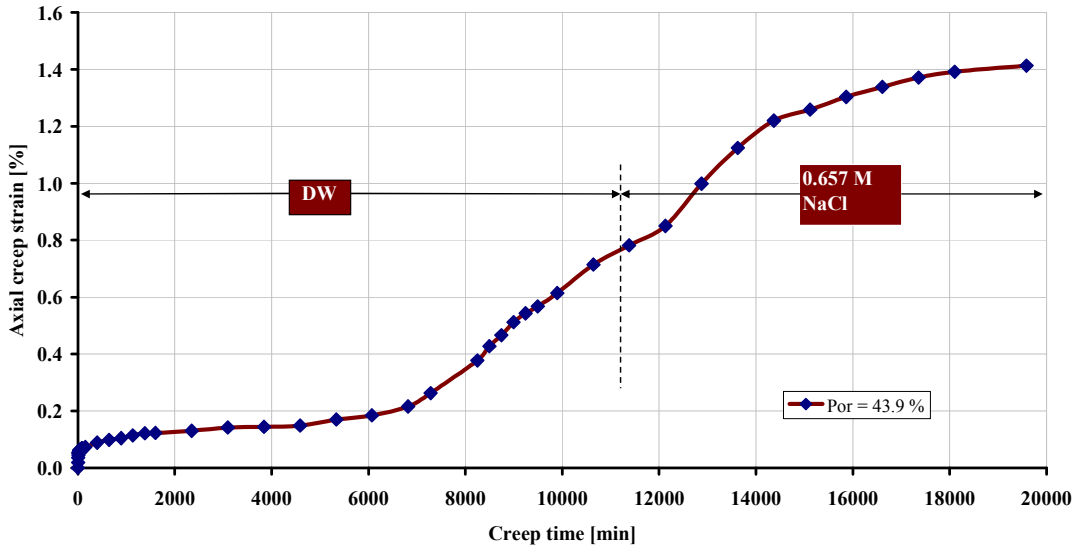

Fig. 5.8 Creep curve for chalk flooded with DW and NaCl (Kulathilagan, 2009)

By observing the creep curve for core D in fig. 5.7, it may seem there was "accelerating-like" creep as observed in cores A and B. This is not necessarily the case because the non-uniform creep curve actually resulted from fluctuation in pore pressure during the test. It happened that at creep time of 4520mins, there was sudden, unexpected drop in pore pressure to 0.1MPa. This resulted in increase in the effective stress on the sample to 12.6MPa. In an attempt to restore the pore pressure, the flooding rate was increased to 0.09ml/min from 0.05ml/min and the pressure became relatively stable around 0.55MPa. After about 2days, the pore pressure was restored to the original 0.7MPa and the flooding rate changed to initial 0.05ml/min. The creep curve then began to take the original trend as it was from the beginning.

Inasmuch as loss of pore pressure is undesirable during the tests, the creep trend in core D reveals that there is increase in axial strain after the flooding rate is reduced or removed entirely. Midtun, (2009)[39] carried out a similar test as on core D on Stevns Klint chalk with 45.93% porosity and a similar trend was observed, fig.5.9. The test procedure involves flooding 0.219M $MgCl_2$, by-pass the core for some days, and then continue flooding again. It was observed that the axial strain increased rapidly during the by-pass and when flooding continued.

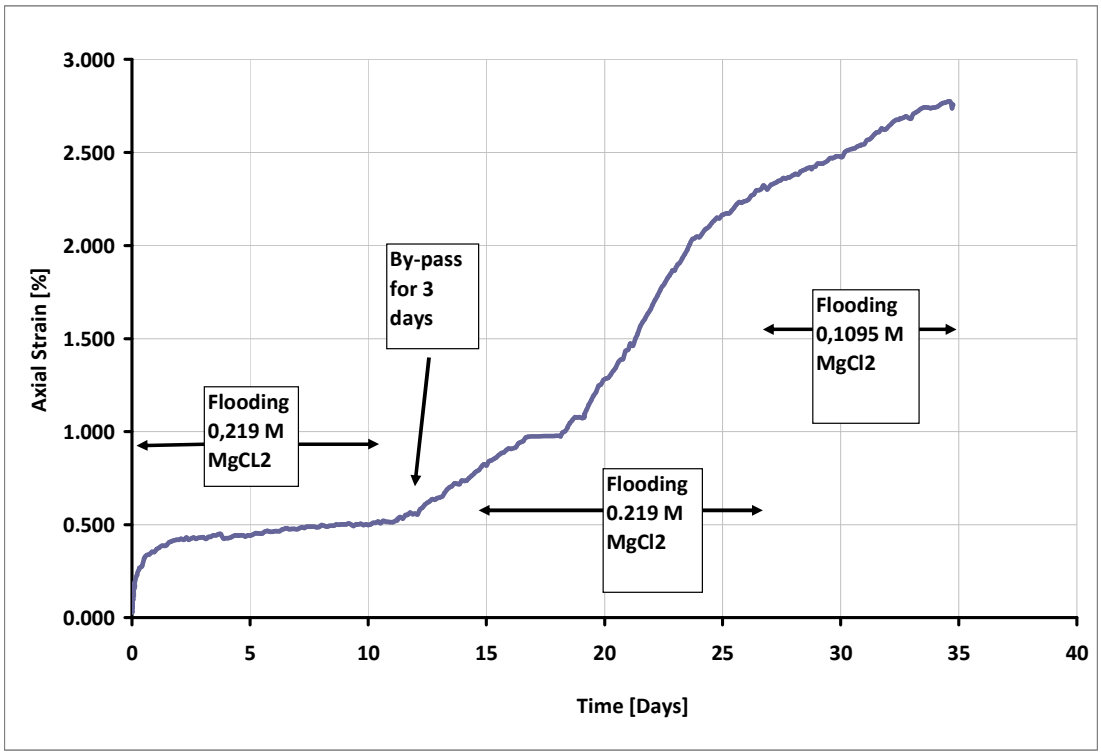

Fig 5.9 Creep curve, flooding with $MgCl_2$, by-pass and continued flooding. Midtun (2009).

5.2.3 Pressure effects, $MgCl_2$ brine

Tests on cores A and B were performed at 40MPa pore pressures and 0.7MPa pore pressures on cores C and D. All the samples were flooded with $MgCl_2$ and exposed to 12MPa effective stress during the creep period.

As can be seen from fig.5.10, it seems that the cores deform more at low pressures than at higher pressures during creep. For instance, core A developed a strain of about 0.233% after 6000mins of creep, core D deformed by as much as 0.482% within the same time period. One may have attributed this to the higher porosity of core D compared to the rest samples but the higher deformation of core C compared to cores A and B reveals otherwise. Cores B and C have similar porosities, and based on the fact that core C is believed to have higher mechanical strength than other samples, it could therefore be that the higher deformations on cores C and D are as result of lower pressures they were subjected to. This is quite contrary to theory of chalk dissolution with respect to pressure. Theory states that $CaCO_3$ (chalk) is less soluble at high temperatures but more soluble at high pressures [Jury, 2009][25] .

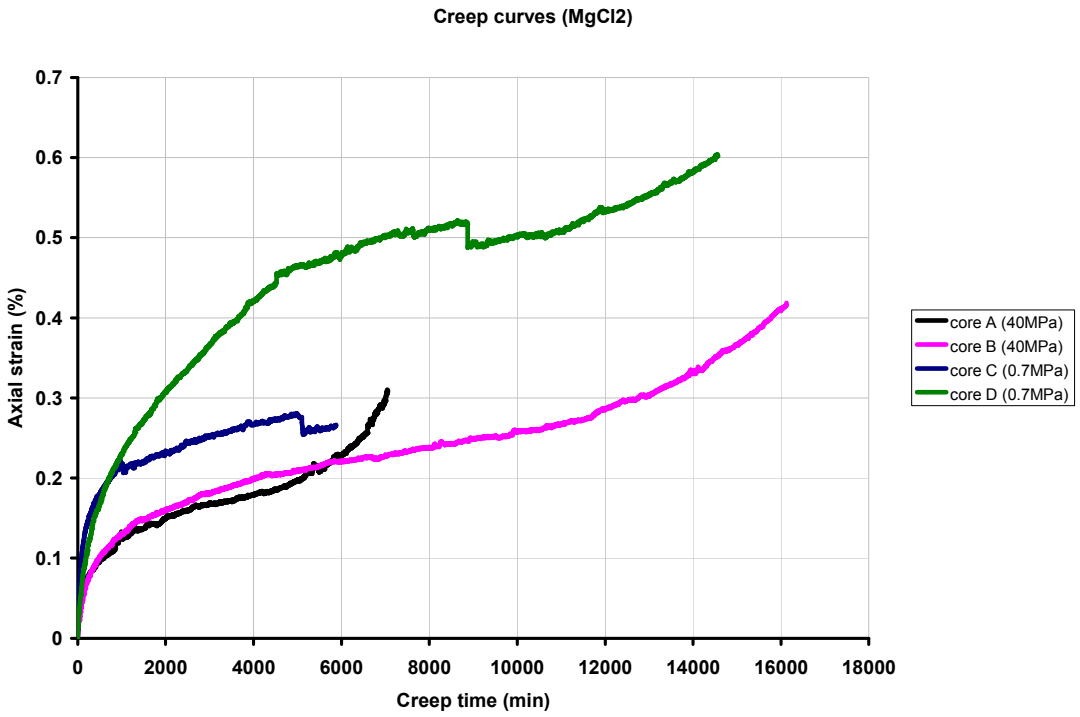

Fig. 5.10 Creep curves for cores A, B, C and D

Another significant difference that can be observed from the figure is that cores exposed to high pore pressures developed "accelerating-like" creep while those subjected to low pressures have no such creep trend observed on them.

5.2.4 Pressure effects, NaCl brine

Fig.5.11 shows the creep curves for cores G and M. Test on core G was carried out at a lower pressure of 0.7MPa while on core M, it was 40MPa. Both samples were flooded with NaCl and exposed to 12MPa effective stress during creep.

From the figure, it can be observed that core M deformed a little more than core G, when the same creep period is considered. For example, at a creep time of 6000mins, the deformation on core M is about 1.104% while it is 0.907 % on core G.

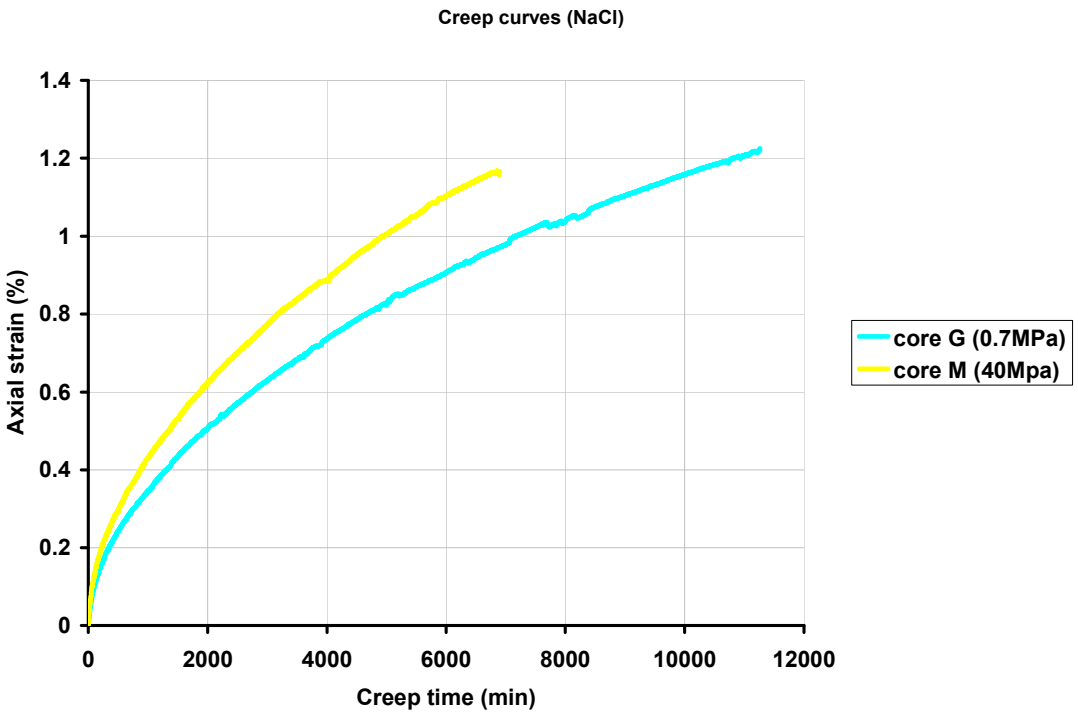

Fig. 5.11 Creep curves for cores G and M

Theory states that $CaCO_3$ (chalk) is less soluble at high temperatures but more soluble at high pressures [Jury, 2009][25]. It could therefore be that the samples dissolve more at high pressures, hence the greater deformation observed on core M. However, the porosity of both samples and their creep trends are quite similar.

5.2.5 Combined creep curve

Fig. 5.12 presents the creep curves for all the samples. Table 5.2 summarises the deformation of each sample under their respective test conditions.

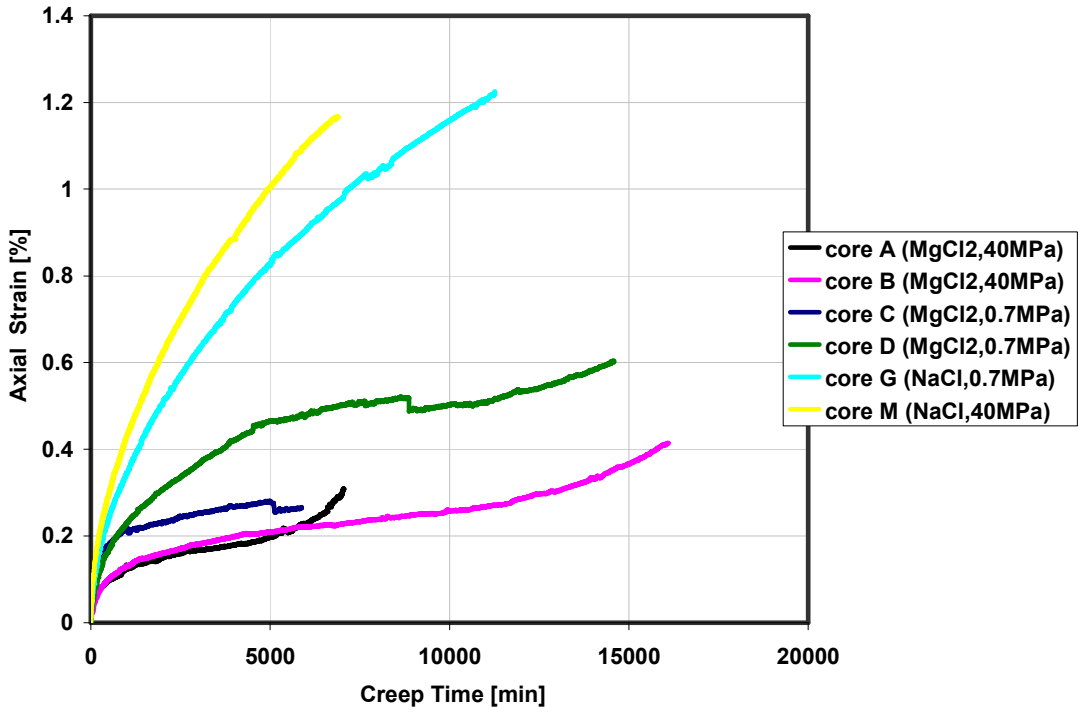

Fig. 5.12 Combined creep curves

It can be seen from the curves that the deformation for cores flooded with NaCl is significantly higher than those flooded with $MgCl_2$. There also seems to be higher deformation for cores flooded with $MgCl_2$ at lower pore pressures compared to the ones at higher pressures, when the same creep period is considered. "Accelerating-like" creep was observed on cores exposed to $MgCl_2$ at high pore pressures but no such creep was observed at low pressure tests and on samples injected with NaCl.

Table 5.2 Deformation summary

Sample name	Flooding fluid	Pore pressure (MPa)	Flooded volume (PV)	Str at max load (%)	Creep strain (%)	Total strain (%)	Str at 6000 mins of creep (%)
A	$MgCl_2$	40.00	12.14	0.58	0.31	0.89	0.23
B	$MgCl_2$	40.00	24.55	0.54	0.41	0.95	0.22
C	$MgCl_2$	0.70	10.93	0.45	0.27	0.71	0.28
D	$MgCl_2$	0.70	27.11	0.81	0.60	1.41	0.48
G	NaCl	0.70	19.49	0.72	1.22	1.94	0.91
M	NaCl	40.00	11.73	0.99	1.17	2.15	1.10
N	$MgCl_2$	40.00	12.24	0.93	–	–	–
O	$MgCl_2$	40.00	14.85	0.62	–	–	–

The influence of pore pressure on chalk deformation seems to depend on the brine. From fig.5.12 it can be observed that core M has higher deformation at high pore pressure than core G at a lower pressure. The period of creep vary for the different

samples. Some of the samples have about 4 days of creep while others creep for more than 11 days. In order to have a uniform comparison on the deformation, the strain developed by each sample after 6000minutes of creep was determined for each sample and tabulated as shown in table 5.2. Also, the total deformation, that is, deformation at maximum hydrostatic load plus deformation during creep for each sample was also determined and shown in table 5.2. From the table, it is obvious that cores flooded with NaCl deformed more than those injected with $MgCl_2$.

5.2.6 "Accelerating-like" creep on cores A and B

From the mechanisms of dissolution and precipitation, theory states that rates of dissolution and precipitation of $CaCO_3$ (chalk) are proportional to the saturation state (Mucci, 1983. Jury, 2009)[25]. When solid $CaCO_3$ is dissolved in a solvent, the resulting solution will either be saturated or under saturated depending on the concentration. If the solution is saturated, precipitation of minerals will take place in order to maintain equilibrium. Mineral precipitation on the other hand will not take place if the solution is under saturated. Usually, ions in injected brines form complexes when in contact with chalk. Hiorth et al., (2008)[29] noted that a lot of minerals are supersaturated at 130^oC when seawater is injected into chalk reservoirs, which subsequently lead to precipitation of several minerals. It could therefore be that when chalk cores are flooded with the respective brines, there will be dissolution followed by a possible precipitation, if a saturated solution is formed. This process may probably lead to enhanced compaction of the chalk.

Magnesium form ion pairs with CO_3^{2-}, and with the knowledge that $MgCO_3$ is more soluble than $CaCO_3$ (Jury, 2009), it may be that when $MgCl_2$ was flooded through the cores, Mg^{2+} from the injected brine form ion pairs with CO_3^{2-} from the chalk. The consequence may therefore be high dissolution of the cores. This may be the case for cores A and B in fig. 4.6 within the first creep phase, that is, the transient creep region. As more $MgCl_2$ is injected more dissolution takes place such the solution becomes saturated. The resulting saturated solution leads to precipitation of minerals. The precipitates will cause more cementation and more friction between the grains because the chalk grains will not be able to slide easily between each other. This may explain the linear deformation with time as observed within the steady-state creep region observed for cores A and B. It is not quite easy to explain what happens in the last creep phases of cores A and B but if considered from equilibrium point of view, it could be that precipitation gradually reduced after the solution became under saturated. That is, while the precipitation process lasts the solution became under saturated and in attempt for the system to maintain equilibrium, further dissolution of the cores has to take place. The more dissolution resulted in further compaction of the cores, such that the "accelerating-like" creep began to form as observed for the two cores.

On the other hand, NaCl has little or no reaction with the cores (as shown in IC result in fig.4.11). However, the very fact that some traces of calcium ions were detected in the effluents for the cores flooded with NaCl signifies there was at least, some dissolution taking place. It could be that the dissolution of the chalk cores with NaCl is quite minimal, such that a saturated solution is never formed and hence no

precipitation takes place. The minimal dissolution is continuous, with a subsequent increase in deformation as observed for core M in fig.4.7.

5.3 Chemical analyses of the fractioned effluents

Sampling of flooding effluent usually began prior to and during hydrostatic loading, and during the entire creep period. The samples were first diluted to 50 times their original concentration in order to stay in the linear region of the calibration curve. Generally, the concentrations of sampled effluents increase remarkably at first before it stabilizes after some time, fig.5.13. This is because the first effluents sampled are usually a mixture of distilled water and the flooded brine since all the cores were saturated with distilled water from the beginning.

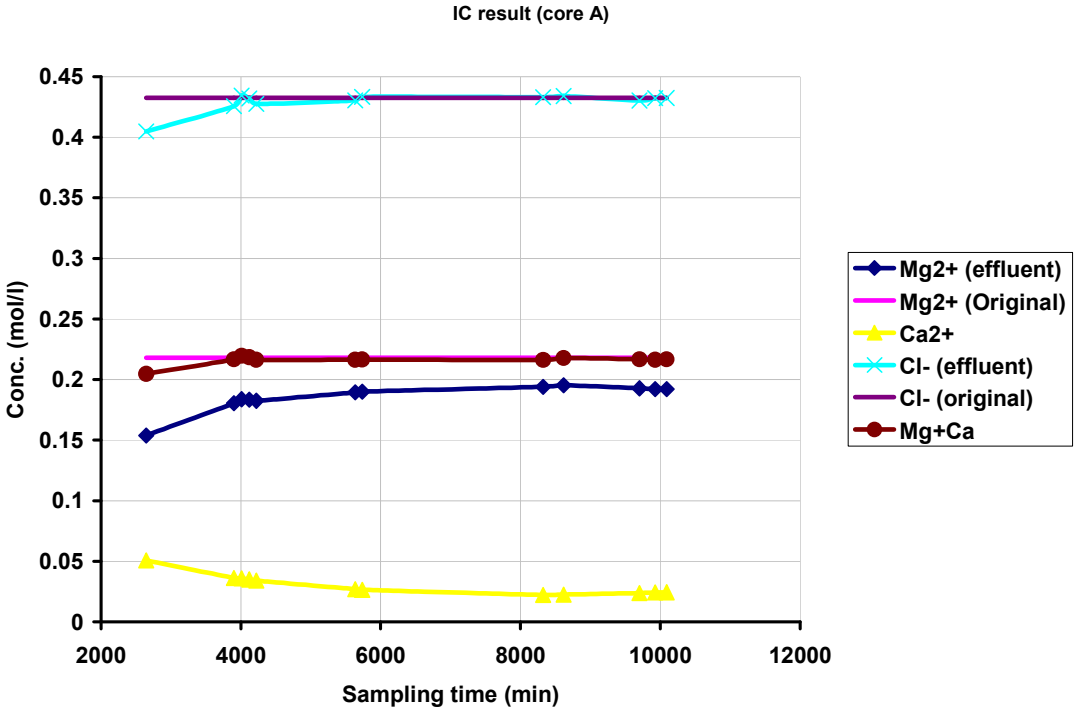

Fig. 5.13 IC result for Mg^{2+}, Ca^{2+} and Cl^{-} ions in sampled effluent for core A flooded with $MgCl_2$

From the chemical analysis of the effluents, it was observed that all the cores flooded with $MgCl_2$ show a significant loss of magnesium inside the core and production of calcium at the same time. There was considerable amount of calcium detected in the effluent, which otherwise, was produced from the cores. From fig. 5.13, it can be seen that the concentration of Mg^{2+} ion in the effluent is less than the original concentration in the injected brine. The amount of magnesium lost inside the core seems to be equal to the amount of calcium produced from the core. That is, there was a one-to-one exchange between Mg^{2+} and Ca^{2+} ions since the summation of magnesium and calcium concentrations in the effluent equals the concentration in the injected brine. For example, at a sampling time of 5736minutes the concentration of magnesium in the effluent reduced to 0.19mol/l while 0.0266mol/l of calcium was detected in the

effluent. The loss of magnesium inside the core increased a little further and then stabilizes as the brine injection is continued. The reverse is the case for calcium in the effluent. Element analysis of core A studied using SEM also confirms significant loss of magnesium inside the core, fig.5.14.

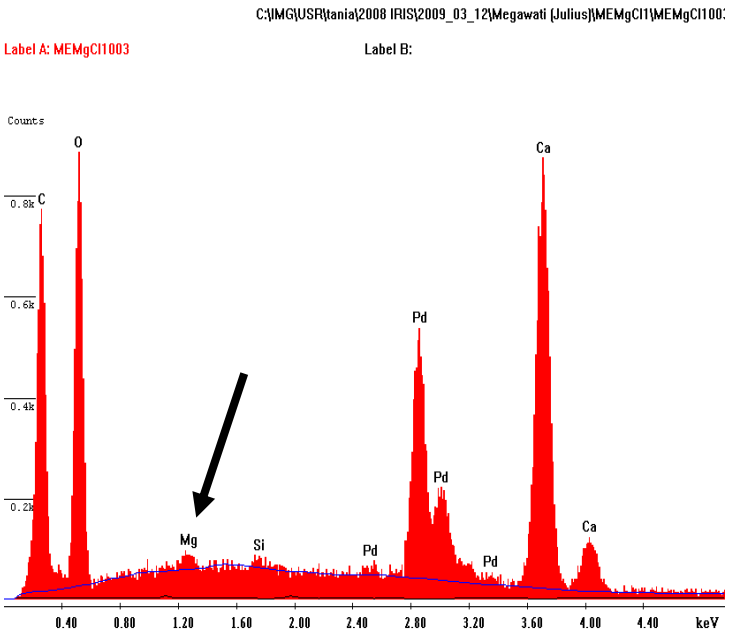

Element	Wt %	At %
C K	08.30	14.38
O K	48.39	62.89
MgK	00.56	00.48
SiK	00.32	00.24
CaK	42.43	22.01

Fig. 5.14 Element analysis result for core A

Fig. 5.15 SEM picture of core A

The SEM picture of core A is as shown in fig. 5.15. From the image, it seems that mineral precipitation was not very high or that the precipitates are not quite visible.

There also seems to be little or no reaction between chlorine and chalk as seen on the fig.5.13. The concentration of chlorine in the effluent gets to its original concentration rapidly after few period of flooding. This is the case for the cores flooded with either $MgCl_2$ or NaCl.

The chemical analysis on cores flooded with NaCl shows that reaction between the chalk cores and NaCl seems to be quite minimal compared to $MgCl_2$, fig. 4.11. From the figure, it can be seen that it takes only 2300 minutes for the Na^+ ion to reach close to its original concentration. Thereafter the concentrations remain almost constant during the remaining period of injection. The amount of calcium detected in the effluent is relatively small compared to the case in $MgCl_2$ injection. For example, at a time of 2400minutes, the concentration of Ca^{2+} is about 0.006125mol/l and the concentration decreases as injection is continued. The fact that calcium is ever produced may signify there was dissolution of the chalk during NaCl injection. This may explain the minimal, continual dissolution, which causes higher deformation observed in cores G and M.

Chapter 6

Conclusion

Several tests were carried out on core samples of Stevns Klint chalk at both high and low pore pressures while injecting $MgCl_2$ and NaCl brines. The average porosity of the test samples is about 43% which is quite low compared to the general higher porosity of about 48% of Stevns Klint chalks. The lower porosity confers some level of mechanical strength on the samples such that the average yield values were relatively high. Average yield strength for the samples is 8.22MPa which is higher than 6.6MPa yield values obtained by Breivik, (2007) and Korsnes et al. on cores with 48% porosity.

It was observed that yield strength and strain developed by the samples at maximum hydrostatic loading does not dependent on the pore pressures. This is in line with studies by Breivik, (2007). However, cores exposed to NaCl at high pore pressures deformed by more than 40% compared to those flooded with $MgCl_2$ at the same pressure. There was no significant correlation in terms of strain at maximum hydrostatic load for the samples flooded with both $MgCl_2$ and NaCl at low pressures.

During the creep phase, it was observed that samples flooded with NaCl deformed by more than a factor of 3 compared to those exposed to $MgCl_2$ at both high and low pressures within the same creep period. It was suggested that the lower creep strain on samples exposed to $MgCl_2$ was as a result of higher chalk dissolution, and a subsequent precipitation of minerals. The argument was based on the theory that rates of dissolution and precipitation of $CaCO_3$ (chalk) are proportional to the saturation state (Mucci, 1983. Jury, 2009)[25]. Injecting the cores with $MgCl_2$ leads to higher dissolution, resulting in a saturated solution. In order to maintain equilibrium, precipitates were formed. The precipitates restrict the chalk grains from sliding freely between each other because of friction, and also increase cementation between the chalk grains, hence reducing the rate of deformation. Cores flooded with NaCl dissolves minimally such that the solution is perpetually under saturated and no precipitates are formed. This may therefore explain the enhanced compaction with NaCl.

Also, samples flooded with $MgCl_2$ show higher creep strain at low pore pressures than at higher pressures. This is contrary to theory which states that $CaCO_3$ (chalk) is less soluble at high temperatures but more soluble at high pressures [Jury, 2009][25]. However, samples exposed to NaCl shows slightly more deformation at higher pressures compared to the one tested at low pore pressure. Further, "accelerating-like" creep was observed on cores injected with $MgCl_2$ at high pore pressures but no such creep trend occurred in other test samples.

As expected, the chemical analysis of fractioned effluents show that all the cores flooded with $MgCl_2$ show a significant loss of magnesium inside the core and production of calcium at the same time. Chlorine was observed to be chemically inert with chalk while traces of calcium were detected in the effluents of cores flooded with NaCl. Detection of calcium in the effluents of cores exposed to NaCl may be a pointer that at least, some dissolution of chalk was taking place.

Chapter 7

FUTURE WORK

In order to have a detailed understanding of the influence of the brines on the mechanical strength of chalk, it is recommended that;

1. Further tests to be performed at high pressures with NaCl since only one test was successfully carried out at this test condition during this thesis work.

2. Tests should be performed at both high and low pressures with a mixture of the two brines in equal proportion. This will help to determine if the deformation will be as high as when NaCl was used, low as in the use of $MgCl_2$, or intermediary between the two.

3. Carry out the tests at high pressures for a prolonged period in order to see the creep trends.

REFERENCES

[1] P.O. Roehl and P.W. Choquette, *Carbonate petroleum reservoirs*. Springer, 1985.

[2] Schlumberger, "Carbonate reservoirs," 2007. www.slb.com/carbonates.

[3] M.V. Madland, "Water weakening of chalk: A mechanistic study," PhD thesis, University of Stavanger, faculty of science and tech., 2005.

[4] R.I. Korsnes, "Chemical induced water weakening of chalk by rock- fluid interactions: A mechanistic study," PhD thesis, University of Stavanger, faculty of science and tech., 2007.

[5] E. Fjær, R.M. Holt, P. Horsrud, A.M. Raaen, R. Risnes, *Petroleum related rock mechanics*, 2nd edition, Develpoments in petroleum science 53, 1992.

[6] T.L. Blanton III, "Deformation of chalk under confining and pore pressure," SPE Science applications inc.,1981.

[7] H. Breivik, "Pore pressure effects in chalk," Masters thesis, University of Stavanger, 2007.

[8] R. Risnes "Deformation and yield in high porosity outcrop chalk," Stavanger university college, Elservier science ltd, 2001.

[9] B.S. Aadnøy, *An introduction to petroleum rock mechanics*, rev.2, University of Stavanger, 2003.

[10] E. Detournay and A.H.-D. Cheng, "Fundamentals of poroelasticity," Ch.5 *comprehensive rock engineering: principles, practice and projects*, vol.11, Pergamon press. Pp.113-171, 1993.

[11] A Dahou, J.F. Shao, M. Bederiat, "Experimental and numerical investigations on transient creep of porous chalk," Mechanics of materials 21(1995) 147-158, Elsevier science BV.

[12] M.V. Madland, A. Hiorth, R.I. Korsnes, S. Evje, L. Cathles, "Rock fluid interactions in chalk exposed to seawater, $MgCl_2$, and NaCl brines with equal ionic strength," Paper presented at 15th *European symposium on improved oil recovery*, Paris, 2009.

[13] R. Risnes, M.V. Madland, M. Hole, N.K. Kwabiah, "Water weakening of chalk – Mechanical effects of water-glycol mixtures," *Journal of Petroleum Science and Engineering*, vol.48, pp21-36, 2005.

[14] R.I. Korsnes, S. Strand, Ø. Hoff, T. Perdersen, M.V. Madland, T. Austad, "Does the chemical interaction between seawater and chalk affect the mechanical properties of chalk," *Eurock 2006*, London, pp. 427-434. ISBN 0415 410010.

[15] T. Austad, S. Strand, M.V. Madland, T. Puntervold and R.I. Korsnes, "Seawater in chalk: An EOR and compaction fluid," University of Stavanger. IPTC11370/SPE 118431, presented at IPTC, Dubai, 4-6 Dec. 2007.

[16] K. Bjørlykke and K. Høeg, "Effect of burial and diagenesis on stresses, compaction and fluid flow in sedimentary basins," *marine petr. geology*14, pp267-276,1997.

[17] F. Dasilva, J.P. Sarda, and C. Shroeder, "Mechanical behaviour of chalks. Second North Sea chalk symposium, Book II," Stavanger, Norway, 1985.

[18] G.H. Newman, "The effect of water chemistry on the laboratory compression and permeability characterization of North Sea chalks," *Journal of petroleum tech*. 35 pp. 976-980, 1983.

[19] M.A. Andersen, *Petroleum research in North Sea Chalk*, Stavanger : RF –

Rogaland Research, 1995.
[20] R. Hellman, P.J.N. Renders, J.P. Gratier, and R. Guiguet, "Experimental pressure solution of chalk in aqueous solutions. Part 2. Deformation examined by SEM, porosimeter, synthetic permeability, and X-ray computerised tomography. Water-Rock Interactions, Ore Deposits, and Environmental Geochemistry: A tribute to David A. Crerar.," *The Geochemical Society* , *Special publication* No.7, 2002b.
[21] R. Hellman, P.J.N. Renders, J.P. Gratier, and R. Guiguet, "Experimental pressure solution of chalk in aqueous solutions. Part 2. Deformation examined by SEM, porosimeter, synthetic permeability, and X-ray computerised tomography. Water-Rock Interactions, Ore Deposits, and Environmental Geochemistry: A tribute to David A. Crerar.," *The Geochemical Society* , *Special publication* No.7, 2002a.
[22] T. Heggheim, M.V. Madland, R. Risnes, and T. Austad, "A chemical induced enhanced weakening of chalk by seawater," *Journal Petroleum Science and Engineering*, vol.46 (2005), pp.171-184, 2005.
[23] S. Homand, and J.F. Shao, "Mechanical behaviour of porous chalk and effect of saturating fluid," *Mechanics of cohesive friction materials*, ch.5, pp.583-606, John Wiley & Sons, Ltd. 2000.
[24] R.I. Korsnes, M.V. Madland, and T. Austad, "Impact of brine composition on the mechanical strength of chalk at high temperature," *Euroock 2006, Multiphysics coupling and long term behaviour in rock mechanics* – Cottheim, A.V., Charlier, R., Thimus, J.F. and Tshibangu, J.P. (eds), Taylor & Francis, London, (2006), pp.133-140. ISBN 0 415 41001 0.
[25] C. Jury, "Aquarium chemistry: The carbonate system in the aquarium, and the ocean, part II: The interacting carbonate," Centre for marine science, biology and marine biology, University of North Carolina Wilmington, Feb., 2009.
[26] B.M. Rai, *Introduction to reservoir engineering*, (unpublished), University of Benin, Nigeria, 1998.
[27] T. Puntervold, S. Strand, and T. Austad, "New method to prepare outcrop chalk cores for wettability and oil recovery studies at low initial saturation." *Energy and fuels*, 21(6) 3425-3430, 2007.
[28] A.Mucci, "The solubility of calcite and aragonite in seawater at various salinities, temperatures, and one atmosphere total pressure," *Am J Sci* 283: 780-799, 1983.
[29] A. Hiorth, L.M. Cathles, J. Kolnes, O. Vikane, A. Lohne, R.I. Korsnes, M.V. Madland, "A chemical model for the seawater-CO2-carbonate system – aqueous and surface chemistry," Paper presented at *International Symposium of the Society of Core Analysts*, Abu Dhabi, 2008.
[30] E. Omdal, H. Breivik, K.E. Næss, R. Ramos, T.G. Kristiansen, R.I. Korsnes, A. Hiorth and M.V. Madland, "Experimental investigation of the effective stresss coefficient for various high porosity outcrop chalk," Paper presented at *International Symposium of the Society of Core Analysts*, Abu Dhabi, 2008.
[31] A. Hiorth, L.M. Cathles, J. Kolnes, O. Vikane, A. Lohne, M.V. Madland, "Chemical model of wettability change in carbonate rocks," Paper presented at *International Symposium of the Society of Core Analysts*, Abu Dhabi, 2008.
[32] M.V. Madland, K. Midtgarden, R. Manafov, R.I. Korsnes, T.G. Kristiansen, and A. Hiorth, "The effect of temperature and brine composition on the mechanical strength of Kansas chalk," Paper presented at *International Symposium of the Society of Core Analysts*, Abu Dhabi, 2008.

[33] P.D. Pattillo, T.G. Kristiansen, G.V. Sund, and R.M. Kjelstadli, "Reservoir compaction and seafloor subsidence at Valhall," SPE Eurock '98, Trondheim, Norway, SPE/ISRM 47274, 1998.
[34] I. Ruddy, M.A. Andersen, P.D. Pattillo, M.Bishlawl, and N. Foged, "Rock compressibility, compaction and subsidence in a high-porosity chalk reservoir: A case study of Valhall field," SPE 18278, 1989.
[35] Y. Kitano, M. Okumura, and M. Idogaki, "Incorporation of sodium, chloride and sulphate with calcium carbonate," *Geochemical Journal*, vol. 9,pp. 75-84, 1975.
[36] R.S. Arvidson, M. Collier, K.J. Davies, M.D. Vinson, J.E. Amonette, and A. Luttge, "Magnesium inhibition of calcite dissolution kinetics," Elsevier, *Geochimica et Cosmochimica* Acta 70 (2006) pp.583-594, 2005.
[37] R. Al Zadjali, Q. Fisher, C.A. Grattoni, and S. Al-Hinaib, "Chemical effects on chalk weakening and fracture deformation," Paper presented at 15th *European symposium on improved oil recovery*, Paris, 2009.
[38] J. Laurent, M.J. Bouteca, J-P. Sarda, and D. Bary, "Pore-pressure influence in poroelastic behaviour of rocks: Experimental studies and results," *SPE Formation Evaluation*, June 1993.
[39] B. Midtun, "Chalk-fluid interaction: The role of Mg^{2+} (using $MgCl_2$) and flooding status," Bachelor's thesis, Faculty of Science & Technology, University of Stavanger, 2009.
[40] P. Kulathilagan, "Chalk-fluid interaction: The role of specific ions ($MgCl_2$, $NaSO_4$ & NaCl) and flooding status," Bachelor's thesis, Faculty of Science & Technology, University of Stavanger, 2009.

Appendix A

Pressure history

The pressure histories of the different test samples are presented in this appendix. They include mainly the confining and pore pressures.

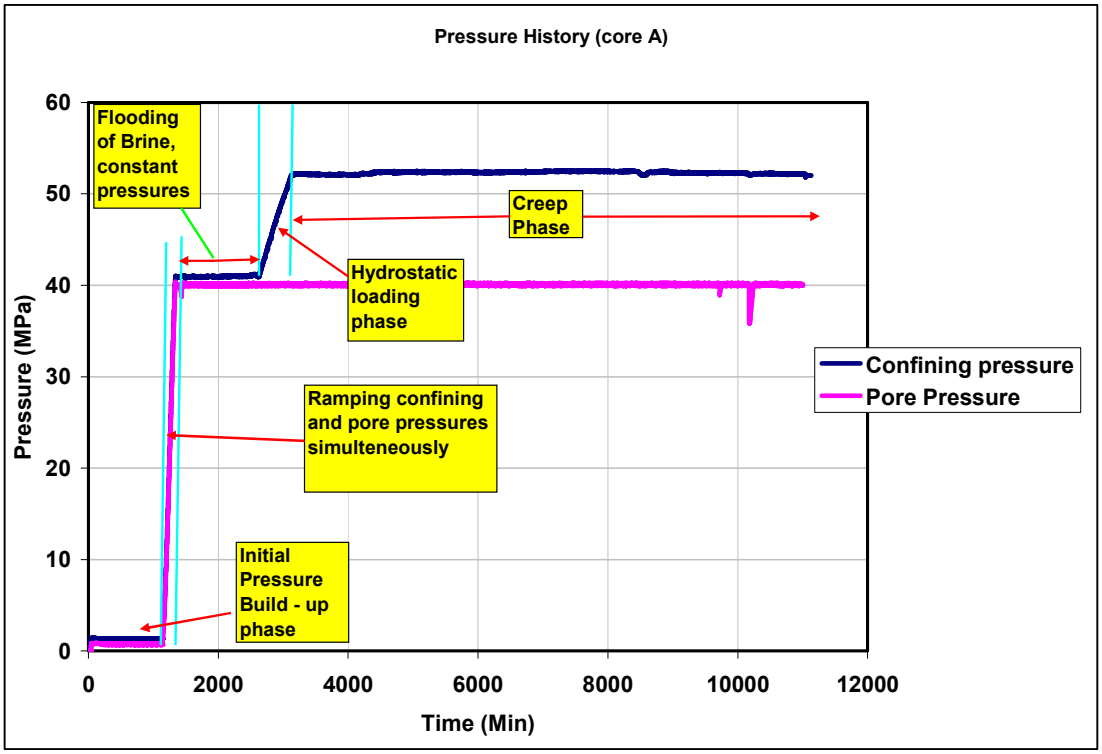

Pressure history for core A

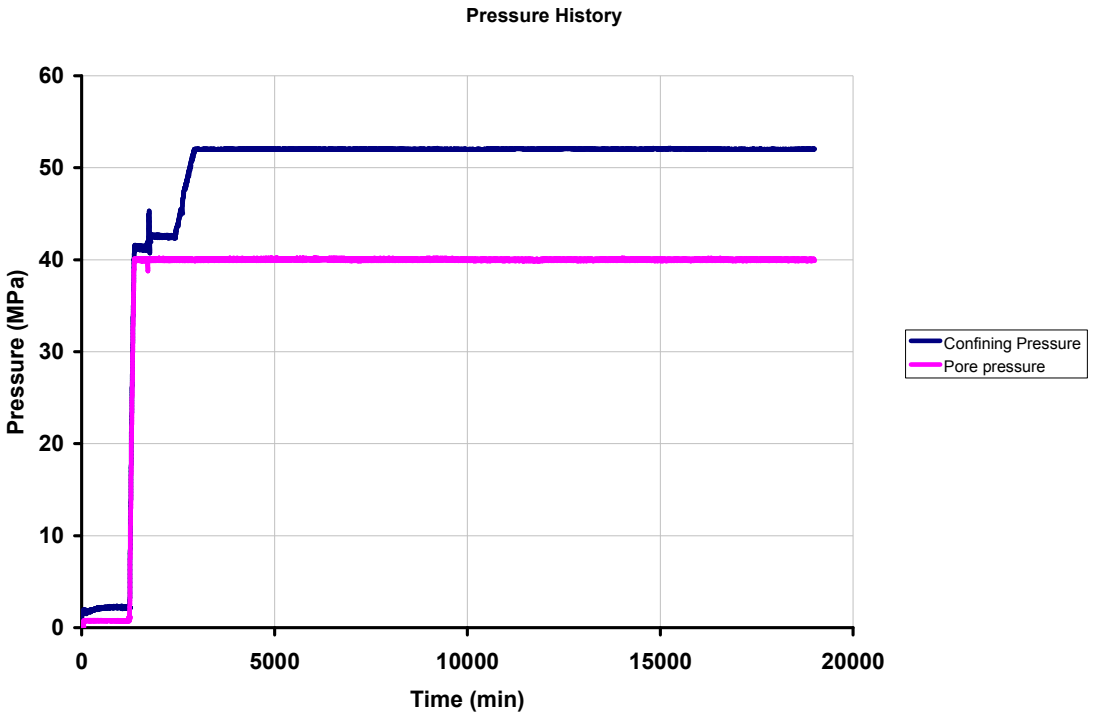

Pressure history for core B

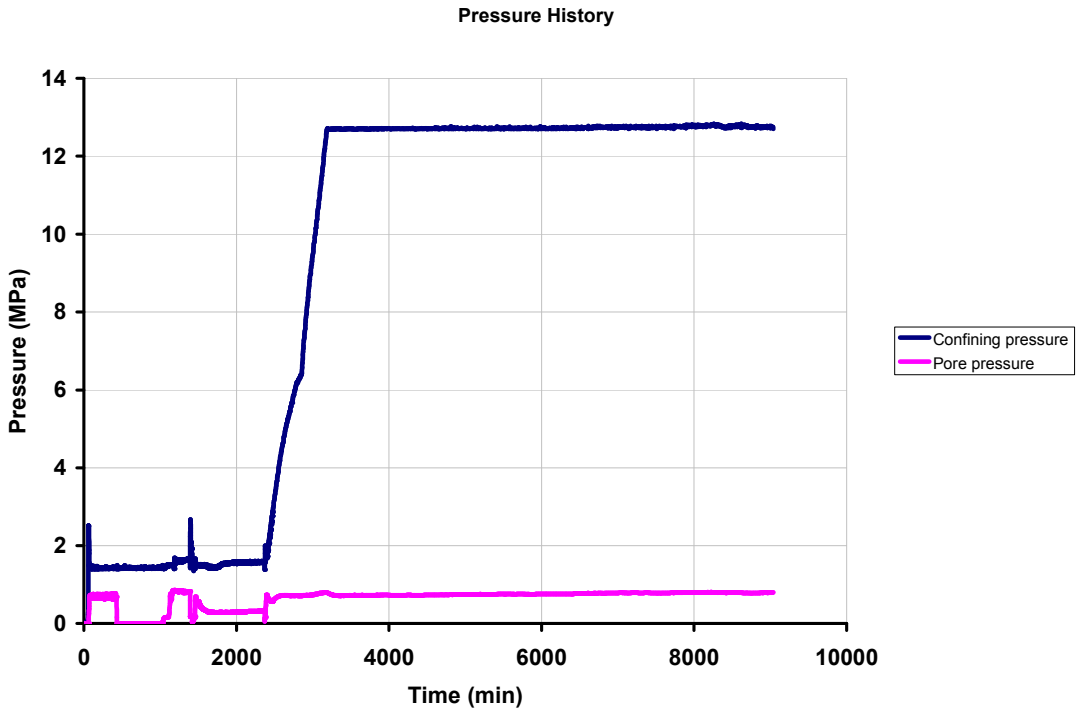

Pressure history for core C

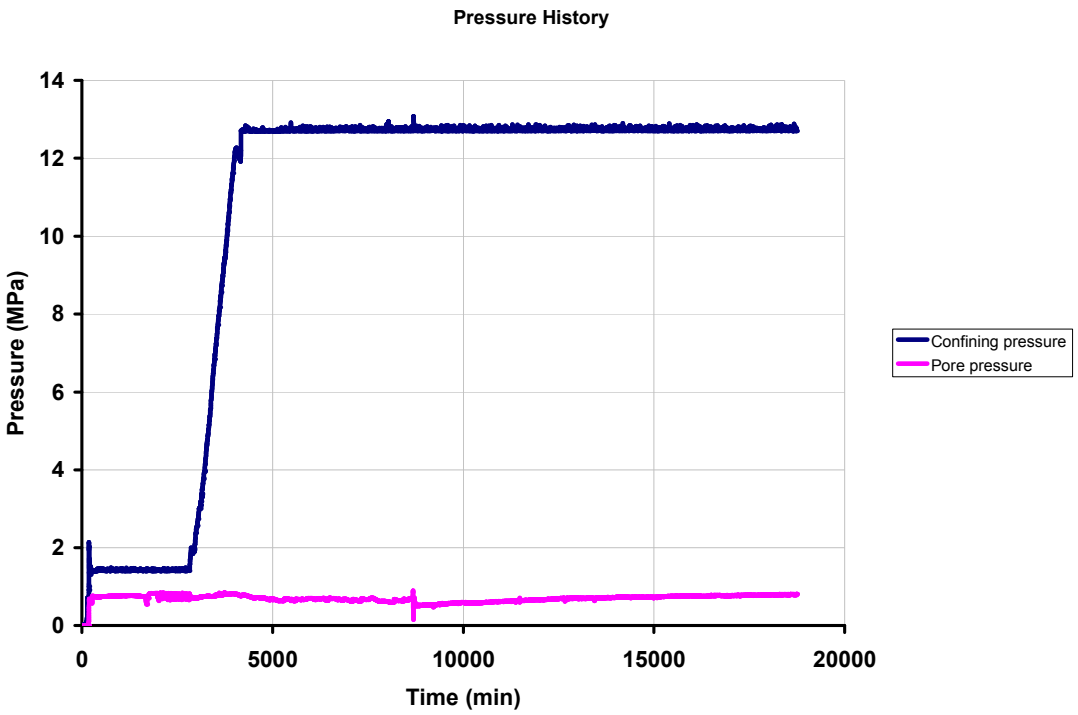

Pressure history for core D

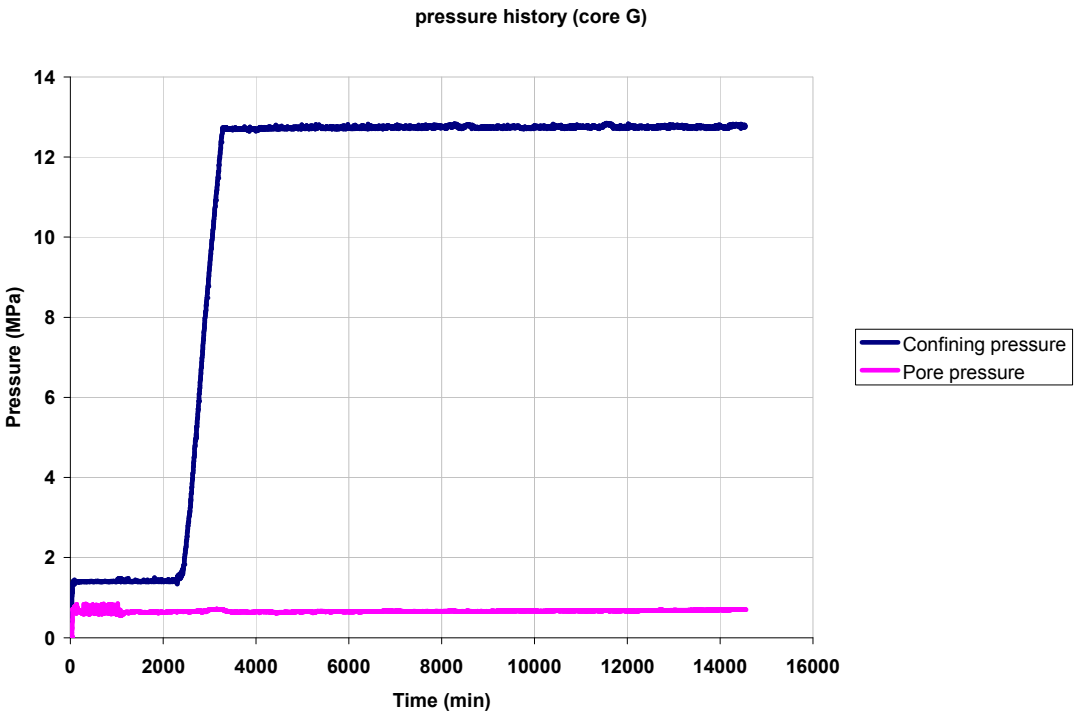

Pressure history for core G

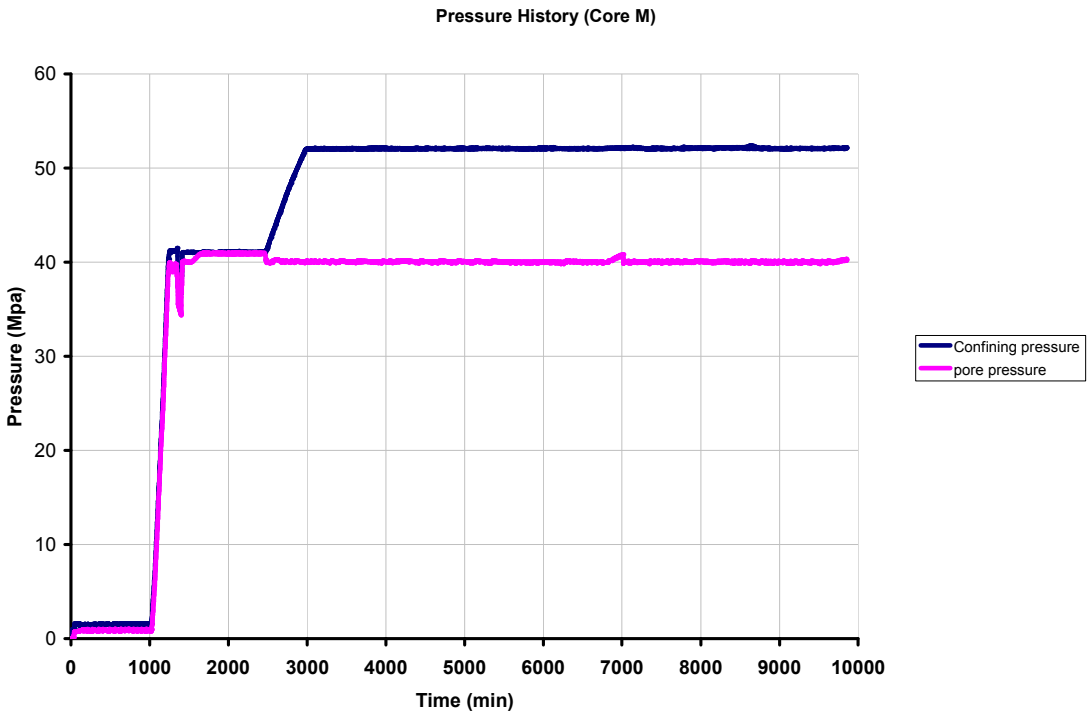

Pressure history for core M

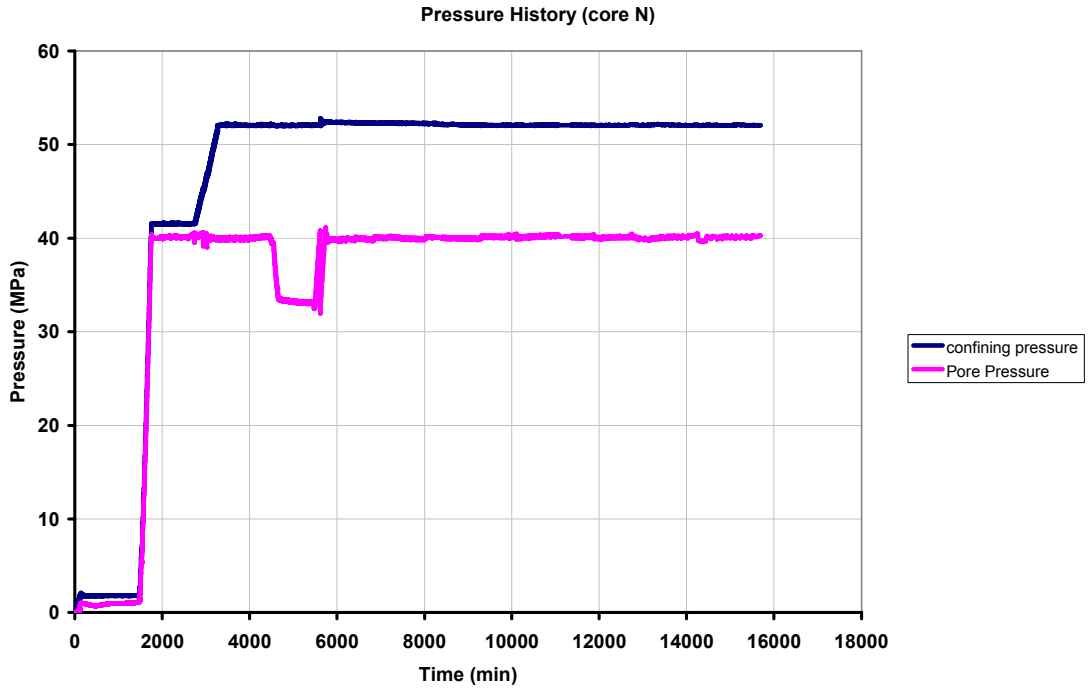

Pressure history for core N

As can be seen on the pressure history of core N, there was drop in pore pressure to 33MPa between 4700 to 5800minutes. This resulted in increase in effective stress on the sample to 19MPa for about 100minutes. The pore pressure was later restored but the core has already been compacted, such that the creep trend was no longer maintained. The creep curve is presented in appendix C.

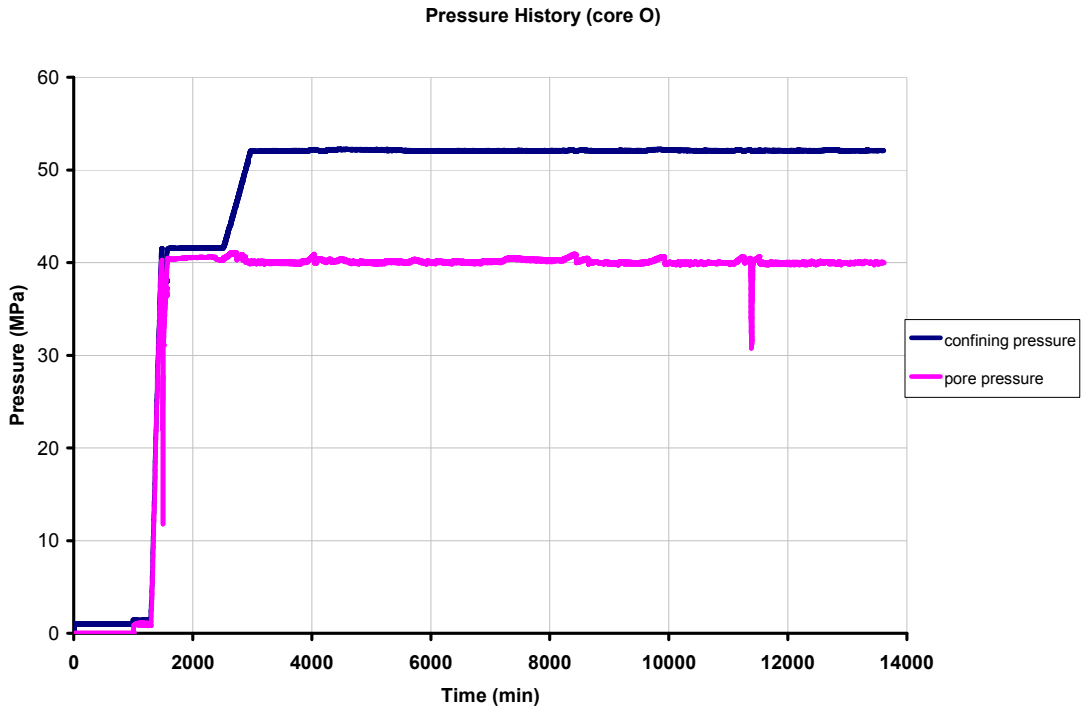

Pressure history for core O

Similar loss in pore pressure on core N was also observed on core O as can be seen on the pressure history. The pore pressure during the test on core O was fluctuating as can be seen on the non-smooth pore pressure curve in the figure. This resulted in non-uniform loading of the sample. Also, there was a sudden drop in pore pressure at about 11300minutes, with a subsequent over-loading and high compaction of the core.

Appendix B

Stress-strain curve for the samples.

In this appendix, the stress-strain plot for the samples will be presented. The plots will involve the stress-strain plots determined by both methods, that is, method 1 which is a plot of effective isotropic stress versus axial strain and method 2 which is a plot of effective isotropic stress versus differential pressure. However, the stress-strain curves plotted by using method 2 are not shown for all the samples because of non-linear increase in differential pressure as explained in section 4.3.

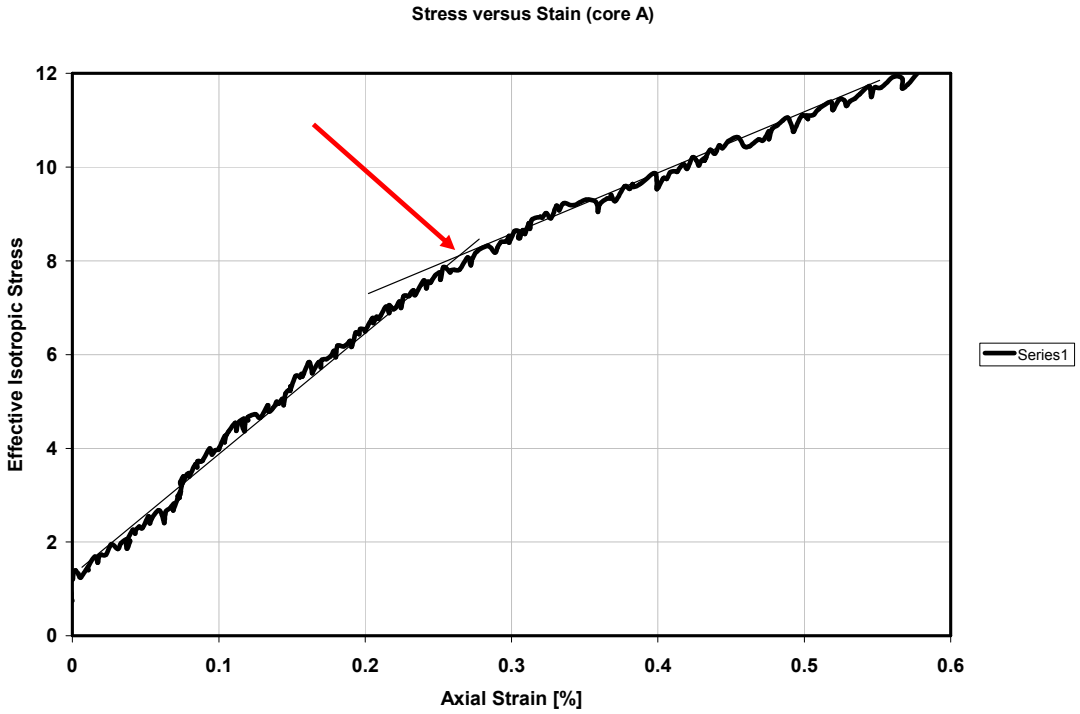

Stress versus strain for core A (method 1)

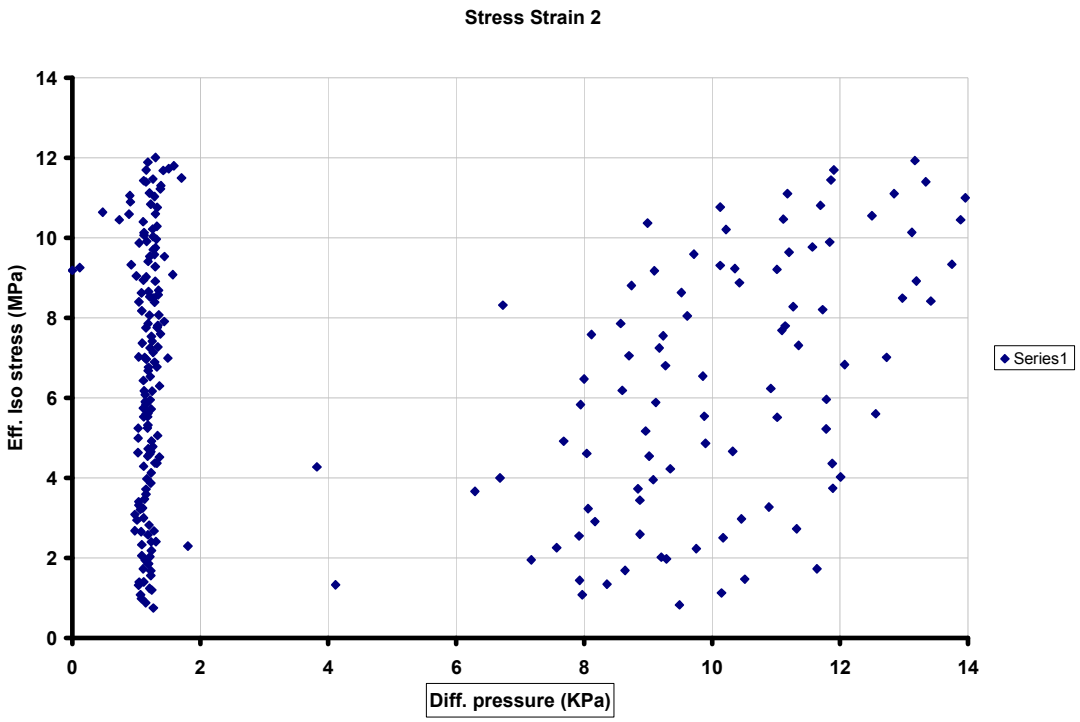

Stress versus strain for core A (method 2)

The yield point for core A using method 2 was quite difficult to determine because of scatter in the plot.

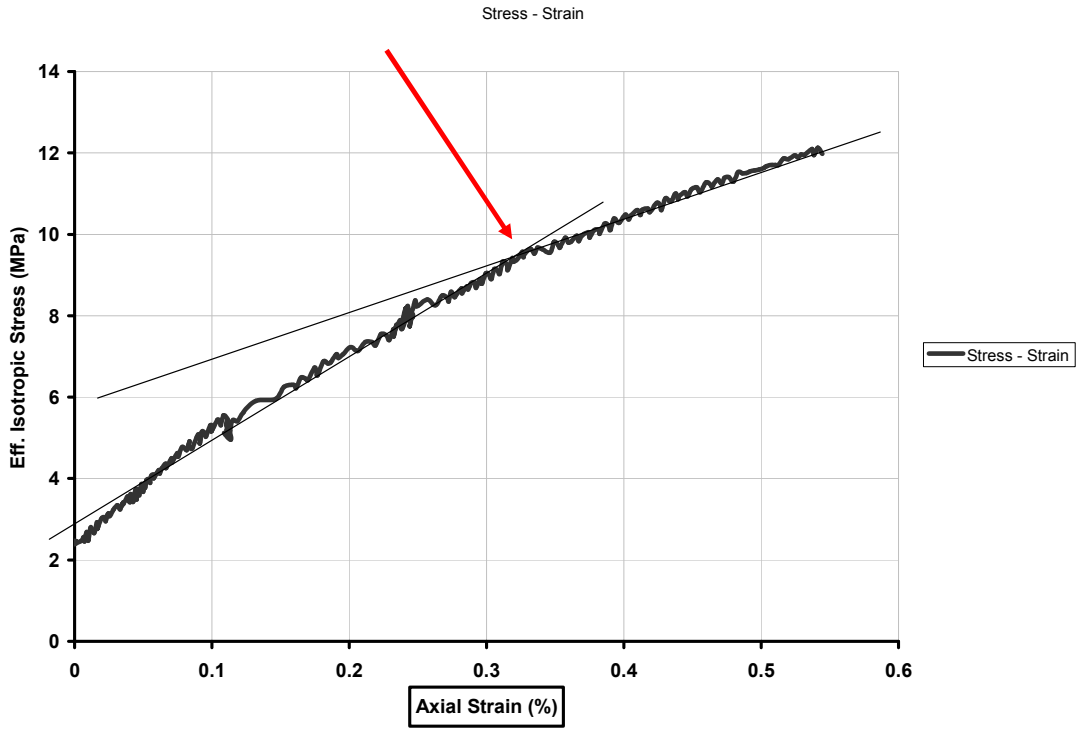

Stress versus strain for core B (method 1)

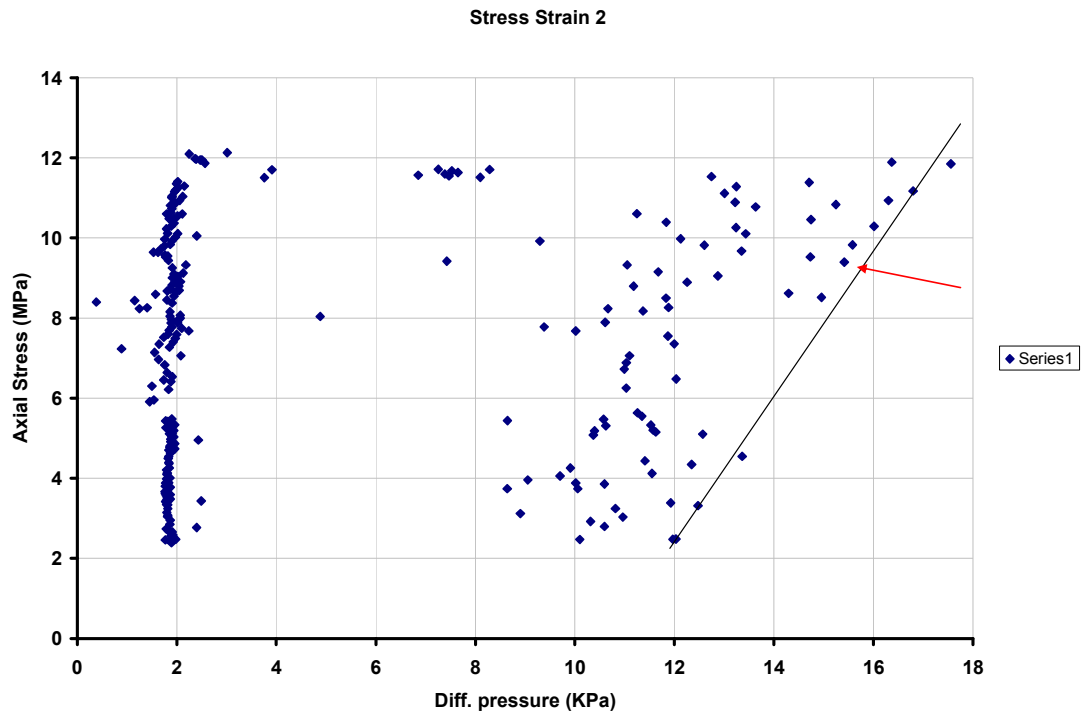

Stress versus strain for core B (method 2)

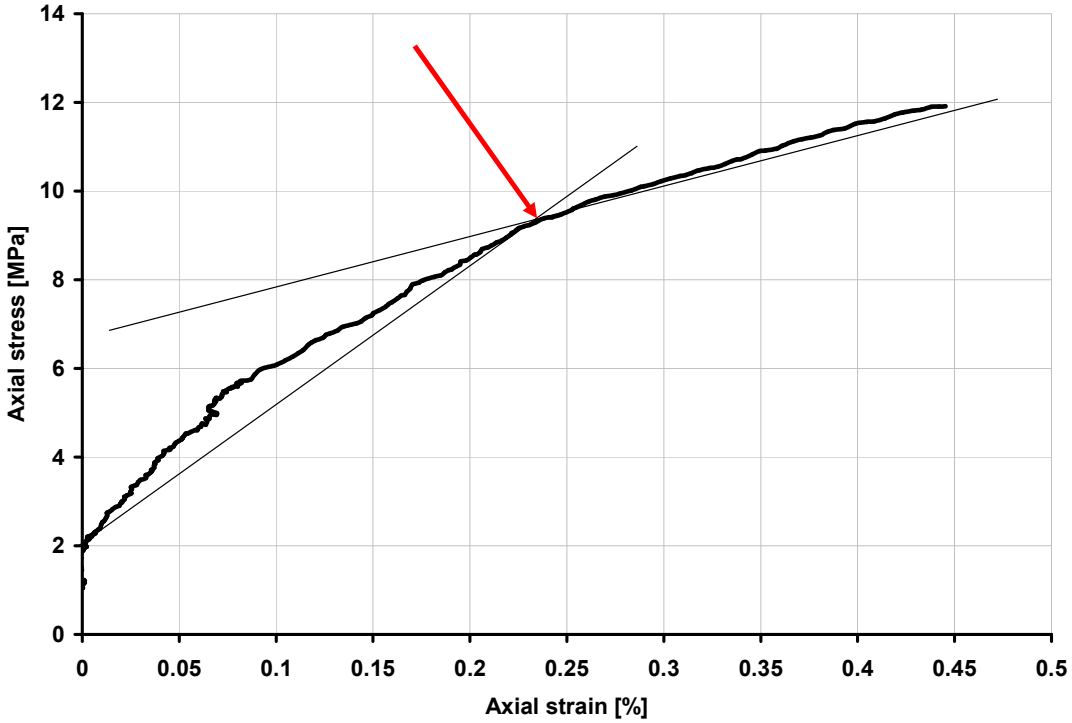

Stress versus strain plot for core C (method 1)

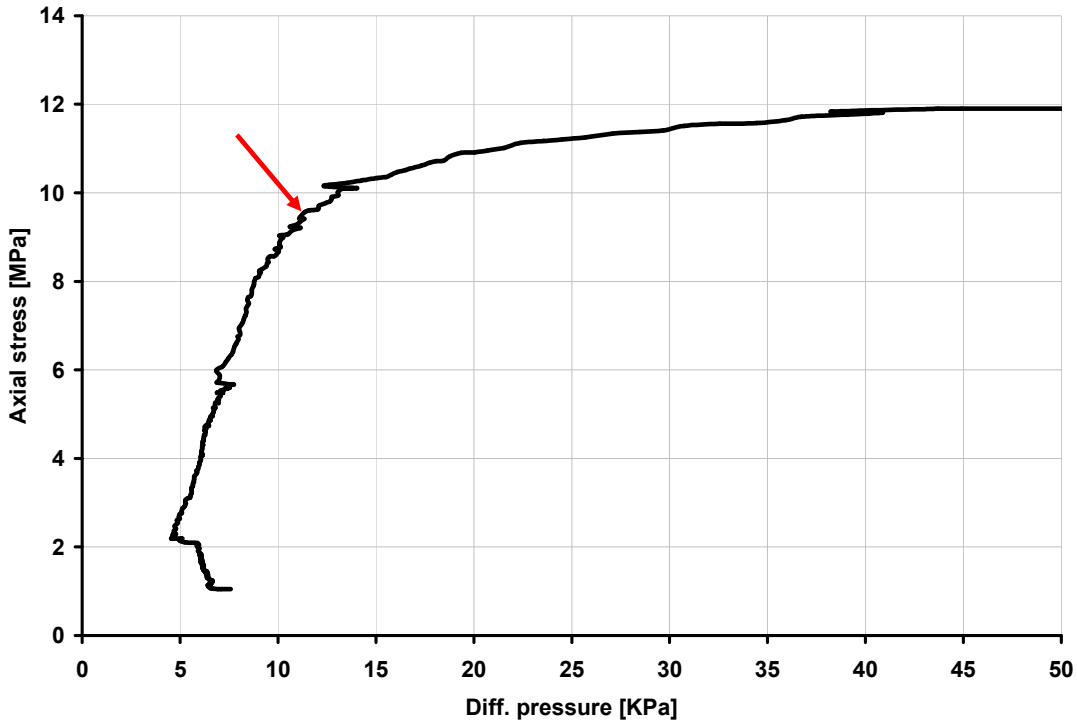

Stress versus strain plot for core C (method 2)

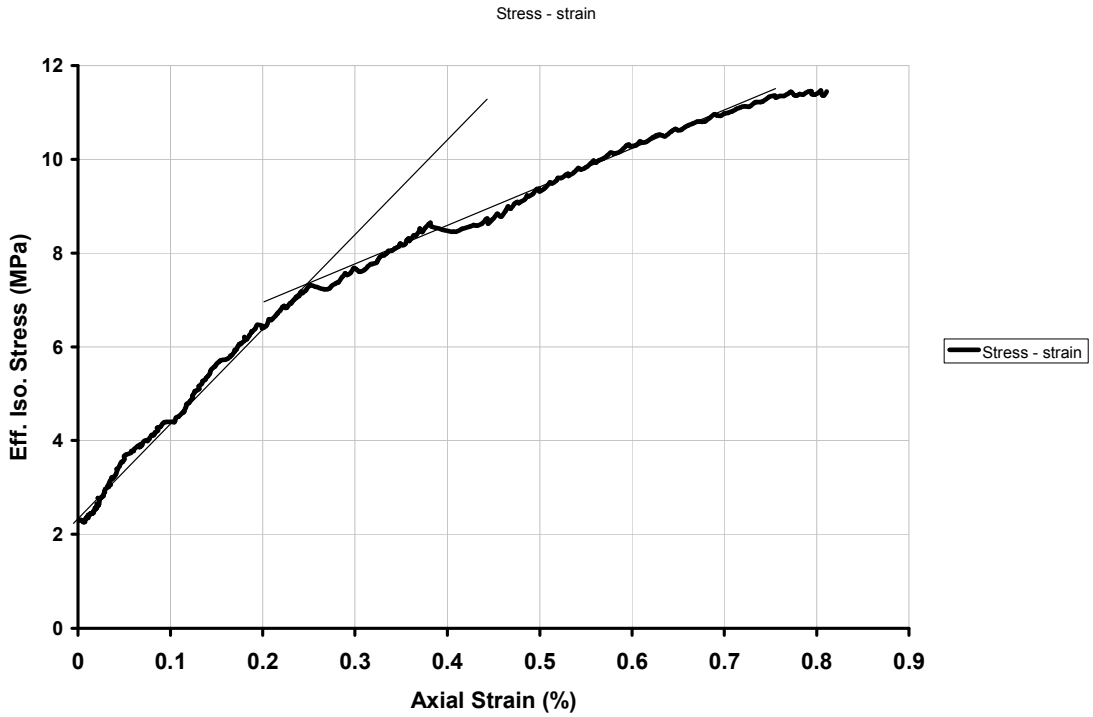

Stress versus strain plot for core D (method 1)

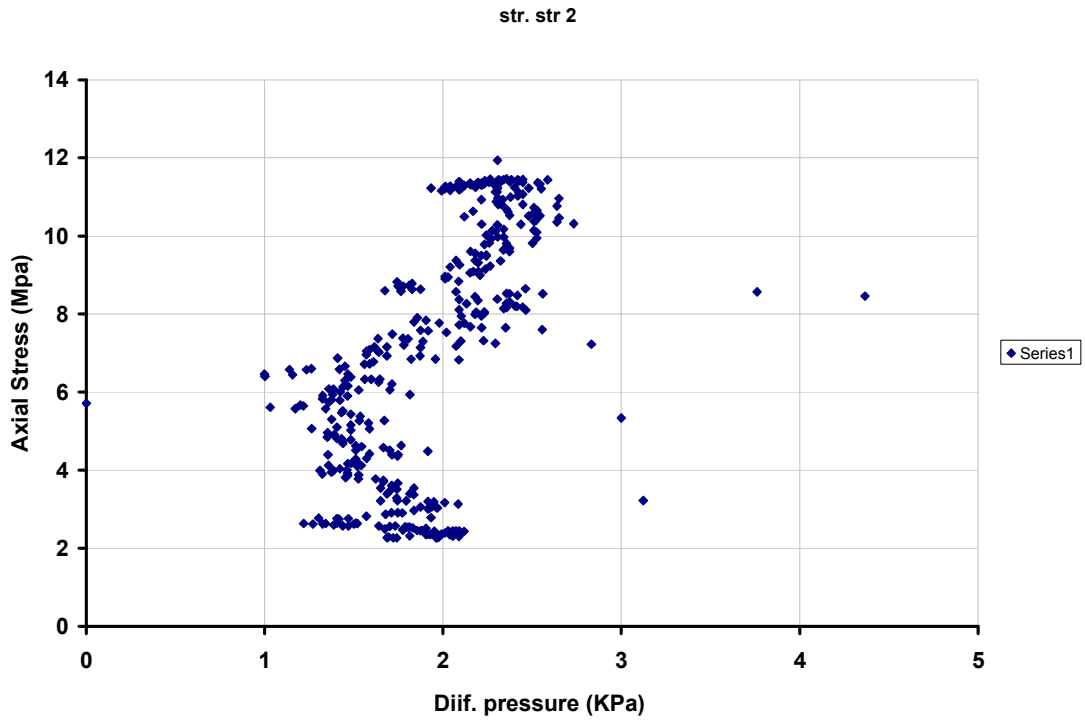

Stress versus strain plot for core D (method 2)

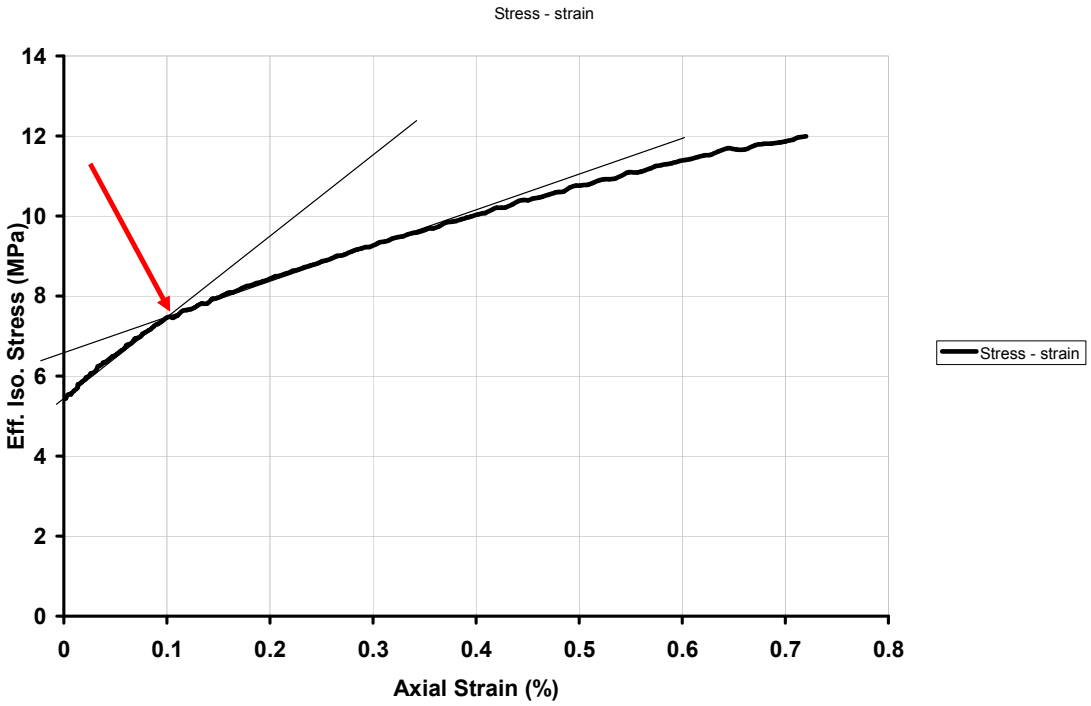

Stress versus strain plot for core G (method 1)

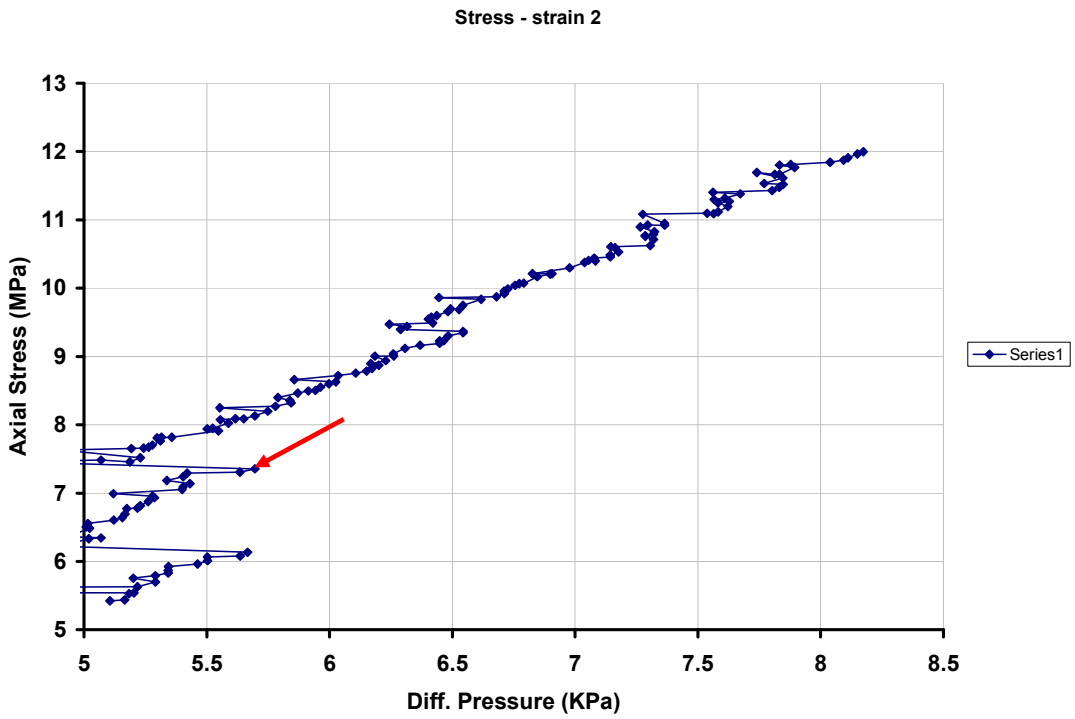

Stress versus strain plot for core G (method 2)

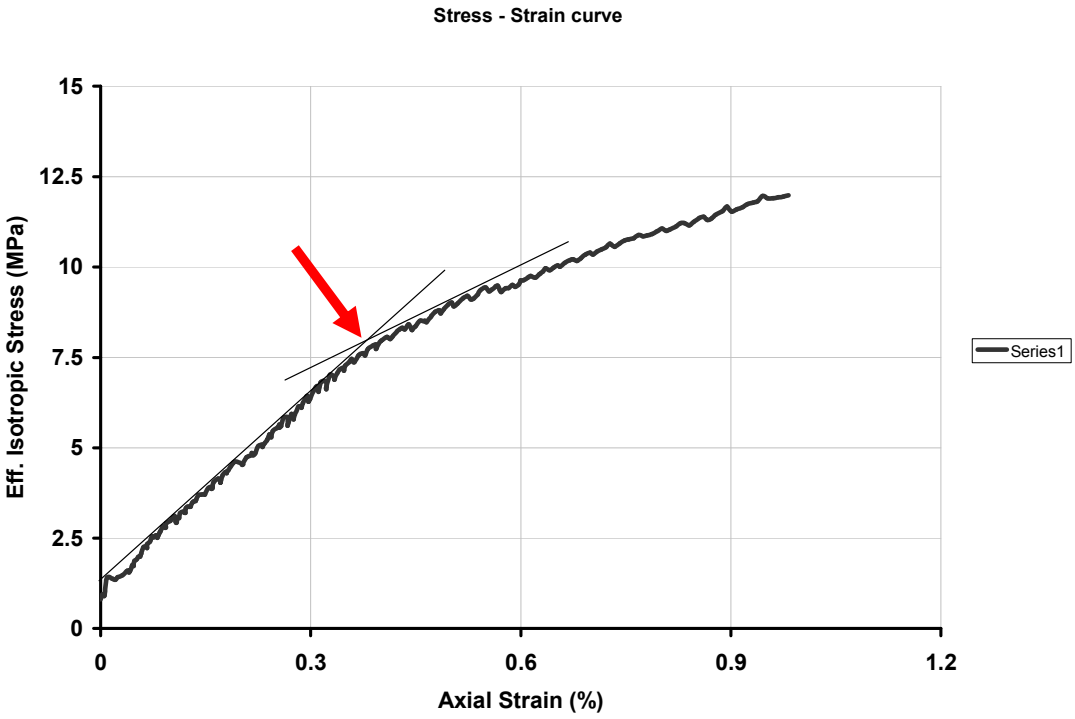

Stress versus strain plot for core M (method 1)

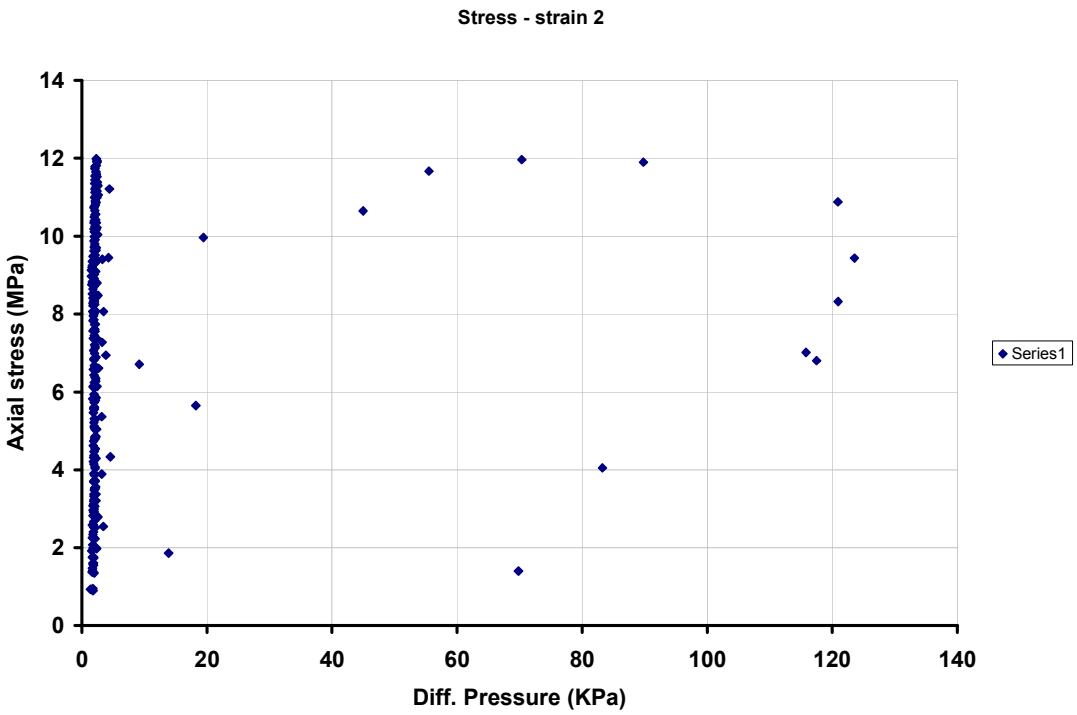

Stress versus strain for core M (method 2

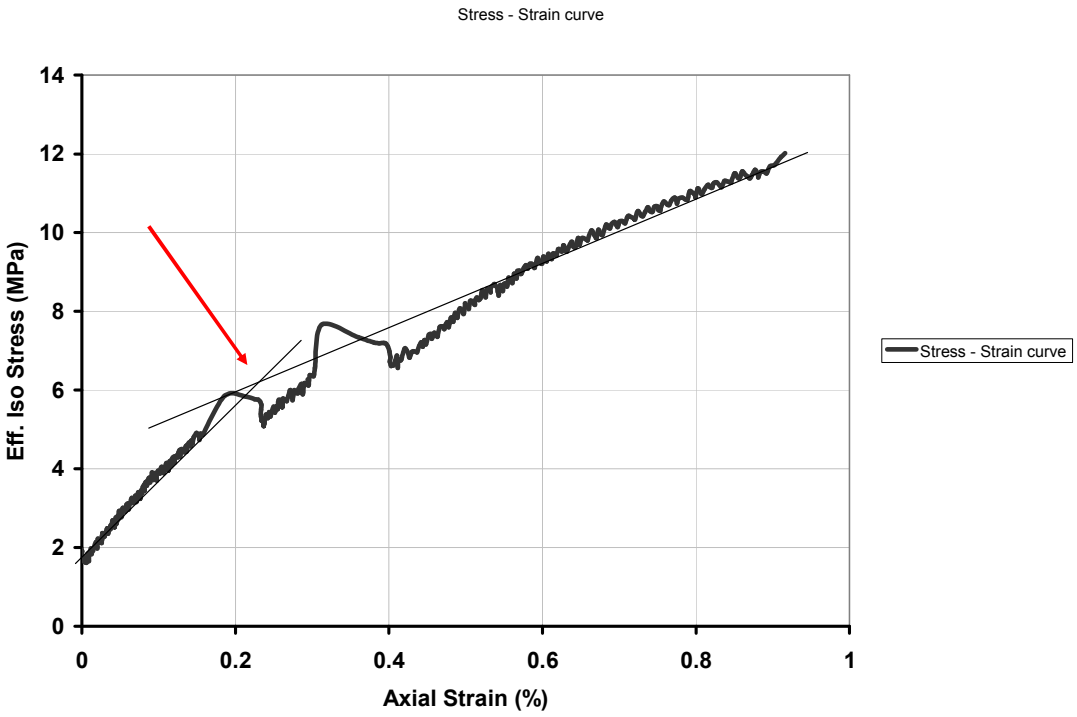

Stress versus strain plot for core N (method 1)

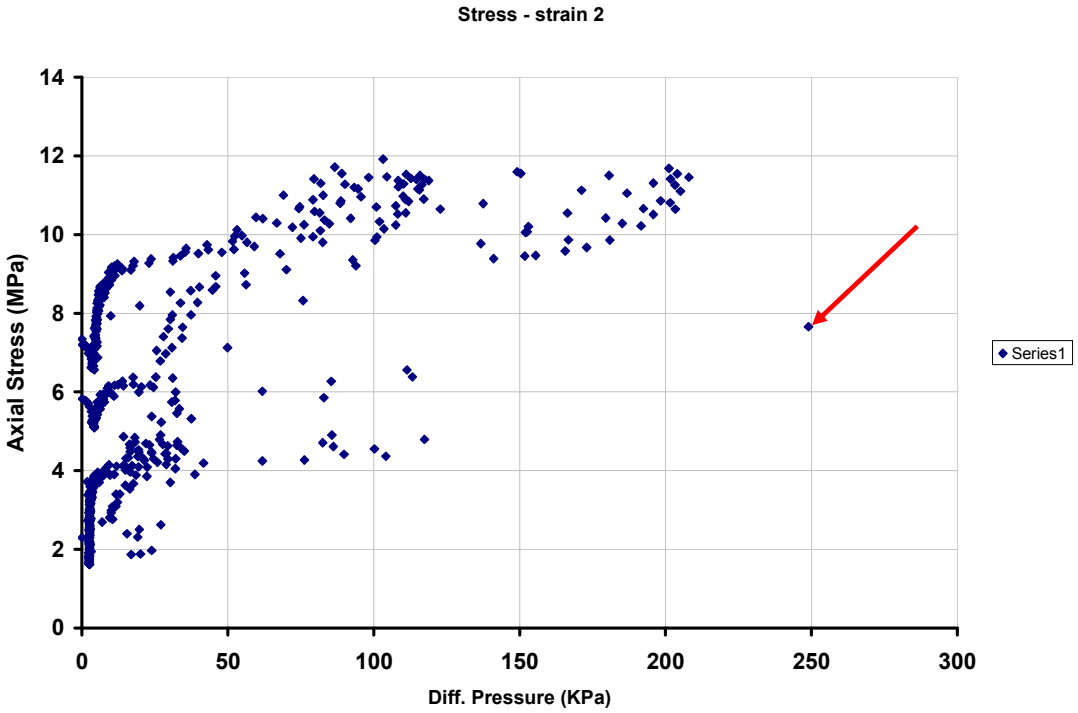

Stress versus strain plot for core N (method 2)

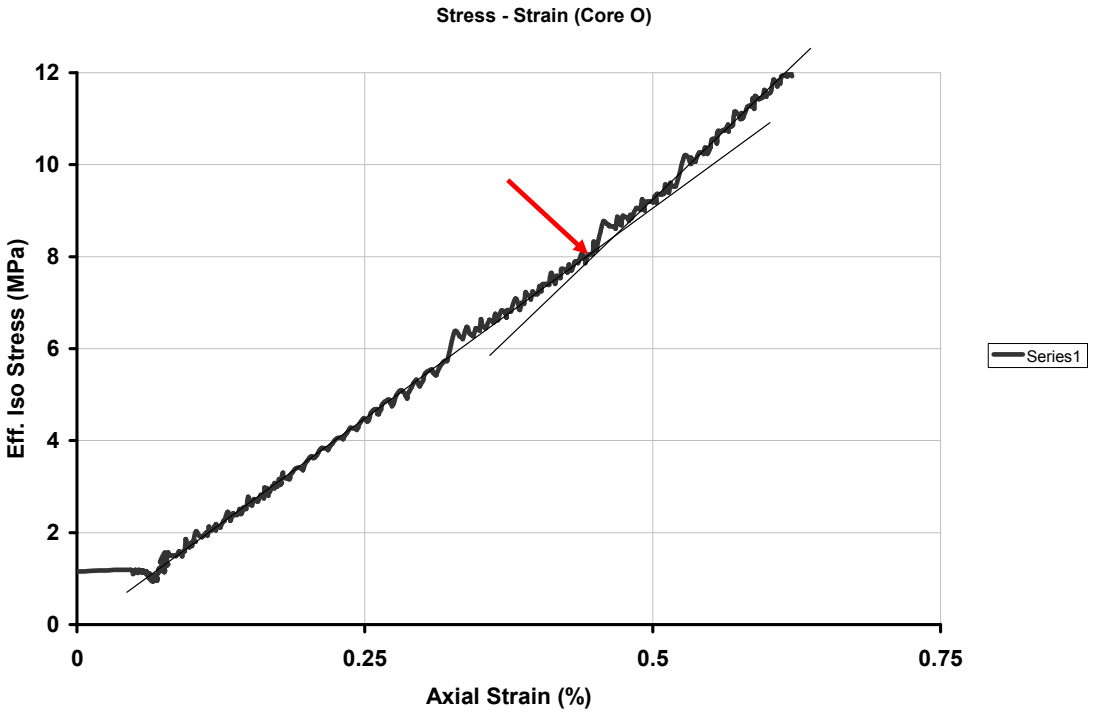

Stress versus strain plot for core O (method 1)

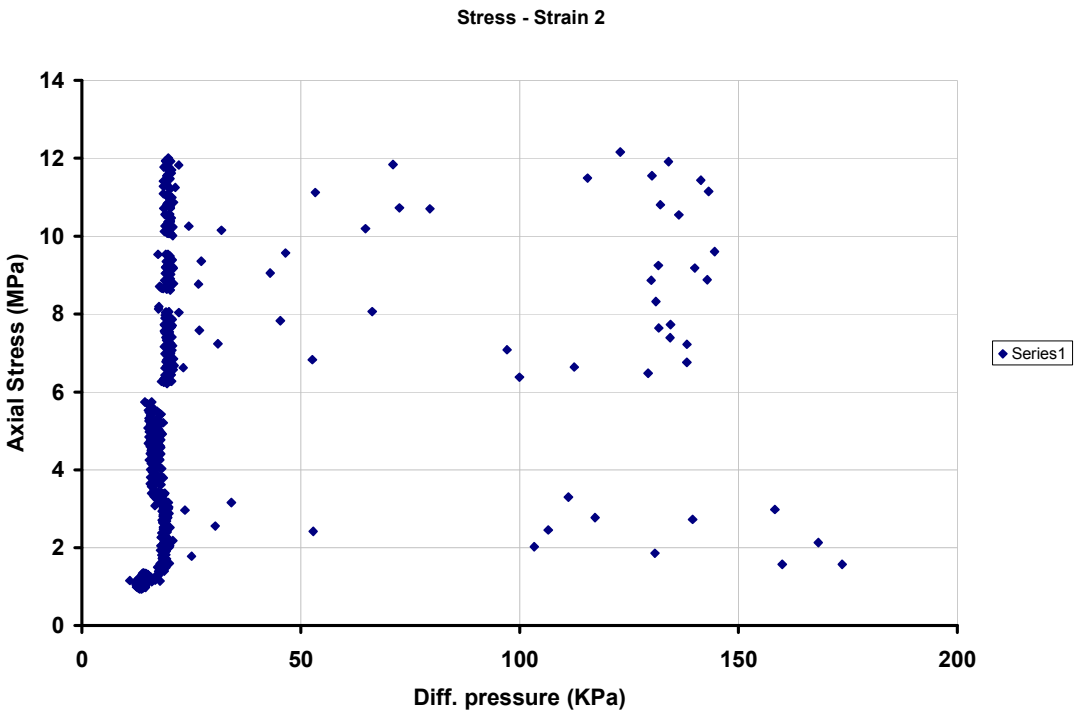

Stress versus strain plot for core O (method 2)

Appendix C

Creep curve for the samples

The creep plot for the samples are presented in appendix C

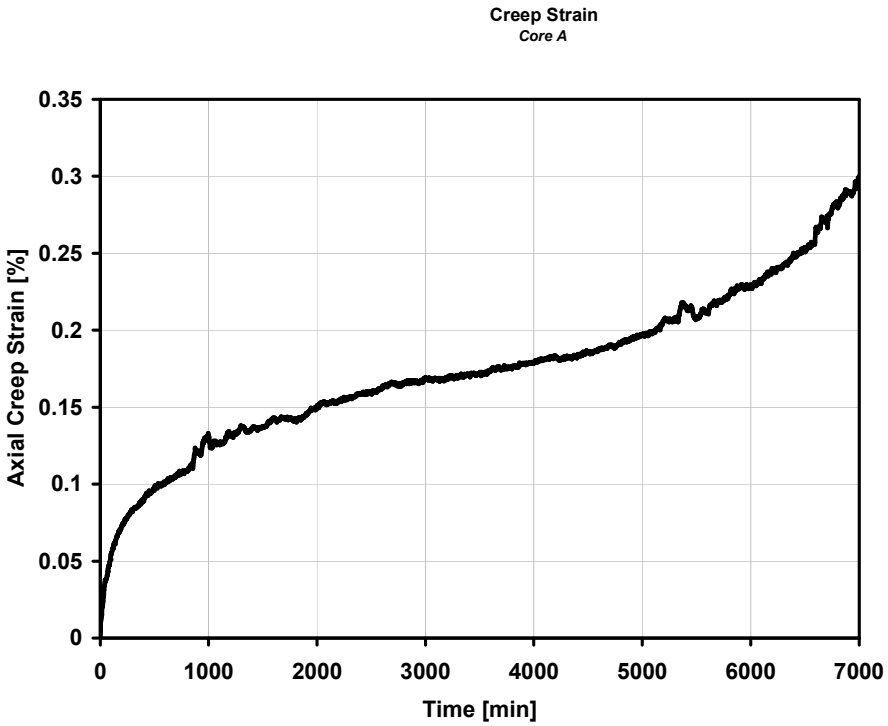

Creep curve for core A

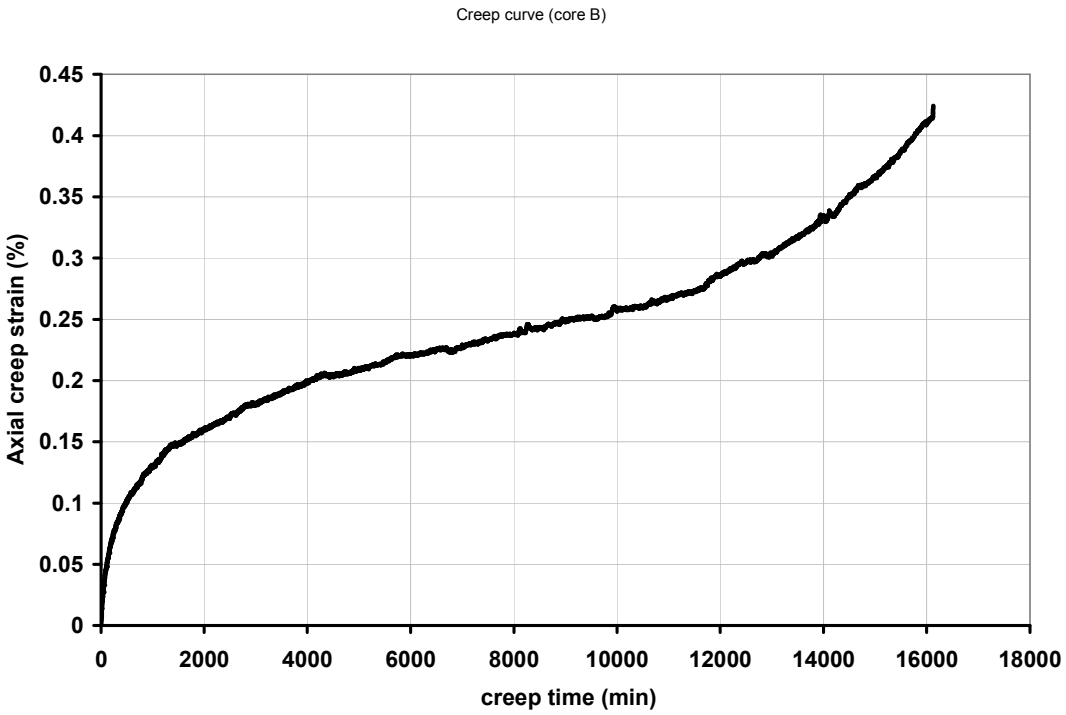

Creep curve for core B

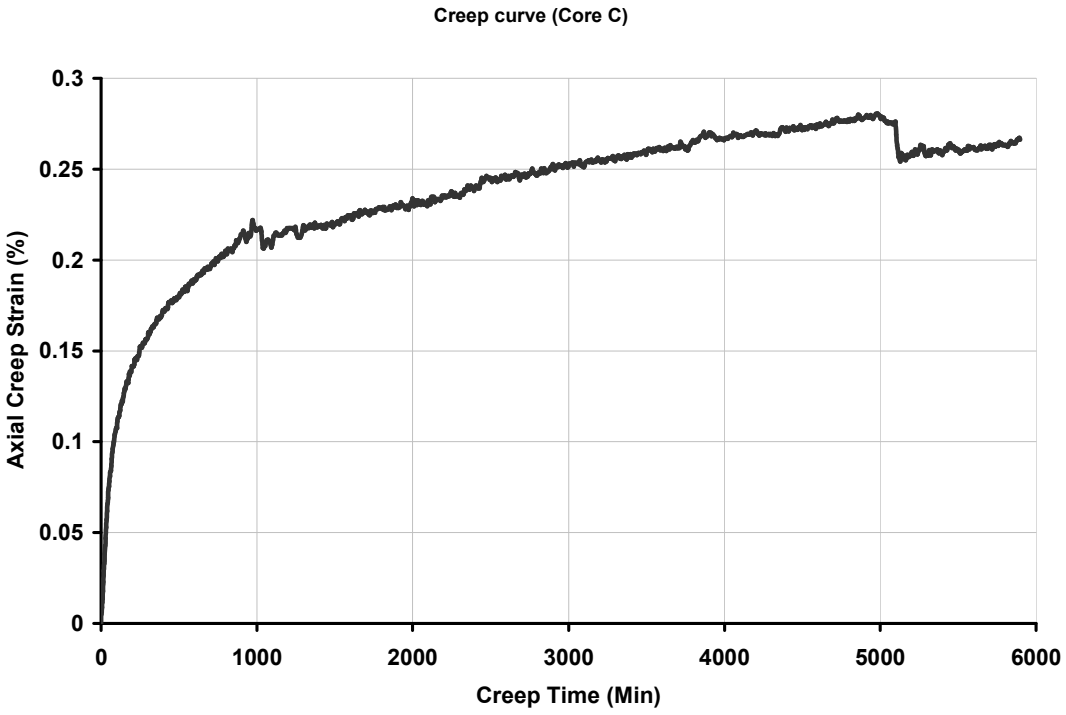

Creep curve for core C

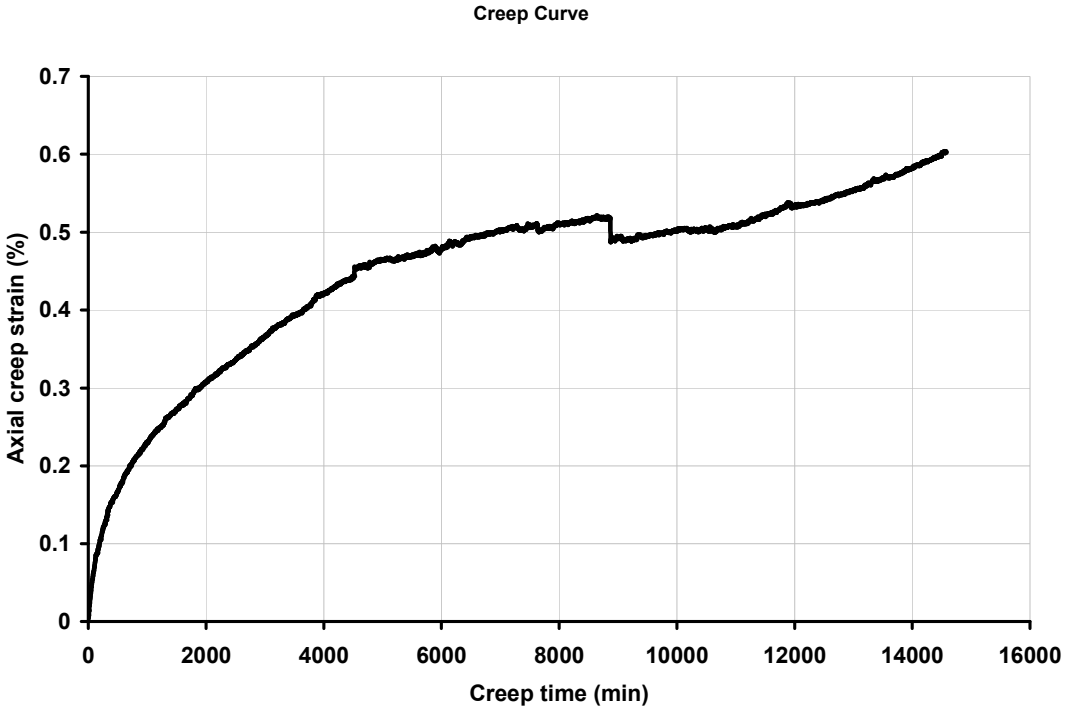

Creep curve for core D

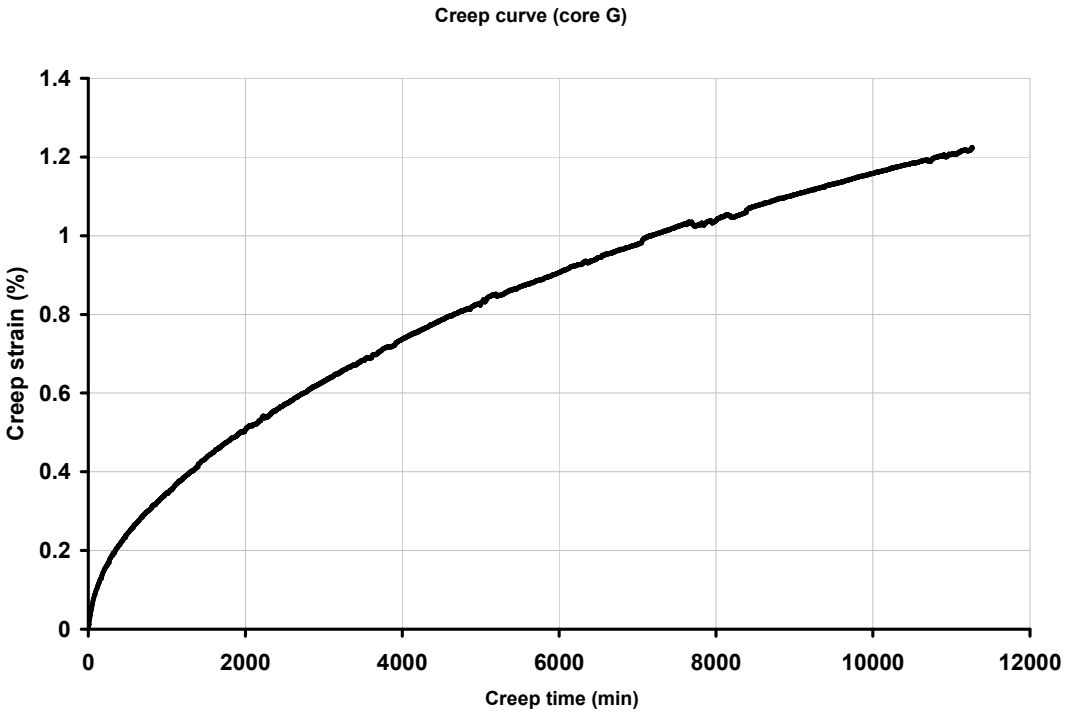

Creep curve for core G

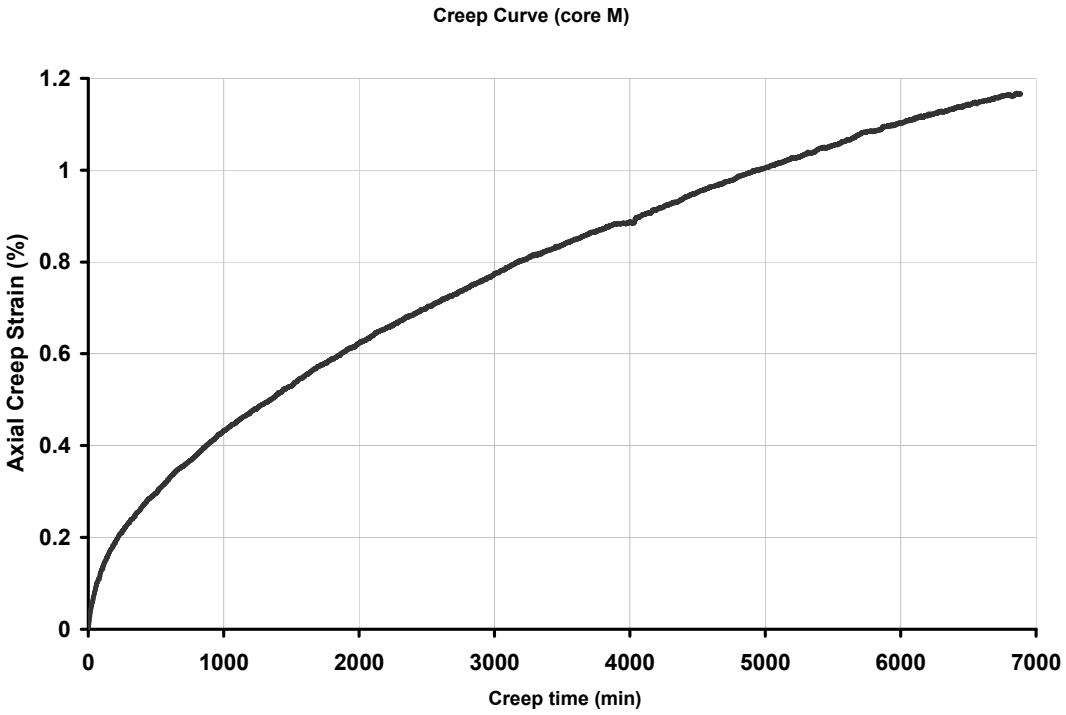

Creep curve for core M

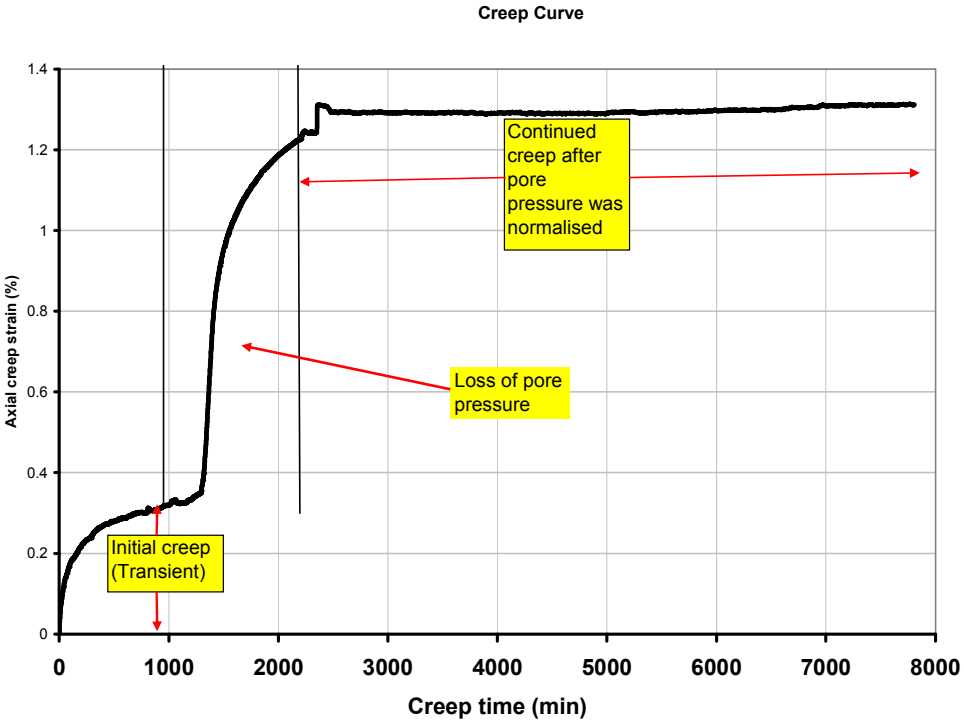

Creep curve for core N

As explained in section 5.2, there sudden drop in pore pressure to 33MPa during the creep period. This was as a result of leakage through the BPR connections. The implication of this was that the effective stress on the sample increased to 19MPa and

the core became highly compacted. The resulting effect was that the previous creep trend was no longer maintained after the pore pressure was normalised.

Appendix D

IC results

In this appendix, the results from chemical analyses of the sampled effluents are presented. Some of the results did not contain the plots for Cl^- because of insufficiency of cartridge used for anion analysis during the test period.

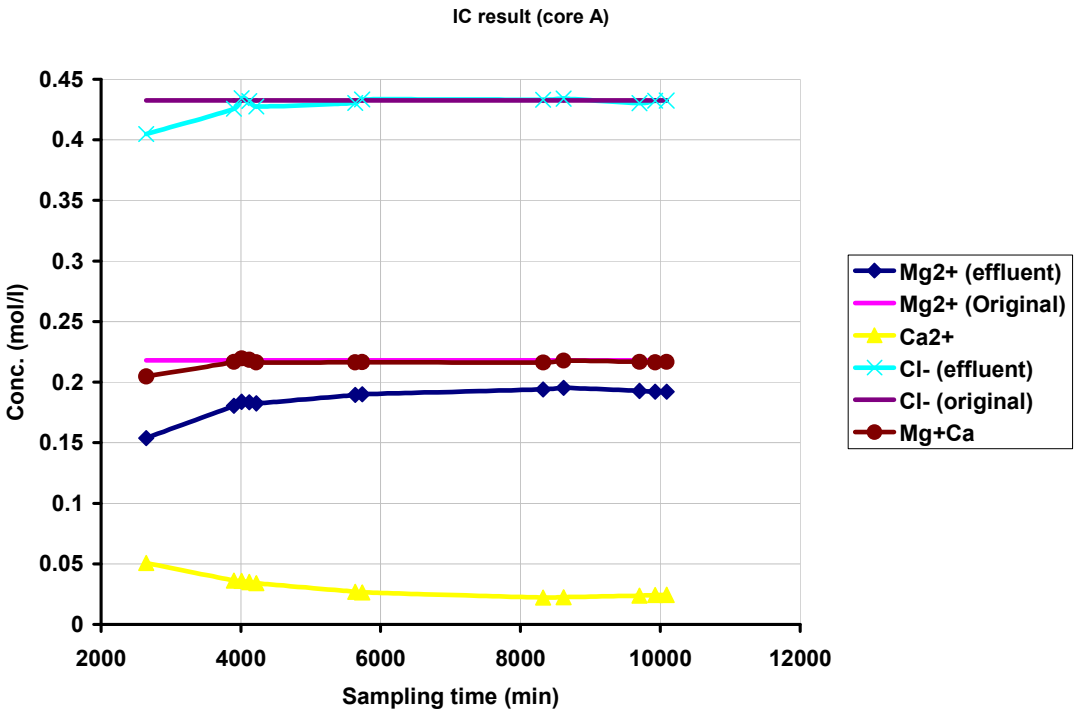

IC result for Mg^{2+}, Ca^{2+} and Cl^- ions in sampled effluent for core A flooded with $MgCl_2$

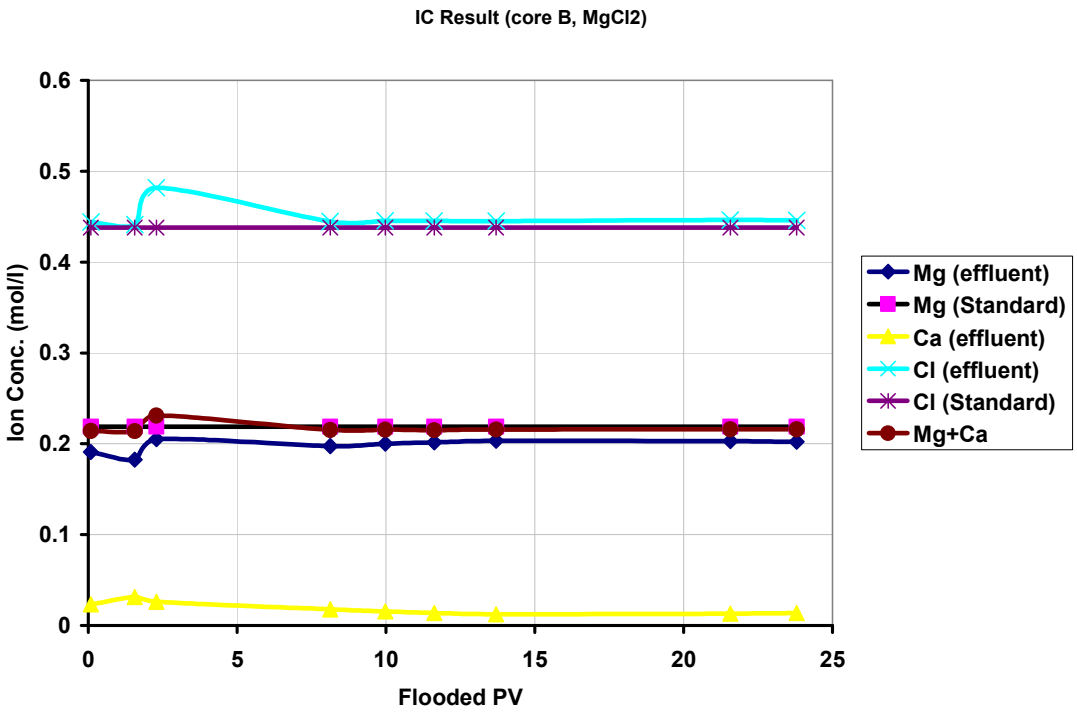

IC result for Mg^{2+}, Ca^{2+} and Cl^- ions in sampled effluent for core B flooded with $MgCl_2$

pH of sampled effluent for core B

Sample number	sampled time (min.)	PV	pH
1	1431	0.09	7.63
2	2462	1.56	7.68
3	2981	2.28	7.69
4	7188	8.12	7.27
5	8519	9.98	7.28
6	9704	11.62	7.75
7	11204	13.7	7.63
8	16869	21.57	7.65
9	18474	23.8	7.77
$MgCl_2$ (standard)		–	5.59
$MgCl_2$ (undiluted)		–	5.71

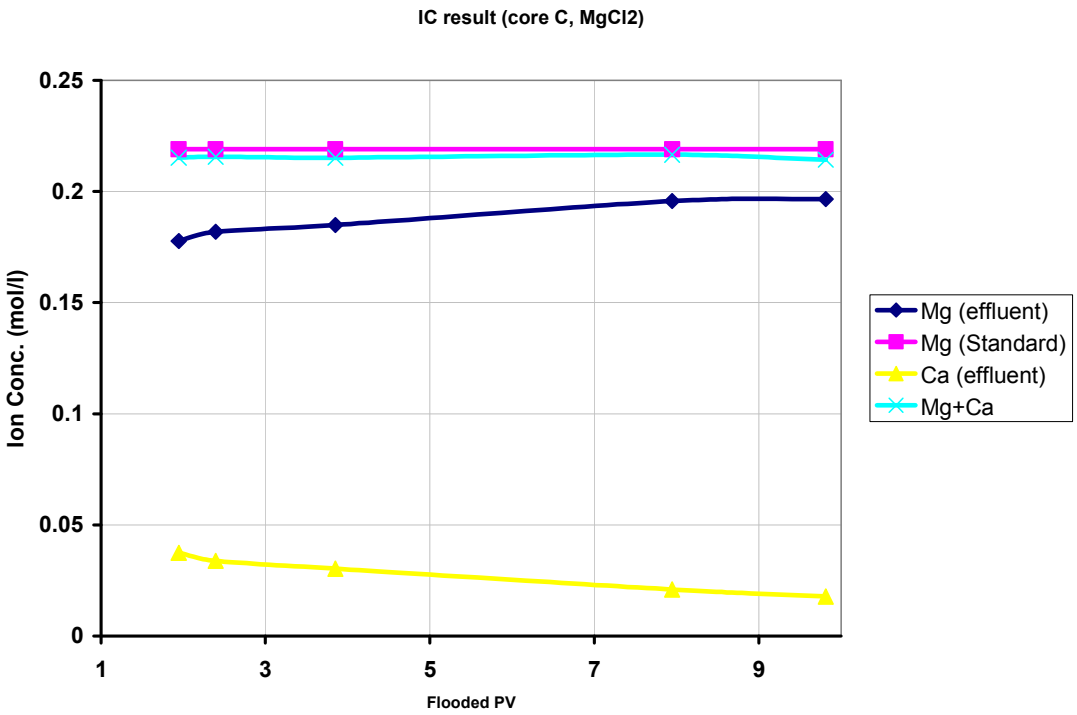

IC result for Mg^{2+}, Ca^{2+} and Cl^{-} ions in sampled effluent for core C flooded with $MgCl_2$

pH of sampled effluent for core C

Sample Number	Sampled time (min)	PV	PH
C1	2574	1.94	7.35
C2	2897	2.39	7.35
C3	3944	3.85	7.41
C4	6894	7.95	7.5
C5	8239	9.81	7.21
$MgCl_2$ (standard)		–	5.59
$MgCl_2$ (undiluted)		–	5.71

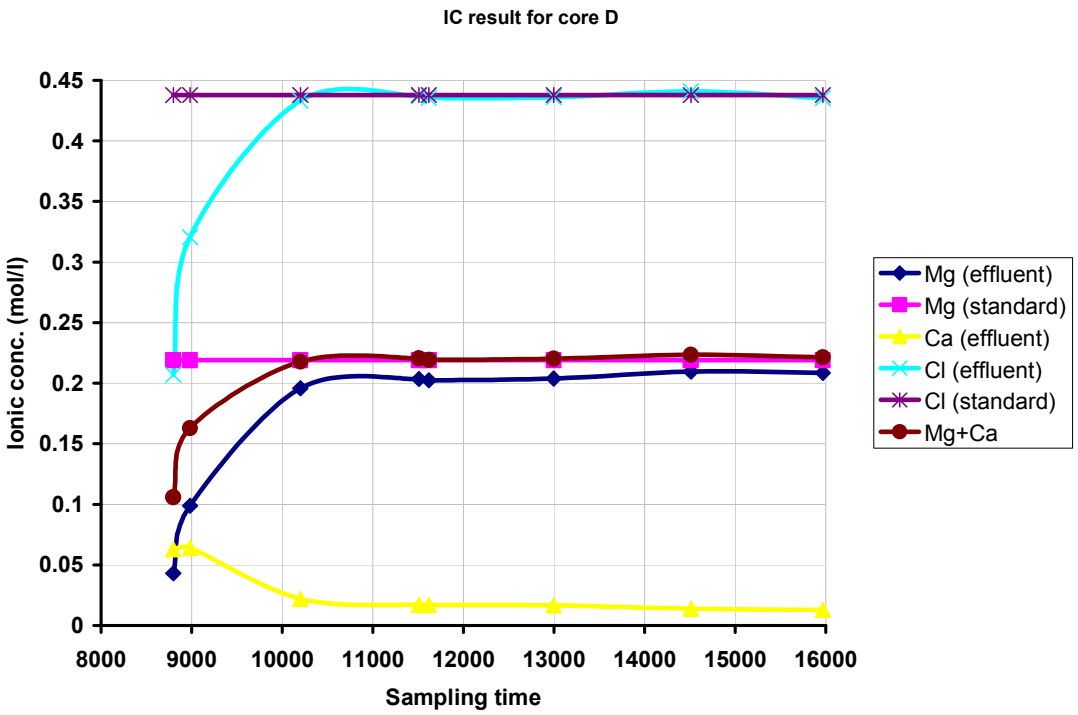

IC result for Mg^{2+}, Ca^{2+} and Cl^{-} ions in sampled effluent for core D flooded with $MgCl_2$.

The first three effluent samples were contaminated during the dilution process. Hence, the effluents tested were therefore, those sampled after over 8500minutes of flooding.

pH of sampled effluent for core D

sample number	sampled time	PV	pH
D1	8797	10.33	7.2
D2	8983	10.77	7.45
D3	10201	13.81	7.8
D4	11509	17.05	7.7
D5	11620	17.21	7.7
D6	12997	19.12	7.84
D7	14512	21.22	7.81
D8	15967	23.25	7.7
$MgCl_2$ (standard)		–	5.59
$MgCl_2$ (undiluted)		–	5.71

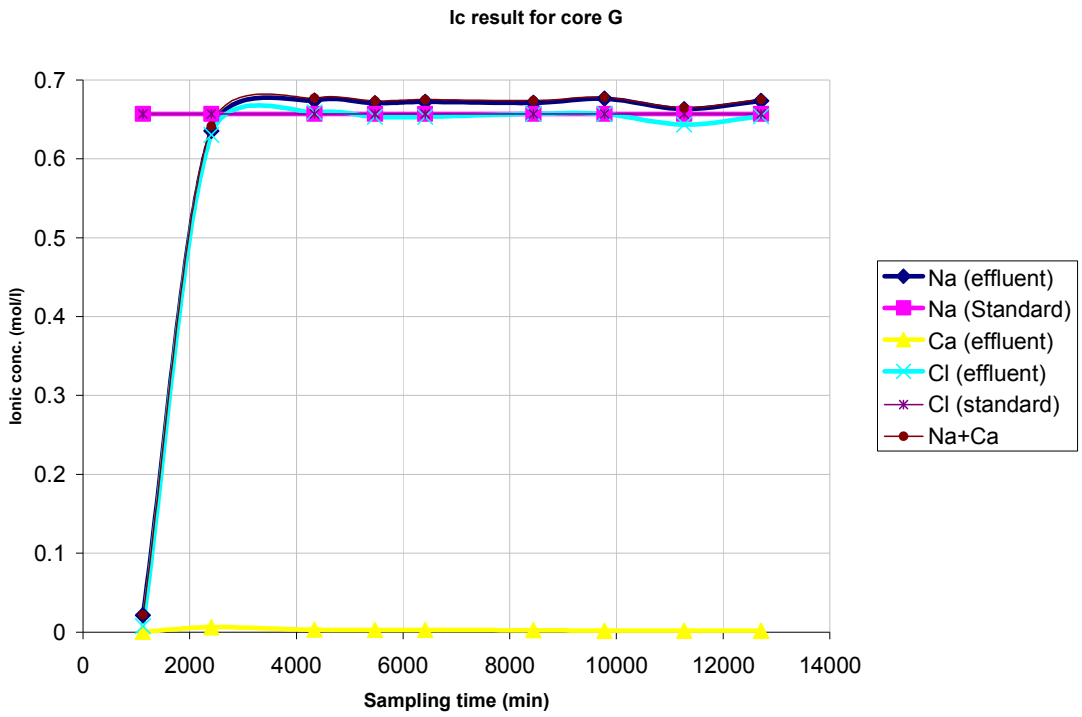

IC result for Na^{+}, Ca^{2+} and Cl^{-} ions in sampled effluent for core G flooded with NaCl

pH of sampled effluent for core G

sample number	sampled time	PV	pH
G1	1124	0.41	8.25
G2	2408	2.63	7.6
G3	4340	5.31	7.88
G4	5477	6.9	7.79
G5	6414	8.19	7.78
G6	8444	11.01	7.65
G7	9776	12.86	7.75
G8	11270	14.94	7.76
G9	12710	16.94	7.74
NaCl (standard)		–	5.76
NaCl (undiluted)		–	5.66

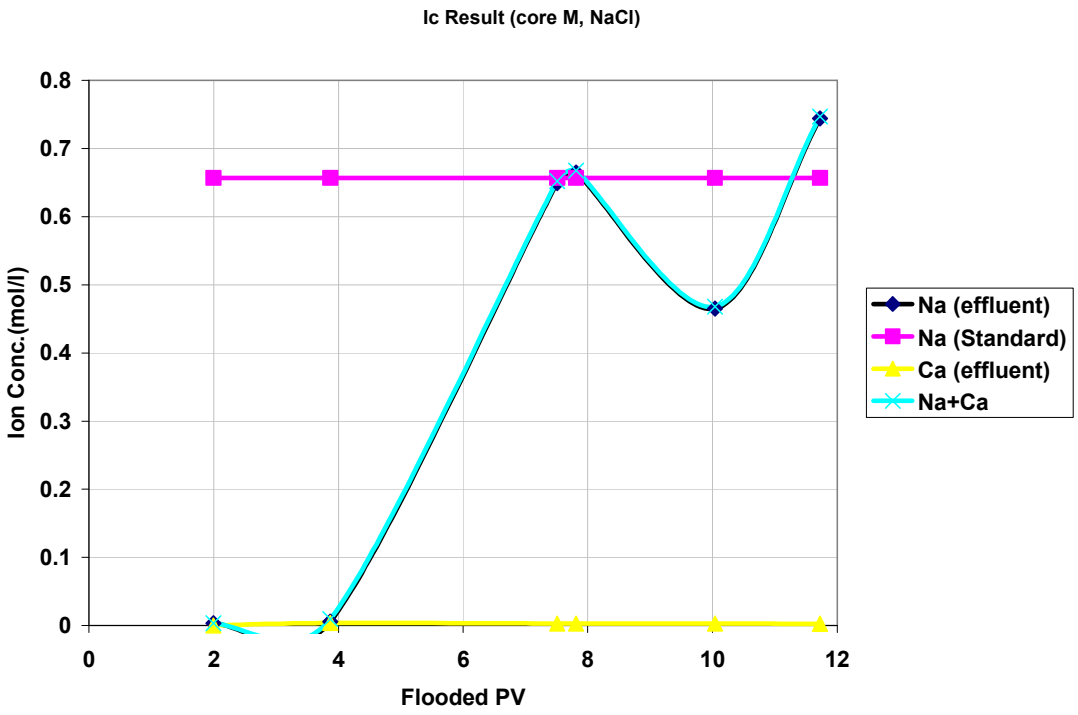

IC result for Na^{+} and Ca^{2+} ions in sampled effluent for core M flooded with NaCl

The fluctuation in concentration of Na and Na+Ca in the effluents of core M was as a result of evaporation during storage. It happened that while the sampled effluents were on storage (before the IC analysis), evaporation of some portion of the samples took place, leaving behind highly concentrated solution of the effluent.

pH of sampled effluent for core M

sample number	sampled time (min)	PV	pH
M1	2859	1.99	-
M2	4207	3.87	7.72
M3	6827	7.51	7.7
M4	7043	7.81	7.73
M5	8649	10.04	7.9
M6	9861	11.73	7.8
NaCl (standard)		–	5.76
NaCl (undiluted)		–	5.66

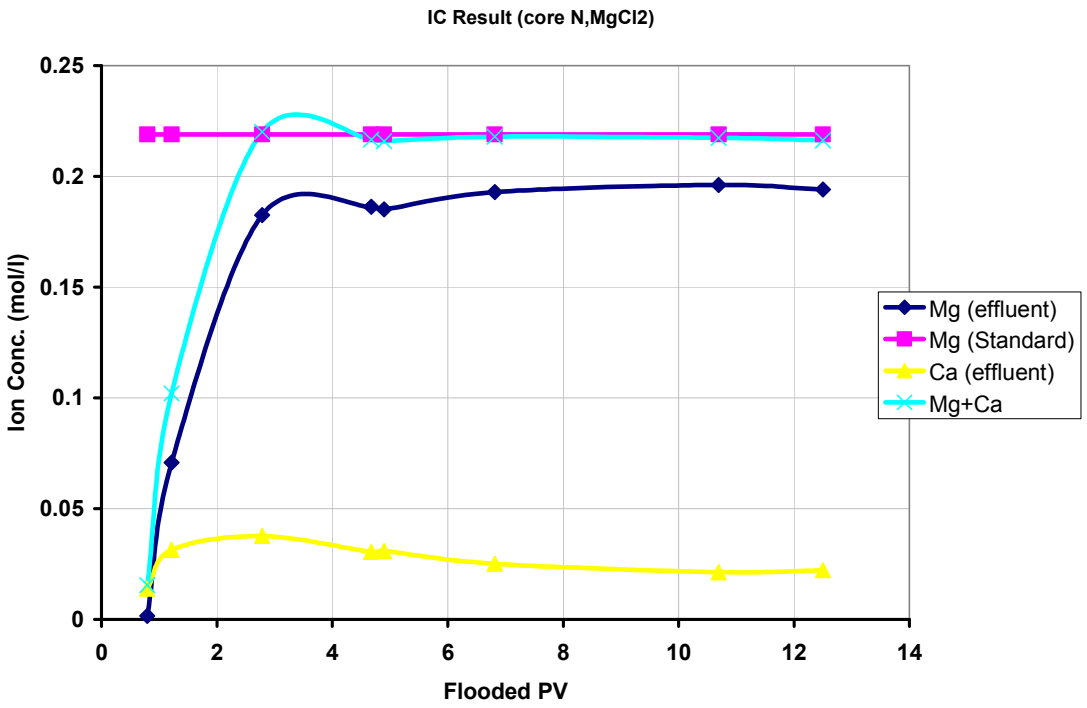

IC result for $Mg^{2+}$and Ca^{2+} ions in sampled effluent for core N flooded with $MgCl_2$

pH of sampled effluent for core N

Sample number	Sampled time(min)	PV	PH
N1	2824	0.8	7.45
N2	3126	1.22	7.61
N3	4256	2.78	7.63
N4	5615	4.67	7.4
N5	5774	4.89	7.72
N6	7157	6.81	7.82
N7	9950	10.69	7.73
N8	11556	12.49	7.67
$MgCl_2$ (standard)		–	5.59
$MgCl_2$ (undiluted)		–	5.71

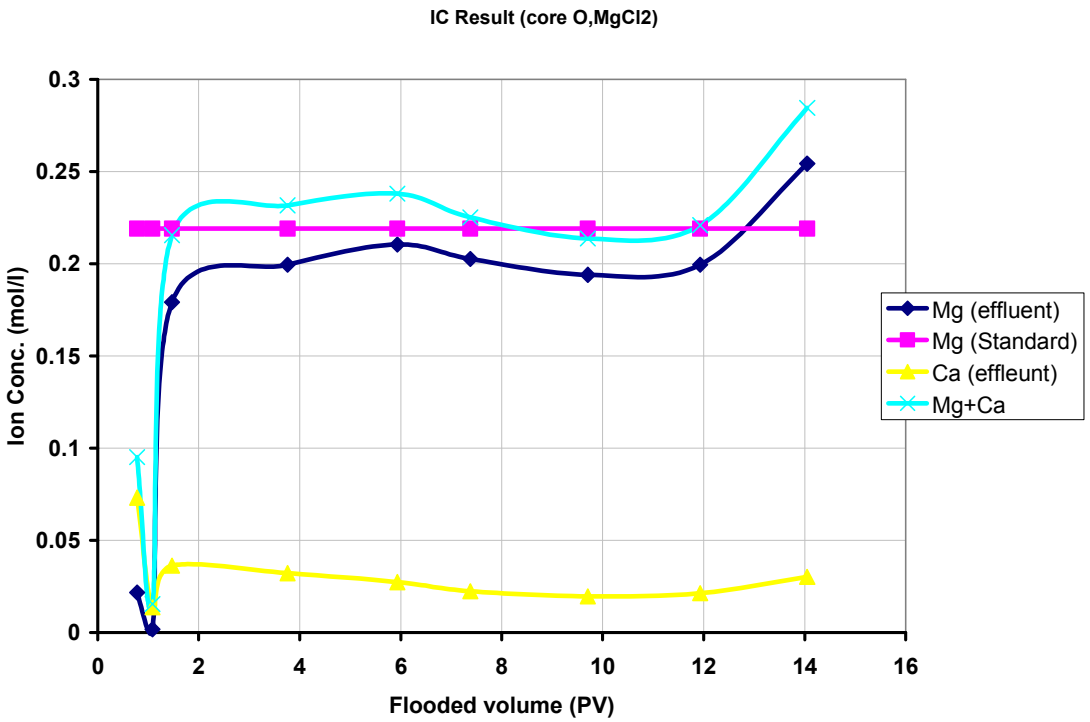

IC result for $Mg^{2+}$and Ca^{2+} ions in sampled effluent for core O flooded with $MgCl_2$

pH of sampled effluent for core O

Sample number	Sampled time(min)	PV	pH
N1	2604	0.78	7.3
N2	2828	1.09	7.61
N3	4022	1.47	7.76
N4	5675	3.76	7.79
N5	7237	5.93	7.86
N6	8277	7.38	7.76
N7	9950	9.7	7.79
N8	11477	11.93	7.81
N9	12998	14.05	7.76
$MgCl_2$ (standard)		–	5.59
$MgCl_2$ (undiluted)		–	5.71